MEA and GDE manufacture for electrolytic membrane characterisation

HH Hoek

20164610

Dissertation submitted in fulfillment of the requirements for the degree *Magister Scientiae* in Chemistry at the Potchefstroom Campus of the North-West University

Supervisor: Prof HM Krieg

November 2013

Acknowledgements

I would like to express my total gratitude towards:

- Our Father from above for giving me the ability to complete this task.
- Professor Henning Krieg for the utmost patience, understanding and guidance.
- My parents for standing beside me supporting me throughout this endeavour.
- For Jenavicka Carney for being patient and supportive throughout the time it took me to complete this research.
- For the School of Physical and Chemical Sciences for the opportunity to visit Germany and receive necessary training for my experimental work.
- Dr Jochen A. Kerres and Andreas Chormick, university of Stuttgart for hosting me their total helpfulness throughout my stay.
- Zentrum für Sonnenenergie- und Wasserstoff- Forschung (ZSW), Ulm, Germany for the time to train me in membrane coating techniques.
- HySA infrastructure for the funding of my research and the bursary that made it possible for me to complete my studies.
- Chemical Resource Beneficiation, North-West University, Potchefstroom campus for the use of their laboratories for all my research purposes.
- And lastly to all my friends for the endless conversations, support and memories that will last me a lifetime.

Abstract

In recent years an emphasis has been placed on the development of alternative and clean energy sources to reduce the global use of fossil fuels. One of these alternatives entails the use of H_2 as an energy carrier, which can be obtained amongst others using thermochemical processes, for example the hybrid sulphur process (HyS). The HyS process is based on the thermal decomposition of sulphuric acid into water, sulphur dioxide and oxygen. The subsequent chemical conversion of the sulphur dioxide saturated water back to sulphuric acid and hydrogen is achieved in an electrolyser using a platinum coated proton exchange membrane. This depolarised electrolysis requires a theoretical voltage of only 0.158 V compared to water electrolysis requiring approximately 1.23 V. One of the steps in the development of this technology at the North-West University, entailed the establishment of the platinum coating technology which entailed two steps; firstly using newly obtained equipment to manufacture the membrane electro catalyst assemblies (MEA's) and gas diffusion electrodes (GDE's) and secondly to test these MEA's and GDE's using sulphur dioxide depolarized electrolysis by comparing the manufactured MEA's and GDE's to commercially available MEA's and GDE's.

Different MEA's and GDE's were manufactured using both a screen printing (for the microporous layer deposition) and a spraying technique. The catalyst loadings were varied as well as the type and thickness of the proton exchange membranes used. The proton exchange membranes that were included in this study were Nafion 117®, sPSU-PBIOO and SfS-PBIOO membranes whereas the gas diffusion layer consisted of carbon paper with varying thicknesses (EC-TP01-030 – 0.11 mm and EC-TP01-060 – 0.19mm). MEA and GDE were prepared by first preparing an ink that was used both for MEA and GDE spraying. The MEA's were prepared by spraying various catalyst coatings onto the proton exchange membranes containing 0.3, 0.6 and 0.9 mg/cm^2 platinum respectively. The GDE's were first coated by a micro porous carbon layer using the screen printing technique in order to attain a suitable surface for catalyst deposition. Using the spraying technique GDE's containing 0.3, 0.6, 0.9 mg/cm^2 platinum were prepared. After SEM analysis, the MEA's and GDE's performance was measured using SO_2 depolarized electrolysis. From the electrolysis experiments, the voltage vs. current density generated during operation, the hydrogen production, the sulphuric acid generation and the hydrogen production efficiency was obtained.

From the results it became clear that while the catalyst loading had little effect on performance there were a number of factors that did have a significant influence. These included the type of proton exchange membrane, the membrane thickness and whether the catalyst coating was applied

to the proton exchange membrane (MEA) or to the gas diffusion layer (GDE). During SO_2 depolarized electrolysis VI curves were generated which gave an indication of the performance of the GDE's and MEA's. The best preforming GDE was GDE-3 (0.46V @ 320 mA/cm^2), which included a GDE EC-TP01-060, while the best preforming MEA's were NAF-4 (0.69V @ 320mA/cm^2) consisting of a Nafion117 based MEA and PBI-1 (0.43V @ 320mA/cm^2) made from a sPSU-PBIOO blended membrane. During hydrogen production it became clear that the GDE's produced the most hydrogen (best was GDE-02 a in house manufactured GDE yielding 67.3 mL/min @ 0.8V), followed by the Nafion® MEA's (best was NAF-4 a commercial MEA yielding 57.61 mL/min @ 0.74V) and the PBI based MEA's. , (best was PBI-2 with 67.11 mL/min @ 0.88V). Due to the small amounts of acid produced and the SO_2 crossover, a significant error margin was observed when measuring the amount of sulphuric acid produced. Nonetheless, a direct correlation could still be seen between the acid and the hydrogen production as had been expected from literature. The highest sulphuric acid concentrations produced using the tested GDE's and MEA's from this study were the in-house manufactured GDE-01 (3.572mol/L @ 0.8V), the commercial NAF-4 (4.456mol/L @ 0.64V) and the in-house manufactured PBI-2 (3.344mol/L @ 0.8V). The overall efficiency of the GDE's were similar, ranging from less than 10% at low voltages (± 0.6V) increasing to approximately 60% at ± 0.8V. For the MEA's larger variation was observed with NAF-4 reaching efficiencies of nearly 80% at 0.7V.

In terms of consistency of performance it was shown that the Nafion MEA's preformed most consistently followed by the GDE's and lastly the PBI based MEA's which for the PBI based membranes can probably be ascribed to the significant difference in thickness of the thin PBI vs. the Nafion based membranes. In summary the study has shown the results between the commercially obtained and the in-house manufactured GDE's and MEA's were comparable confirming the suitability of the coating techniques evaluated in this study.

Key words: Membrane electrocatalyst assemblies (MEA), Gas diffusion electrodes (GDE), Catalyst loadings, Proton exchange membrane, SO_2 depolarized electrolysis.

Table of content

Chapter 3: Experimental

Chapter 5: Evaluation and recommendations

List of tables

Chapter 2: Literature study

Chapter 3: Experimental

Chapter 4: Results and discussion

List of figures

Chapter 1: Introduction

Chapter 2: Literature study

Chapter 3: Experimental

Chapter 4: Results and discussion

Chapter 5: Evaluation and recommendations

Nomenclature

List of abbreviations

CH_4	Methane
CL	Catalyst layer
CO	Carbon monoxide
CO_2	Carbon dioxide
Cu-Cl	Copper Chlorine cycle
DI	Deionized water
e^-	Electron
EDS	Energy Dispersive Spectroscopy
ESA	Electrochemical active surface area
GDE	Gas diffusion electrode
GDL	Gas diffusion layer
H_2	Hydrogen
H_2O	Water
H_2SO_4	Sulphuric acid
HyS	Hybrid Sulphur process
I_2	Iodine
MEA	Membrane electrocatalyst assembly
MPL	Micro porous layer
N_2	Nitrogen
NaOH	Sodium hydroxide
NWU	North-West University
O_2	Oxygen
SEM	Scanning Electron Microscopy
SI	Sulphur Iodine cycle

sFS-PBIOO	Sulfonated fluorophenyl sulphone polybenzimidazole
SO_2	Sulphur dioxide
SPE	Solid Polymer Electrode
S-PEEK-WC	Sulfonated poly ether ether ketone with cardo groups
sPSU-PBIOO	Poly arylene ethersulphone polybenzimidazole
PBI	Polybenzimidazole
PEM	Proton exchange membrane
PEMFC	Proton exchange fuel cell
TAB	Tetra-aminobiphenyl
VI	Volt vs. Ampere
ZSW	Zentrum Für Sonnenenergie- Und Wasserstof Forchung

List of symbols

A_{Ga}	Geometric active catalyst area	(cm^2)
A_{theo}	Theoretical active surface area	(cm^2)
d	Average diameter of Platinum particle	(cm)
F	Faradic constant	(Ampere.second)
I	Current	(Ampere)
L_d	Desired loading	(mg $Pt.cm^{-2}$)
L	Loading	(mg $Pt.cm^{-2}$)
m	Mass of platinum in platinum on carbon	(g)
N	weight % Nafion® in Nafion® solution	
N_e	Mole of electrons produced	(mole)
P	% Pt/C	
Q	Charge	(coulomb)
t	time	(seconds)
ρ	Density of the platinum bulk	($g.cm^{-3}$)

Chapter 1: Introduction

1.1 Background

With finite energy sources like fossil fuels and nuclear power making up most of the world's energy sources (Figure 1.1) and the negative effect that these fossil fuels and, potentially, nuclear energy have on the environment, more impetus has to be placed on renewable energy sources.

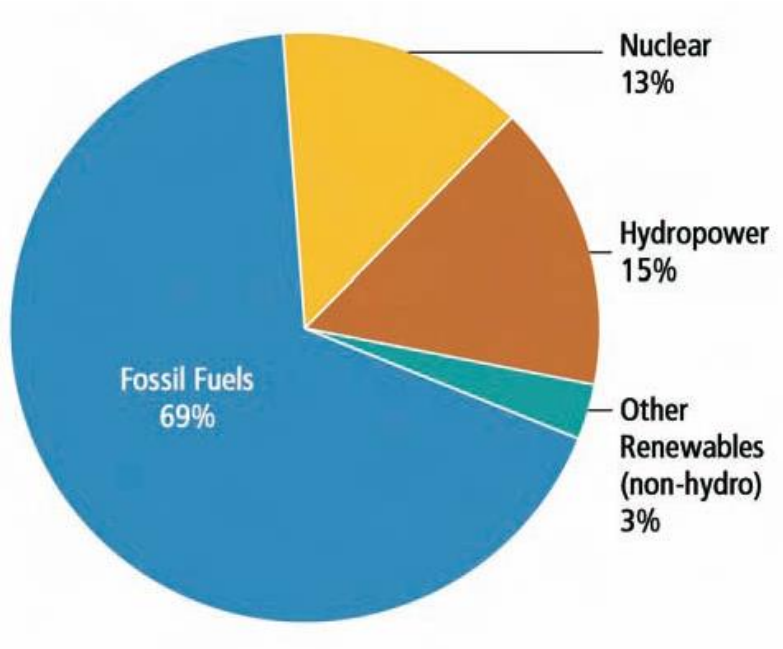

Figure 1.1: Global electricity from renewable and non-renewable energy sources[1].

It is known that the carbon dioxide produced by fossil fuels is continuously increasing (Figure 1. 3). Since the infrared light, which is emitted by the sun and re-emitted by the earth's surface, is readily absorbed by carbon dioxide (Figure 1.2) and re-emitted as heat, an increase in carbon dioxide is thus directly connected to global warming, making fossil fuels one of the largest contributors to global warming.

Nuclear power has the advantage that vast amounts of energy can be produced from little source material, while few by-products are produced by the nuclear fission process. The biggest problem with nuclear power, however, arises when the reactor fails. The dangers of reactor failure were again shown recently in Fukushima, Japan.

In light of the shortcomings of fossil and nuclear-based energy sources it is vital that more research be done on alternative, environmentally friendly energy sources.

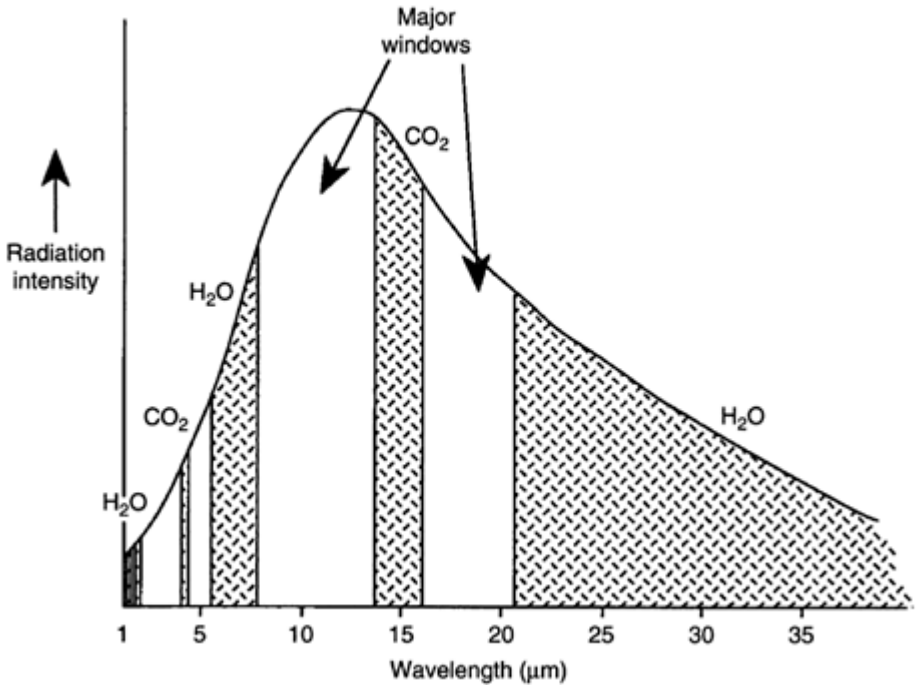

Figure 1.2: Relative intensity of radiation of energy emitted by the earth's surface together with the major absorption bands of CO_2[2].

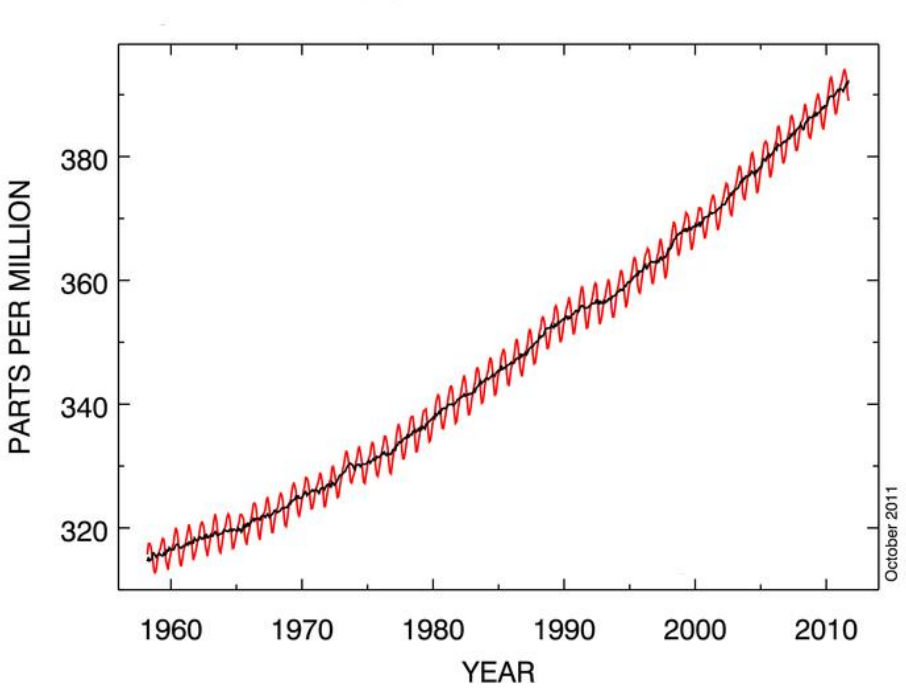

Figure 1.3: Yearly CO_2 increase at Mauna Loa observatory, Hawaii[3].

1.1.1 Hydroelectric power

Various forms of alternative energy sources exist, of which the biggest is hydroelectric power generation, the principle of which is shown in Figure 1.4. Hydroelectric power generation harnesses the natural movement force of water from a reservoir to turn turbines, thereby generating electricity. The main drawback of hydroelectric power generation is that it is dependent on rainfall, leading to reduced electrical output during dry periods, which is traditionally balanced by fossil fuels or nuclear powered energy generation methods. The seasonal dependency factor results in dams being built in areas where regular rainfall is certain. These areas are usually areas containing rainforests and large scale deforestation and habitat loss are therefore normal results of hydroelectric dam building.

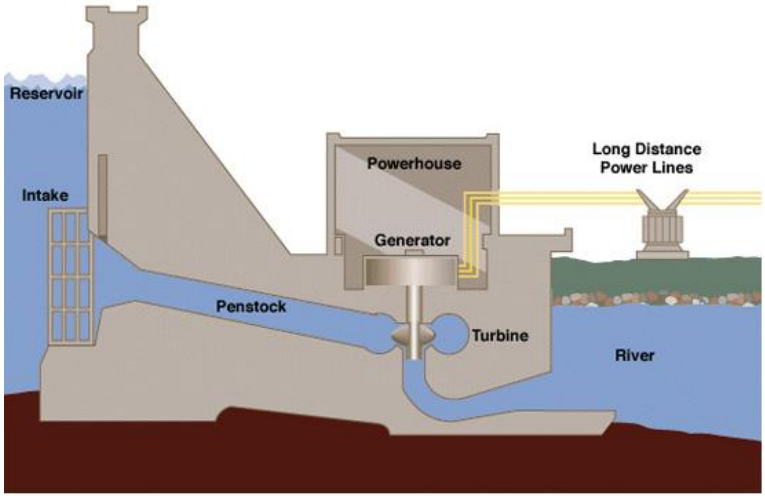

Figure 1.4: Schematic representation of a hydroelectric power plant[4].

1.1.2 Solar energy

Solar energy has been used for decades and is an ever evolving energy producing method. Solar energy arrays rely on a photovoltaic system where solar energy is converted to electrical energy. Photons from the sun excite electrons inside a layer of silicon, raising the electron energy and thus freeing them, while a potential barrier inside the voltaic cell deduces an electric potential which is then used to drive an electric current[5]. The main drawback to a photovoltaic system is the expensive installation and unit costs and also the low voltaic cell conversion rates varying from 12% to 29% for very expensive units[6]. Therefore, although this would be an adequate and clean energy source, significant research is still required to make this source commercially more accessible.

1.1.3 Wind turbines

Wind is another natural renewable source and can be relatively easily harnessed and converted to electrical power using wind turbines (Figure 1.5). The biggest drawback to wind turbines is that wind is unreliable and sporadic. The Institut de recherche sur l'hydrogène, Université du Québec in Canada has been working on ways to eliminate the unreliability by developing a system where they operate a 10kW wind turbine in conjunction with a 1 kW solar array and a 5 kW electrolyser system. The electrical energy from the wind turbine and solar array is sent to the electrolyser where it is

used to generate hydrogen. The hydrogen is then stored and can be reused later to generate electricity[7].

Figure 1.5: Wind turbines generating electricity[8].

1.1.4 Hydrogen-based energy sources

Hydrogen is considered a suitable energy carrier[9] in some energy production methods. It was shown that hydrogen-based energy sources are probably one of the most promising renewable and clean ways of producing energy[10]. Hydrogen can be obtained using either traditional sources (e.g. methane reforming) or novel approaches (e.g. electrolysis).

1.1.4.1 Methane reforming

Methane reforming (Reactions 1 + 2) is a well-established process for the catalysed production of hydrogen and syngas for use in, among others, the Fischer-Tropsch process[11]. An advantage of methane reforming is that it produces the highest H_2 yield compared to several other processes used to obtain hydrogen[12]. The major drawback to methane reforming, however, is the huge amount of greenhouse gases produced when the process is used on an industrial scale.

$$CH_4 + CO_2 \rightarrow 2CO + 2H_2 \quad (1)$$

$$CH_4 + H_2O \rightarrow CO + 3H_2 \quad (2)$$

$$CO + H_2O \rightarrow CO_2 + H_2 \quad (3)$$

1.1.4.2 Membrane-based electrolysis

There are numerous proton exchange membrane (PEM) based hydrogen production methods available (like the copper chloride cycle, sulphur iodine cycle and the hybrid sulphur cycle (HyS) to name a few[13,14,15,16]), of which water electrolysis is probably best known.

1.1.4.3 Water electrolysis

During water electrolysis, water is split into protons, electrons and oxygen using an electrical current and catalyst[17]. The protons migrate across a PEM and are reduced by the electrons for the water splitting delivered through an external circuit on the cathode side of the PEM to form hydrogen. Water electrolysis is a clean energy process with no by-products and it is reported that water electrolysis is probably one of the most promising alternative energy producing methods available[18]. The biggest drawback, however, is the high voltage (V= 1.2) required to split water into hydrogen and oxygen[18], which makes water electrolysis less attractive because it is not able to compete with fossil fuel-based energy production methods[9].

1.1.4.4 Hybrid sulphur cycle (HyS)

The HyS cycle is a two-step process where the first part entails the thermal decomposition of sulphuric acid (Reaction 3) and the second part entails an electrolysis step (Reaction 4). These types of cycles are generally referred to as thermo/electrochemical hybrid processes. The decomposition step occurs at approximately 850°C, producing SO_2, H_2O and O_2. After separating the SO_2 from the O_2 it is used to saturate H_2O, which is subsequently fed into a SO_2 depolarized electrolyser, where it is electrochemically oxidised to form sulphuric acid and protons at the anode (Reaction 5). The protons migrate through the PEM and are reduced to hydrogen at the cathode (Reaction 6) to complete the electrolysis step.

General reactions

Decomposition

$$H_2SO_4 \rightarrow SO_2 + H_2O + 1/2O_2 \quad (3)$$

Electrochemical

$$SO_2 + 2H_2O \rightarrow H_2SO_4 + H_2 \quad (4)$$

Specific electrochemical reactions

Anode: $SO_2 + 2H_2O \rightarrow H_2SO_4 + 2H^+ + 2e^-$ (5)

Cathode: $2H^+ + 2e^- \rightarrow H_2$ (6)

Overall reaction: $SO_2 + 2H_2O \rightarrow H_2SO_4 + H_2$

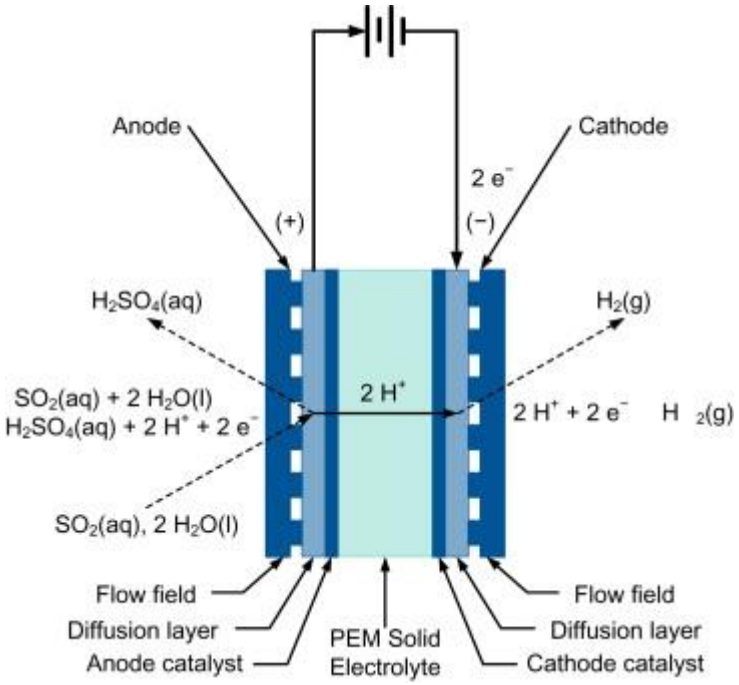

Figure 1.6: PEM SO_2 depolarized electrolyzer setup[19].

1.2 Problem statement

From the above background, it is clear that the development of successful PEMs is central to the success of PEM-based electrochemical and thermochemical techniques, thus membrane electrocatalyst assemblies (MEAs) or gas diffusion electrodes (GDEs) are vital to the operation and testing of proton exchange membranes (PEMs) using SO_2 depolarized electrolysis. To test a variety of different PEMs, MEA and GDE manufacturing capacity had to be established within the HyS research group at the North-West University (NWU) to reduce cost as well as fast tracking screen PEMs. In order to meet our specific lab-scale testing requirements for PEM testing, a variety of coating techniques were investigated in order to establish the most efficient technique. From an initial study, the two most promising techniques were the screen printing technique and the spraying technique, due to advantages of both techniques including the repeatability and consistency of coatings applied, especially for microporous layers (MPLs) with the screen printer and the versatility and ease of use of using the spraying technique.

1.3 Aim and objectives

In view of the problem statement, the aim of this study was to establish MEA and GDE manufacturing technology and capabilities at the North-West University by establishing screen printing and spraying techniques.

In order to attain this aim the objectives were to manufacture MEAs and GDEs with various Pt/C loadings, using the screen printing and spraying technique and comparing them to commercial MEAs and GDEs using various characterisation techniques.

1.4 Outline of thesis

Chapter 1: Introduction

In Chapter 1, different energy sources are outlined, focussing on renewable energy sources. Subsequently, the advantages and disadvantages of the different energy generation processes are elaborated on, finally focussing on the hybrid sulphur cycle (HyS). The importance of establishing MEA and GDE manufacturing capabilities at the NWU for characterisation of membranes using SO_2 depolarized electrolysis is discussed.

Chapter 2: Literature study

In Chapter 2, different thermochemical and electrochemical cycles are discussed in more detail, again focusing on the HyS cycle. Subsequently, the different components of a functioning electrolyser and the different membranes used in this study in order to meet the specific objectives are discussed. Furthermore, the difference between electrolysers and fuel cells is discussed before elaborating on different MEA and GDE manufacturing techniques, explaining their advantages and disadvantages.

Chapter 3: Experimental

In Chapter 3, the experimental procedures followed to meet the objectives of this study are explained. The catalyst ink preparation, micro porous layer coating, GDE manufacturing and MEA manufacturing are described. H_2 pump, SO_2 depolarized electrolysis, scanning electron microscopy (SEM), energy-dispersive spectroscopy (EDS) and sulphuric acid titration were used as evaluation techniques, all of which are explained in more detail in this chapter.

Chapter 4: Results and discussion

In Chapter 4, the results of the experimental work needed to meet the aim of this study are discussed. The PEMs evaluated in this chapter were Nafion® 117, sPSU-PBIOO, sFS-PBIOO as well as EC-TP1- 030 and EC-TP1-060 gas diffusion layers. These MEAs and GDEs were compared in this chapter to their commercial counterparts. The evaluation techniques described in Chapter 3 were applied on the MEAs and GDEs, resulting in SEM and EDS photos, VI-curves, acid concentration graphs, hydrogen production graphs and efficiency graphs, all of which are presented and discussed in detail in this chapter.

Chapter 5: Evaluation

In Chapter 5, a critical evaluation on the extent to which the aim of this study was met is presented. Recommendations are presented for possible future research in the field of MEA and GDE manufacturing for the characterisation of PEMs using SO_2 depolarized electrolysis.

Chapter 2: Literature study

2.1 Introduction

In line with the topic of this thesis, the focus of this chapter is on hydrogen production. There are numerous different production methods available which can be subdivided based on their sources as shown in Figure 2.1. These sources can be further subdivided into two main groups, i.e. renewable and non-renewable sources. Although there are numerous different renewable hydrogen production cycles available[20], only two types are relevant for this study: thermochemical cycles and water electrolysis.

After the discussion of different cycles, some of the important components of an electrolyser are discussed. An overview is given on some membranes being used for the making of membrane electrode catalyst assemblies (MEAs) before discussing the different techniques commonly used for the manufacturing of membrane electrode assemblies (MEAs) and gas diffusion electrodes (GDEs).

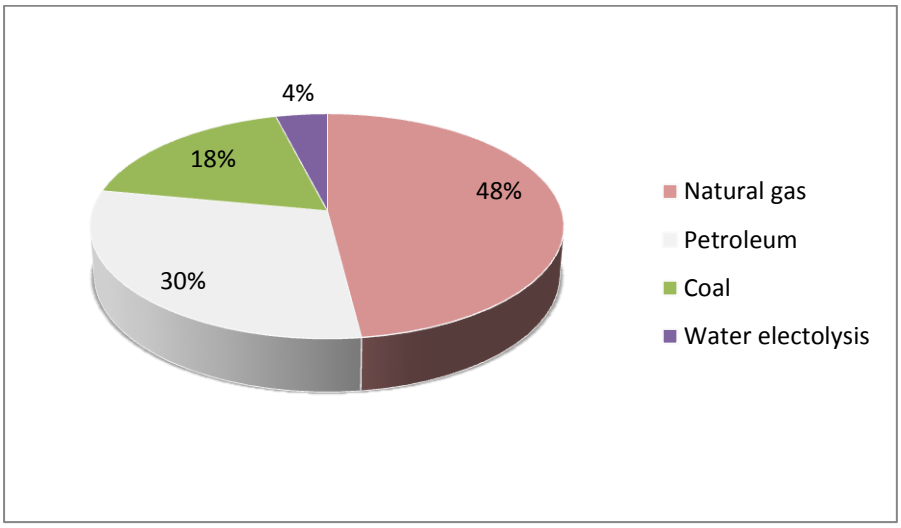

Figure 2.1: World Hydrogen Production[21]

2.2 Thermochemical and electrochemical cycles

2.2.1 The Copper chlorine cycle

The copper chlorine (Cu-Cl) cycle is one of the more promising thermochemical cycles currently available and is considered to be a promising alternative to steam-methane reforming for the generation of hydrogen[22]. There are several advantages to the copper chlorine cycle, for example the low working temperature (<550˚C)[20] required for production, which means that the cycle can be linked to multiple heat sources[23]. Lewis et al[24] gave a diagram illustrating the copper chlorine cycle as shown in Figure 2.2.

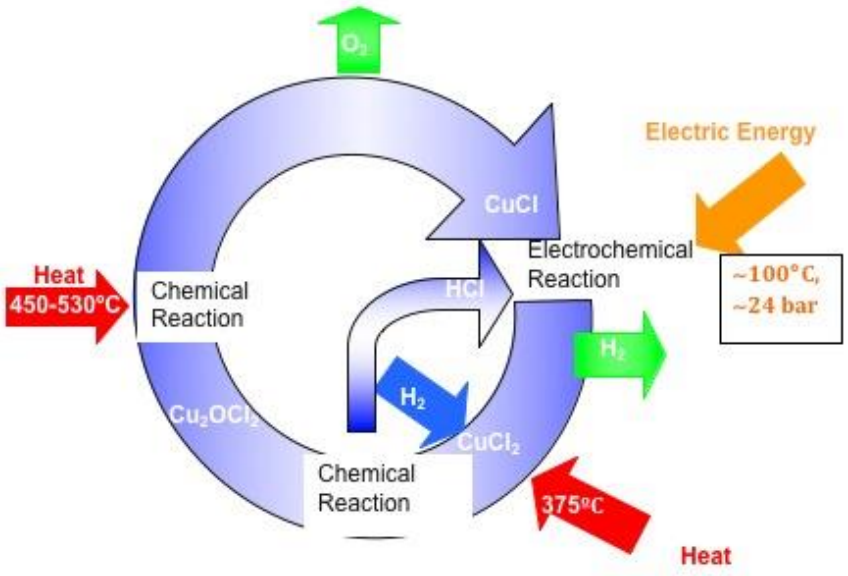

Figure 2.2: Schematic representation of the Cu-Cl cycle[24].

As seen in Table 2.1, the copper chloride process can be subdivided into several different steps according to the entailed chemical reactions. There are thermally driven reactions (1, 3, 4 and 5) and a subsequent electrochemically driven reaction (reaction 2).

Table 2.1: Reactions constituting the copper chlorine cycle[25]

Step	Reaction	Temperature, ˚C
1	$2Cu + 2HCl(g) \leftrightarrow 2CuCl + H_2(g)$	425 - 450
2	$4CuCl \leftrightarrow 2CuCl_2 + 2Cu$ (electrochemical)	25 - 80
3	$2CuCl_2(s) + H_2O(g) \leftrightarrow Cu_2OCl_2(s) + 2HCl(g)$	310 - 375
4	$Cu_2OCl_2(s) \leftrightarrow 2CuCl(l) + 1/2\ O_2(g)$	450 - 530
5	$2CuCl_2(s) + H_2O(g) \leftrightarrow 2CuCl(l) + 1/2\ O_2(g) + 2HCl$	550

However, in spite of the advantages of the cycle, possibly due to the limited research on the subject, there are still numerous problems with the cycle that have to be addressed, including the high energy cost of the electrochemical step[23].

2.2.2 The sulfur iodine cycle

The sulfur iodine (SI) cycle is another promising thermochemical cycle focusing on water splitting[26]. Originally researched by General Atomics (GA) [27], the reactions involved in the sulfur iodine cycle (Figure 2.3) are known as the Bunsen reactions and are presented in Table 2.2.

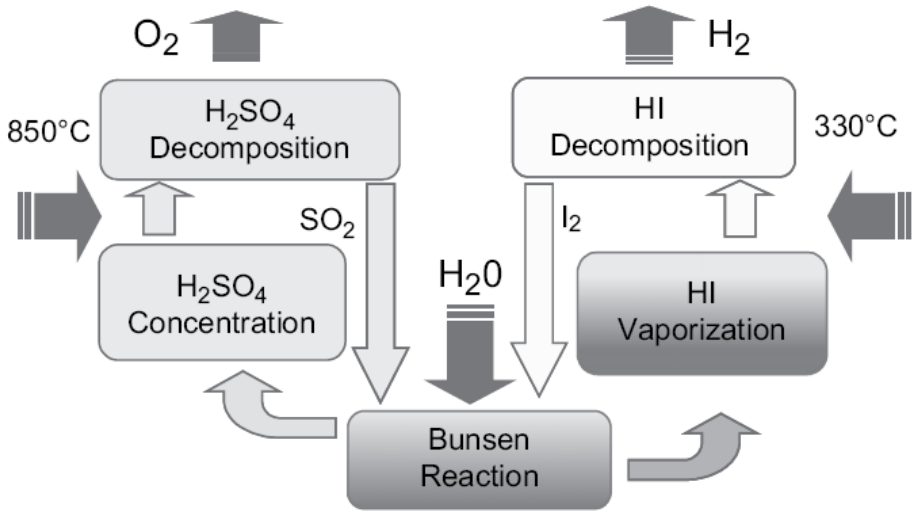

Figure 2.3: A general scheme of the sulfur iodine cycle[26].

During the Bunsen reaction iodine, water and sulfur dioxide react to form two liquid phases (step 1). The one phase consists mainly of sulfuric acid and the other consists mainly of hydroiodic acid. The sulfuric acid is then subsequently decomposed to sulfur dioxide, water and oxygen in step 2 of the process.

The oxygen can be refined, stored and sold, while the sulfur dioxide is reintroduced into the Bunsen reaction. The hydroiodic acid is decomposed to H_2 and I_2, of which the hydrogen is removed and stored while the iodine is then reintroduced back into the Bunsen reaction[28].

Table 2.2: Reactions comprising the Sulfur Iodine cycle.

Step	Reaction
1	$XI_{2(i)} + SO_{2(g)} + 2H_2O_{(l)} \rightarrow 2HI_{x(aq)} + H_2SO_{4(aq)}$
2	$H_2SO_{4(g)} \rightarrow H_2O_{(g)} + SO_{2(g)} + 1/2O_{2(g)}$
3	$2HI_{x(g)} \rightarrow H_{2(g)} + I_{2(g)}$

One of the major advantages of the sulfur iodine cycle is that it is a purely thermochemical cycle; this means that the cycle requires only thermal input and no electrical input like other leading cycles. Furthermore, when this cycle is combined with a renewable heat source, the cycle's attractiveness increases dramatically[26].

On the other hand, in order to drive the Bunsen reaction, an excess amount of water and iodine has to be added to the system. The water is introduced to keep the reaction exothermic, while the iodine facilitates the forming of the two acidic phases. The recovery of the water and iodine causes one of the cycle's major drawbacks as this reduces the thermal efficiency of the overall cycle. Much energy is lost in the recovery of these two substances[29]. A novel technique proposed by General Atomics uses phosphoric acid as a concentrating medium for the hydroiodic acid[30]. This, however, creates another separate cycle step in order to remove the phosphoric acid. Another problem of the cycle entails the high demand (on the materials) due to the corrosiveness caused by the chemicals involved[26]. While numerous other solutions for the optimization for the cycle have been proposed, no final solution to the optimization problem has been presented[26].

2.2.3 Solid polymer electrolyte (SPE) water electrolysis cycle

Water electrolysis is currently seen as the frontline hydrogen producing, membrane-based process in use in industry[31]. Water electrolysis is a process based on the splitting of water into oxygen and hydrogen using an SPE (solid polymer electrolyte), PEM (proton exchange membrane) and a catalyst[32].

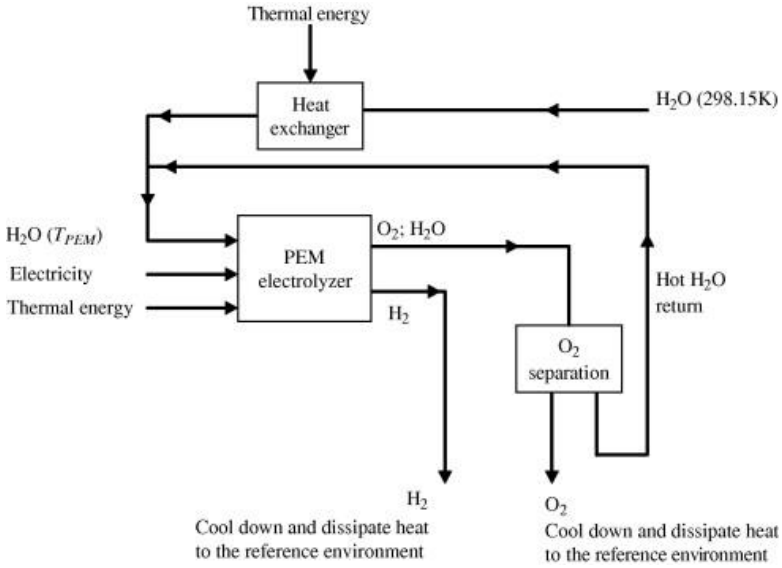

Figure 2.4: PEM electrolyser used for hydrogen production[33].

As illustrated in Figure 2.4, water is fed through a heat exchanger to equilibrate the water temperature with the proton exchange membrane (PEM) electrolyser's temperature. In the electrolyser, the water is split into oxygen and hydrogen. After the hydrogen has migrated through the PEM, it is cooled and collected. The oxygen water mixture remains on the anode side, from where the oxygen is then removed, cooled and collected[33].

The MEA (membrane electrode assembly) used in the PEM electrolyser differs from fuel cell MEAs in the sense that it often uses iridium as anodic catalyst and platinum as the cathodic catalyst[34], where in fuel cells both the anode and cathode catalysts usually consist of platinum[35].

Although water electrolysis using PEM electrolysers is a promising technology for the replacement of processes like hydrocarbon reforming[33], currently only 4% of the worldwide hydrogen is produced via this method[34]. One of the disadvantages of water electrolysis is that the process requires an electrical input of approximately 1.23 V at 25˚C[36], where other processes like the thermochemical Cu-Cl cycle only require an electrical input of 0.35 – 0.9V[37], or 1.7V[38] as in the case of the hybrid sulfur cycle

2.2.4 The hybrid sulfur cycle

The hybrid sulfur cycle (HyS) was developed by Westinghouse as an alternative, improved method for water electrolysis[39]. The HyS cycle forms part of the numerous sulfur-based, thermochemical hydrogen producing cycles currently available[40]. The advantage this cycle has over some other cycles is that it is not only a thermochemical, but also an electrochemical cycle, which means that the energy source for the functioning of the process is divided into a thermal and an electrical energy supply. As a result, higher efficiencies can be reached. Furthermore, the standard working potential for the HyS cycle is only 0.17 V, compared to the 1.23V for water electrolysis[38]. Also, when the thermal decomposition step of ± 850˚C of the cycle is compared to the direct thermal decomposition of water at (2500˚C), the HyS cycle requires less energy[41].

The Hybrid sulfur cycle (Figure 2.5) is a two-step cycle where the first step is the thermal decomposition of sulfuric acid (where sulfuric acid is decomposed at ± 850˚C to form water, oxygen and sulfur dioxide).

$$H_2SO_4 \rightarrow H_2O + ½\ O_2 + SO_2 \qquad (1)$$

The second step is the electrochemical step which occurs in an electrolyser.

$$\text{Anode: } SO_2 + 2H_2O \rightarrow H_2SO_4 + 2H^+ + 2e^- \qquad (2)$$

$$\text{Cathode: } 2H^+ + 2e^- \rightarrow H_2 \qquad (3)$$

On the anode side of the electrolyser, sulfur dioxide and water react to form sulfuric acid, two protons and two electrons. The protons travel over the membrane to the cathode side and recombine with the two electrons to form pure hydrogen[39].

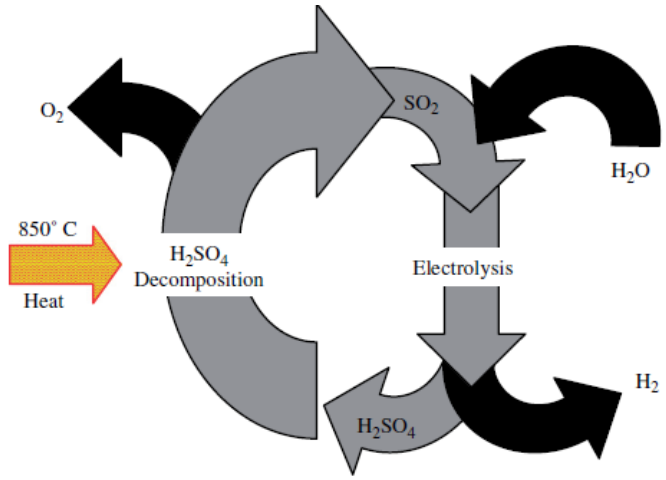

Figure 2.5: Schematic representation of the Hybrid sulfur cycle[41].

2.3 Electrolyser components

2.3.1 Bipolar plates and flow fields

Bipolar plates are responsible both for conducting the current and removing heat from the active area[42]. This means that the bipolar plates need to be corrosive-resistant, while having a high conductivity and a high thermal uptake. The bipolar plates can be machined from a variety of materials[42], including current conducting graphite, bipolar plates with thin noble metal coatings, graphite polymer composite, and sheet metal (e.g. stainless steel).

Flow fields make up a crucial part of the electrolyser[42], as they are responsible for directing the flow of the gases to the gas diffusion layer and the catalyst layer. Different designs of flow fields exist (Figure 2.6), each with their own advantages and disadvantages. From left to right are examples of serpentine, parallel, and fractal flow field designs. For each of these designs, different sub-designs can be found, as in the case of serpentine flow fields, where single, double, cyclic and symmetric designs can be found[43]. When considering fractal designs, a basic principle of design applies and an infinite amount of structures exist.

Serpentine flow fields have some major disadvantages, since gas flows in one continuous line, pressure drops can occur over the inlet to outlet, while the flow field can easily become clogged[44].

Figure 2.6: Different flow field designs[44]

The specific application dictates the type of material that can be used to manufacture the bipolar plates. In the case of the HyS cycle, which produces sulfuric acid, or when polybenzimidazole (PBI) membranes, which use phosphoric acid, are used, special care must be taken to prevent corrosion[45]. In the aforementioned cases, plates made from stainless steel cannot be used as the plates will corrode and the performance of the electrolyser will decrease.

2.3.2 Gas diffusion layer

The most important function of a gas diffusion layer (GDL) is the even distribution of gases from the flow fields throughout the catalyst layer[46]. They also play a role in providing a pathway for electrons to flow between the bipolar plates and the catalyst layer on the PEM[47]. The main factors that dictate the performance of a GDL include the thickness, porosity and permeability of the GDL, as well as its affinity for water[48]. These factors have to be considered carefully when choosing a GDL for a specific application. When considering PEM fuel cells (PEMFCs), where hydrogen is converted to H_2O, a hydrophobic GDL is required to prevent H_2O flooding. In the case of SO_2 electrolysis in the HyS process, where hydrogen is consumed, the GDL ideally needs to be hydrophilic. An example of the microstructure of a carbon paper GDL and a carbon cloth GDL can be seen in Figure 2.7 and Figure 2.8 respectively.

Instead of placing the catalyst on a PEM as is the case with an MEA, the catalyst can also be placed on the GDL, resulting in a gas diffusion electrode (GDE), where the GDL acts as a rigid support for catalyst deposition. Numerous properties of the GDE are determined by the GDL material chosen for GDE manufacturing. GDL material usually includes carbon cloth, carbon fibre paper[49] or carbon nanotubes[50].

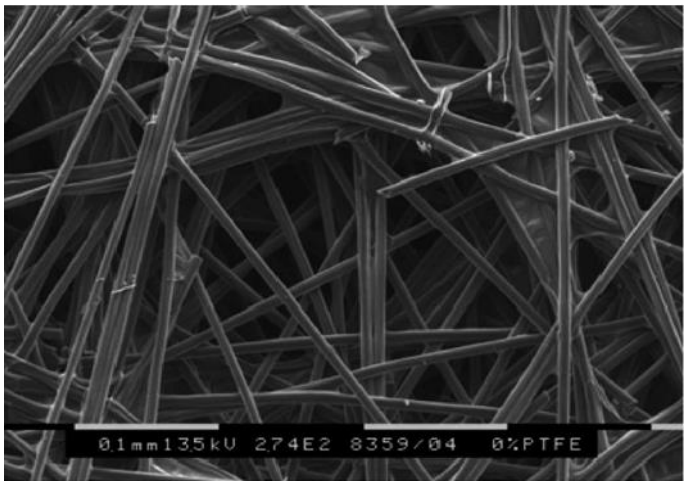

Figure 2.7: SEM micrograph of an untreated carbon paper[51].

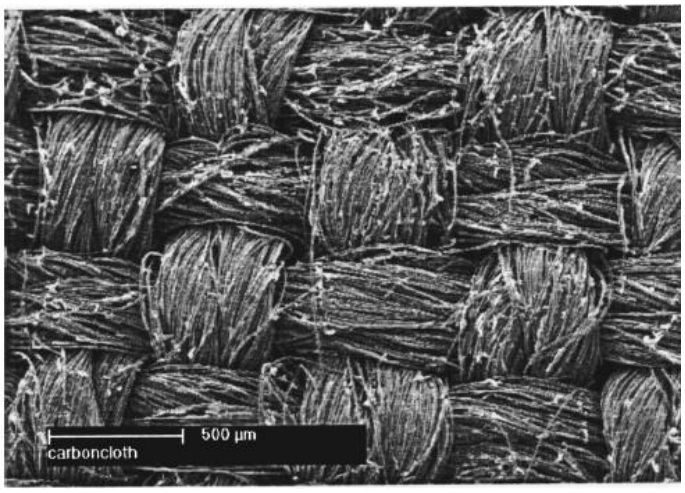

Figure 2.8: SEM micrograph of commercially available carbon cloth[52].

2.3.3 Catalyst and catalyst layer

Many different catalysts exist today and great advances have been made since the first catalysts were developed for fuel cells and electrolysers to be used as catalyst layers[53]. The catalyst is crucial for the working of any electrolyser or fuel cell as the catalyst layer serves as the electrochemical reaction site. This is also called the three phase interface[54]. The three phase interface is crucial because this is the area where the catalyst is in contact with both the membrane as well as the reaction gas and is the only electrochemical active area[55].

The catalysts usually used vary from single metal catalysts like Pt/C or Ir/C, binary catalysts like Pt – Ru/C or Pt – Mo/C, to tertiary catalysts like Pt – Ru – Mo/C[56]. As the catalysts contain mostly noble metals, they are very expensive. To reduce cost while maintaining efficiency, these noble metals are combined with carbon particles (Figure 2.9) to retain a large surface area whilst using the least amount of metal.

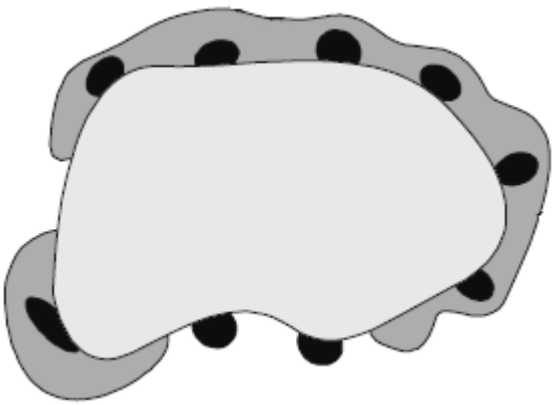

Figure 2.9: Particle made from carbon with smaller noble metal on the surface[54].

The catalyst is used in conjunction with a proton conducting membrane to form an MEA, or with a GDL to form a GDE, both of which will be discussed in detail later. Apart from the requirements for the expected catalytic activity of an effective catalyst layer, this layer must fulfil some additional requirements. Firstly, it needs to allow for protons to pass through the catalyst layer and secondly it needs to be able to conduct electrons.

The first property is usually incorporated in the catalyst layer (CL) in the form of a binder which serves as a proton conductor. For fuel cells this binder is often perfluorosulfonate or Nafion®-based, which will possibly be suitable for electrolysers as well. The second requirement, i.e. the conducting of electrons, is achieved by using carbon particles to which the noble metals are attached[54].

One of the most important factors determining the effectiveness of the CL is related to the amount of catalyst deposited on the PEM or GDL. The amount of deposited catalyst can be measured by determining the actual amount of platinum per cm^2 used vs. the loading applied (Table 2.3). The %Pt utilization can be calculated by dividing the theoretical active area of the catalyst by the electrochemical active surface area (ESA). The theoretical active surface area can be determined using the following equation:

$$A_{theo} = 6\frac{m}{\rho d} \quad (1)$$

Where m is the mass of the platinum in the Pt/C (g), ρ is the density of the platinum bulk ($g.cm^{-3}$) and d is the average diameter of the platinum particles (cm)[57].

Table 2.3: Amount of platinum used versus amount of platinum loading[57]

Pt loading, mg/cm^2	Electrochemical active area, ESA/cm^2	Theoretical active area, A_{theo}/cm^2
0.4	301.6	495.8
0.8	557.9	979.3
1.3	885.5	1595.9
2.34	1182.8	2882.4
4.02	1472.2	4943.4

As previously discussed, the catalyst is very expensive due to the use of noble metals. It is therefore important to determine the upper and lower limit in terms of the maximum and minimum amount of platinum used.

It is clear from Figure 2.10[58] that the over potential increases dramatically at loadings below approximately 1 mg Pt/cm^3, as the distance between the Pt/C particles grows too large (Figure 2.11), hindering the electrons from moving between Pt/C particles.

However, above a catalyst loading of approximately 0.2 mg/cm^2, according to Figure 2.10, little is gained by adding more catalyst. Above 0.2 mg/cm^2 the Pt/C particles are close enough to allow the flow of electrons between them with ease. Another factor that can contribute to a lower efficiency is seen in Figure 2.12, where too much catalyst is employed, resulting in a mass transfer limitation that exists because of the thicker CL and the longer distance the protons have to travel.

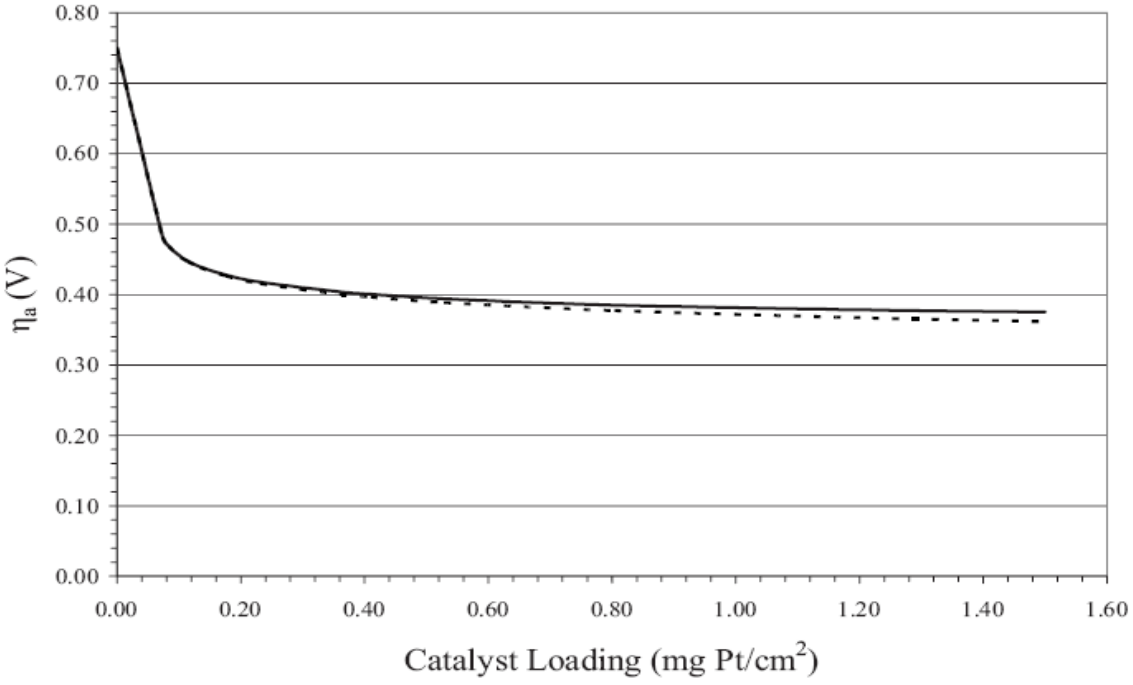

Figure 2.10: The anodic over potential as a function of the catalyst loading as a weak or strong function of loading[58].

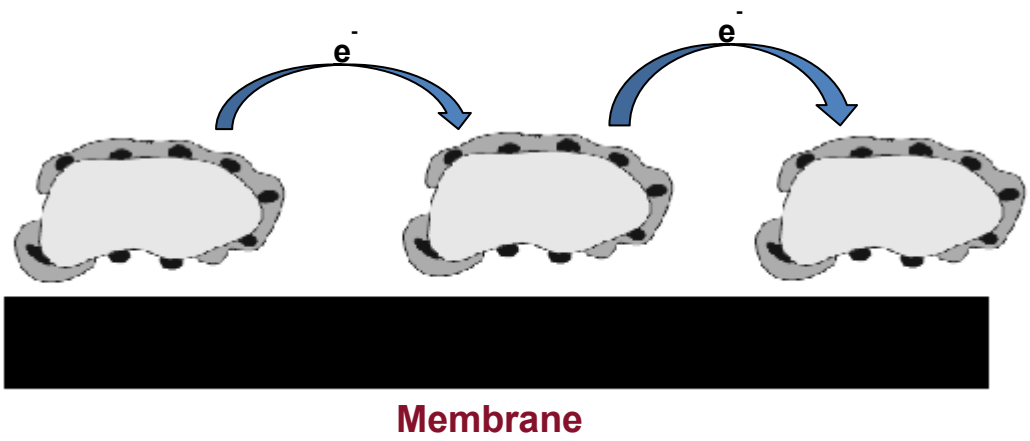

Fig 2.11: Distance between catalysts particles is too large, causing a large over potential[58].

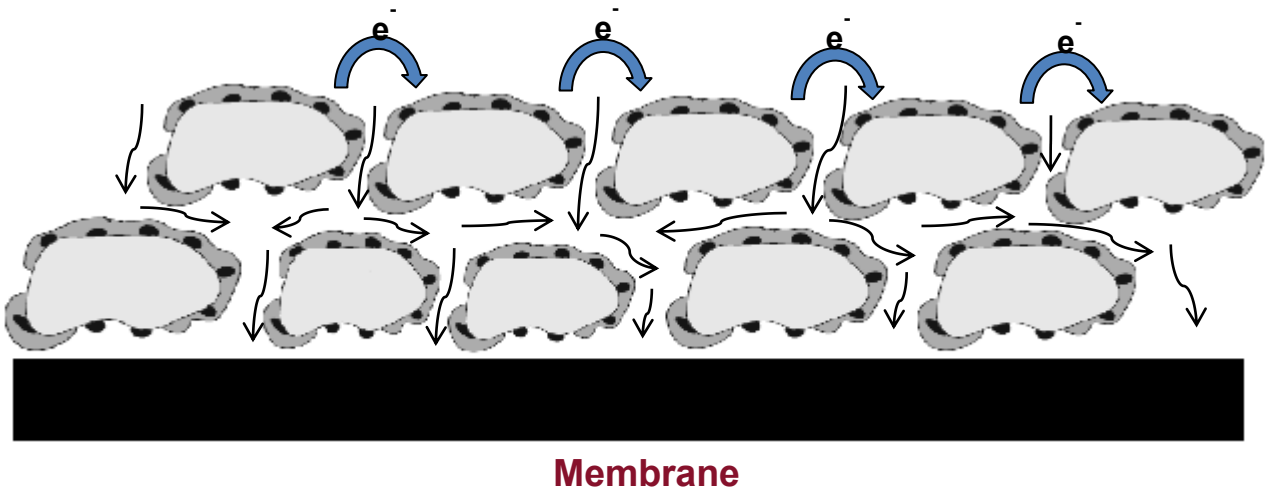

Fig 2.12: Too much catalyst loading and the increased mass transfer limitation caused by the thicker CL[58].

2.3.4 Proton exchange membranes

2.3.4.1 Nafion® membranes

The most proton exchange membranes (PEM) used today are based on perfluorosulfonic acid-based polymers like Nafion®[59]. Nafion® was first developed and is produced to this day by E. I. DuPont. Nafion® is synthesized by a copolymerization reaction of a perfluorinated vinyl ether co-monomer with tetrafluoroethylene. This results in the following polymer structure shown in Figure 2.13[60]:

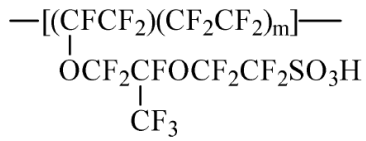

Figure 2.13: Nafion® polymer structure.

The wide use of Nafion® is due to its intrinsic chemical and thermal stability[61] as well as its low ionic resistance[62]. One of Nafion's® few drawbacks is that it is not stable at temperatures above 90˚C and hence performs poorly[63]. This is due to the evaporation of water at ambient pressure and thus the dehydration of the membrane which leads to diminished proton conductivity[61], resulting in a decreased performance of the PEM. The benchmark Nafion® membrane is Nafion®N117, where 117 refers to an equivalent weight of 1100 g/mol and a membrane thickness of 0.007 inches[60].

Hydrated Nafion® uses two main mechanisms for the transportation of protons[64]; firstly the vehicular transport mechanism and secondly the Grotthuss mechanism. The principle on which both of these mechanisms operate is that they subsequently lack a stable electron shell and thus have strong interactions with their surrounding environments[65]. In the case of highly hydrated Nafion® membranes, vehicular transport is the main mechanism found. In the vehicular transport mechanism, protons diffuse through the membrane in the form of H_3O^+ (Figure 2.14). When considering less hydrated membranes, the mode of transport swings to the Grotthuss mechanism, because the dependence on the mobility of the $-SO_3^-$ groups and their part in the conducting process grows larger[66]. The Grotthuss mechanism involves the diffusion of protons via the reorganization of the polymer structure[67]. The reorganization entails the forming and breaking of hydrogen bonds in the water and the strong electrostatic attraction of the $-SO_3^-$ groups[68] as shown in Figure 2.15.

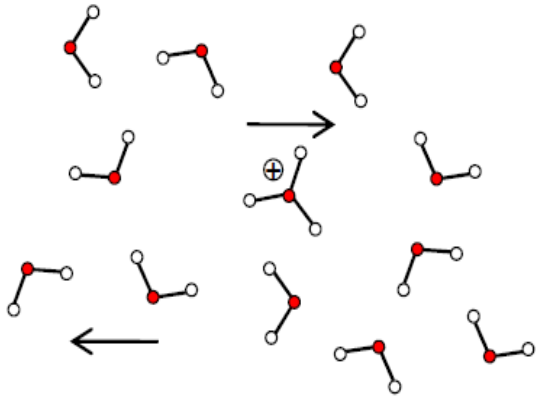

Figure 2.14: Vehicular transport mechanism[67].

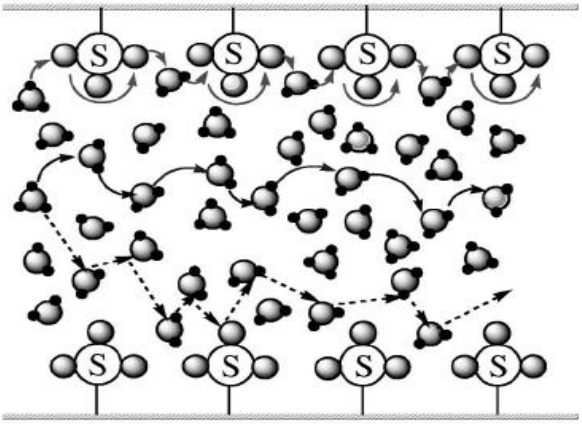

Figure 2.15: Grotthuss mechanism[68].

2.3.4.2 PBI membranes

Since Nafion® only functions optimally at high hydration levels and thus temperatures below approximately 80°C[69], an emphasis has been put on the development of PEMs that function at temperatures above 100˚C[70].

One of the promising membrane materials is based on polybenzimidazole polymers (PBI). The main advantage of PBI is that it does not require water for proton transport and thus can operate at higher temperatures than Nafion®. PBI membranes function on the principle that, when doped with an amphoteric acid like phosphoric acid, the acid acts both as a proton donor and proton acceptor. This means that protons can be readily transferred via hydrogen bond forming and breaking (Grotthuss mechanism)[69]. While the general reference to PBI implies a group of aromatic heterocyclic polymers containing benzimidazole units, the trademarked PBI in fuel applications refers to the structure presented in Figure: 2.16.

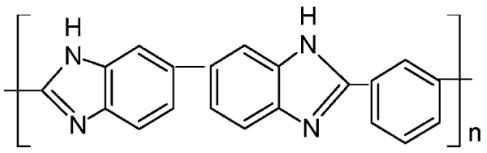

Figure 2.16: Poly 2, 2'-m-(phenylene)-5, 5'-bibenzimidazole, Celazole®[69].

There are many possible synthesis pathways for PBI and a few are listed below, for example using tetra-aminobiphenyl (TAB) and diphenyl isophthalate as monomers, PBI can be synthesized in the following two step reaction[71]:

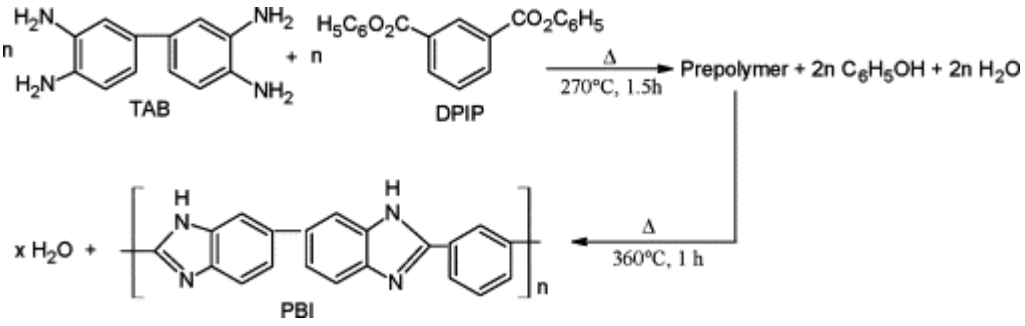

PBI can also be synthesized using the following one step reaction using TAB and isophthalic acid[72]:

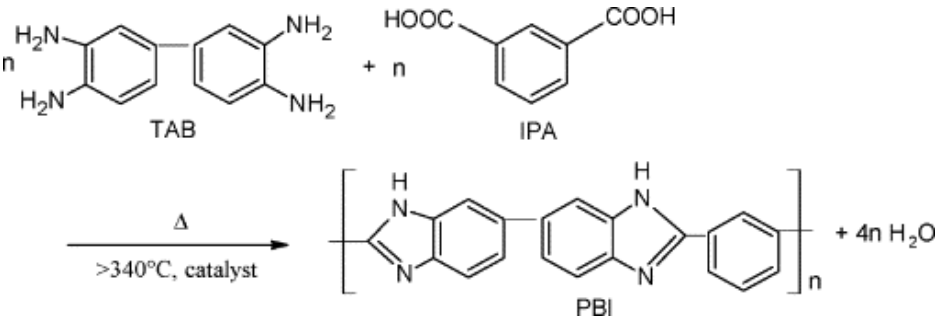

2.3.4.3 Poly (ether ether ketone) with cardo group (PEEK – WC) membranes

Another type of membrane that has arisen to meet the need of high temperature application PEMs is PEEK - WC PEMs[72]. The sulfonated poly (ether ether ketone) with cardo group (S - PEEK – WC) membrane structure is amorphous and exhibits excellent resistance to mechanical and chemical degradation[73]. It is soluble in organic solvents which is an advantage above most other PEEK only materials[74]. S – PEEK – WC is generally synthesized by reacting PEEK – WC with 98% sulfuric acid. However, substitution of 0.8 sulfonic molecules per repeating unit is approximately the maximum, since a higher degree of substitution leads to the degradation of the polymeric chain[74]. More recently chlorosulfuric acid has been used to sulfonate the PEEK – WC, resulting in a polymer with a higher sulfonic substitution without degradation [74]. A general structure is shown in Figure 2.17.

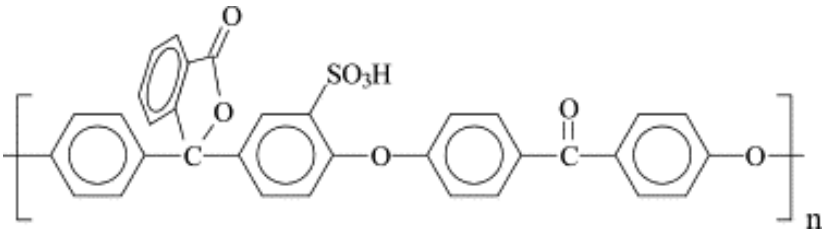

Figure 2.17: Structure of sulfonated PEEK – WC polymer

2.3.5 MEAs and GDEs

The MEA and GDE represent two different approaches that both result in a PEM/ catalyst/GDL assembly as illustrated in Figure 2.18. The only difference is that in MEAs, the catalyst is deposited on the PEM first and the GDL is hot pressed together after the catalyst PEM assembly has been manufactured, and in the case of the GDE, the catalyst is deposited on the GDL first and the PEM is added afterwards by hot pressing. These assemblies are used in both fuel cells as well as electrolysers.

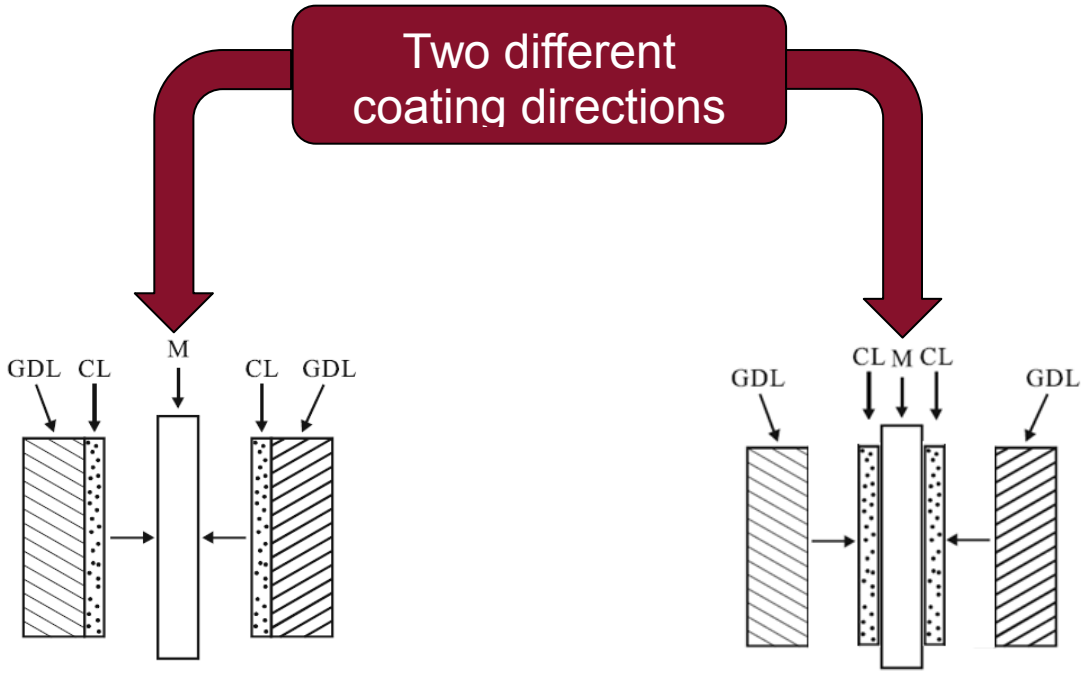

Figure 2.18: The two different coating directions of the PEM, electrocatalyst (CL) and GDE assembly.

2.3.6 PEM Fuel cells and PEM Electrolysers

2.3.6.1 PEM Fuel cells

The function of the MEA, in the case of fuel cells, is to convert H_2 at the anode to protons and electrons. The protons are transported over the PEM and reassembled at the cathode in the

presence of oxygen to form H_2O. The electrons travel in an external circuit, because the PEM is electrically insulating, generating electrical current which can then be used as a power source (Figure 2.19).

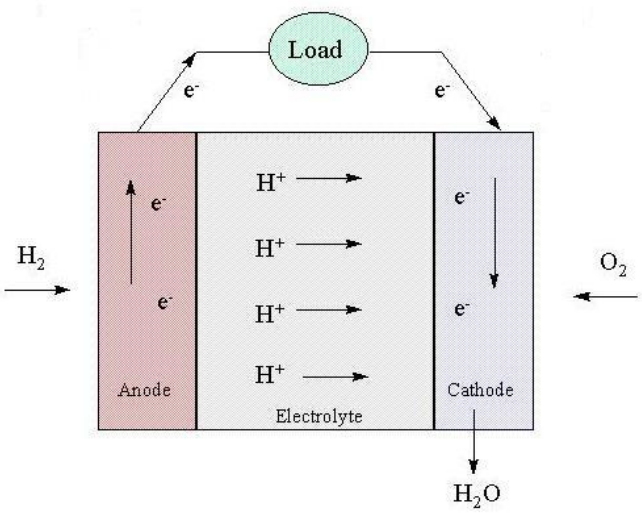

Figure 2.19: Typical working of a proton exchange membrane fuel cell (PEMFC)[75].

2.3.6.2 PEM Electrolysers

The function that a MEA plays in an electrolyser is to convert H_2O at the anode into two protons, oxygen and two electrons. The protons migrate over the PEM while the electrons travel via an external circuit and recombine with the protons at the cathode to form H_2. The oxygen is recovered from the anode side of the electrolyser (Figure 2.20).

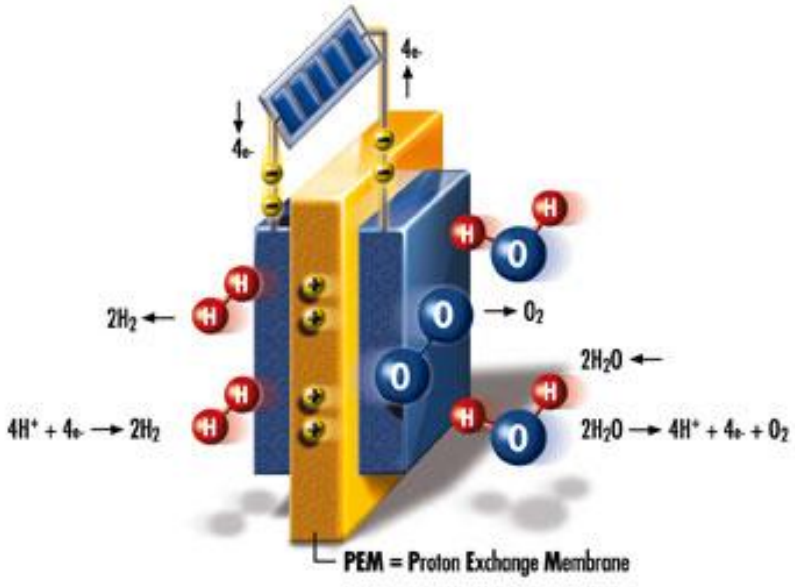

Figure 2.20: Typical working of PEM electrolyser[4].

2.4 MEA manufacturing techniques

2.4.1 Decal method

The decal method, which is a technique where a paintbrush is used to transfer ink onto a Teflon sheet and decaled onto a membrane or GDL, is a simple method[35] compared to some of the other methods available. However, it is less accurate than other methods and thus delivers MEAs that are less refined and less repeatable[76]. The decal method has its origins in the early years of MEA manufacturing and is explained comprehensively by Wilson et al[35] as illustrated in Figure 2.21.

The procedure is as follows:

A) A thin square Teflon sheet (blank) is used. It is supple and the size of the required catalytically active area. It serves as a base on which the painting of the ink will take place. It is non-stick and makes it perfect for the fabrication process.
B) The ink (prepared forehand) is painted onto the Teflon blank using a fine brush.
C) The coated Teflon square is then baked in a force convection oven at around 135˚C.
D) The baked, ink-coated Teflon square is then flipped over onto a membrane or GDL with the ink facing the membrane. It is then hot pressed onto the membrane.
E) The Teflon blank is then slowly and carefully peeled off to reveal the electro catalyst membrane assembly.

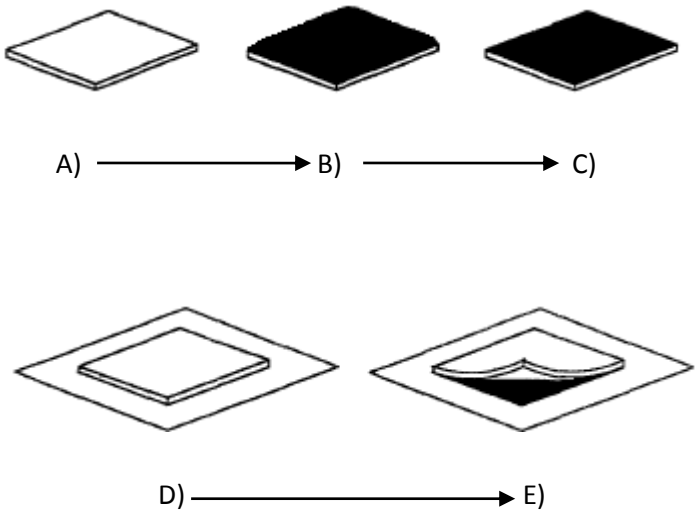

Figure 2.21: The primary steps in fabricating an MEA using the decal method[35]:

2.4.2 Direct spraying method

The spraying technique which is a fast process is one of the most popular techniques available because the ink can be applied (onto the membrane or GDL) in very precise amounts[76]. The technique is relatively simple (Figure 2.22), but care has to be taken to dry the membrane beforehand because the membrane is constantly weighed during coating in order to determine the amount of catalyst applied on the membrane.

When using the spraying technique, the membrane being coated has to be clamped inside a frame due to the constant drying and re-wetting. If the membrane is not clamped inside a frame it will shrink and distort because of the moisture inside the ink. To simplify the spraying process; the inner dimensions and shape of the frame are chosen to be the same as the catalytically active area. The ink viscosity can easily be changed to suit the spray density.

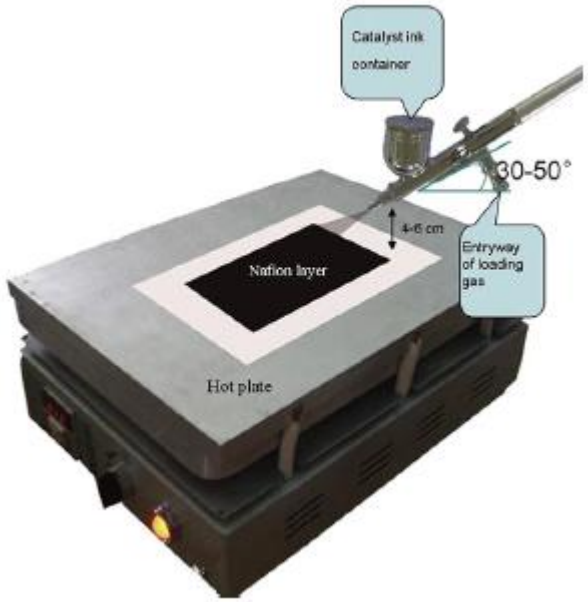

Figure 2.22: A typical spraying setup[76]

2.4.3 Doctor blade method

The doctor blade method is a method that is adapted more recently to MEA manufacturing. It is an efficient method to obtain high precision loadings on MEAs. Another advantage of the technique is that it is suitable for the mass production of MEAs[77]. The method is simple. It uses a hopper which contains catalyst ink, and a reel of wetted membrane is fed through the bottom of the hopper. When exiting the hopper, a doctor blade limits the amount of ink applied onto the membrane (Figure 2.23). The height of the doctor blade can easily be adjusted and thus controls the amount of ink applied on the membrane.

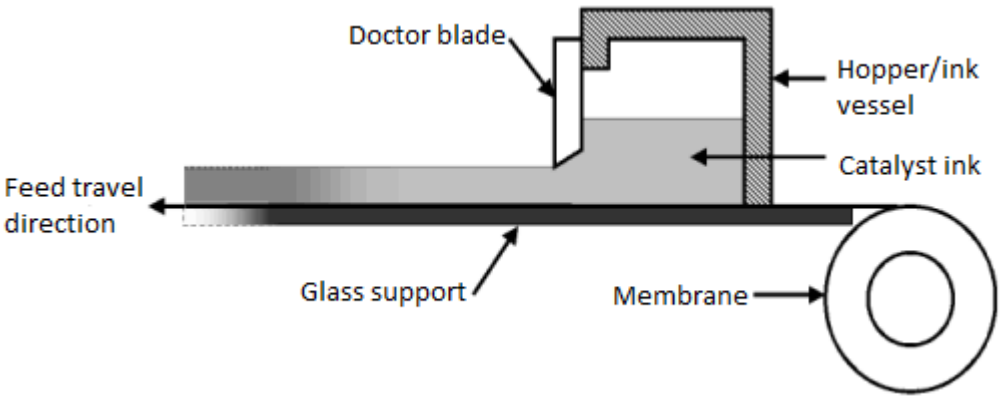

Figure 2.23: Typical automated doctor blade setup.

2.4.4 Screen printing method:

The screen printing technique is a well-known and effective alternative technique[78]. While it is not suitable for mass production, it is a reliable and effective technique to produce high quality MEAs in the laboratory environment as shown by Kim et al[79].

The setup consists of a squeegee head, screen and a vacuum table. The head and vacuum table are part of the screen printer, while the screen is detachable. The screen is attached between the head and the vacuum table. The role of the head is to spread ink over the screen forcing the ink through the screen in an area on the screen that has been designed so that it only allows ink to be released over an area equal to the required area (if a 5 cm^2 active area of catalyst is desired, the screen is used that only allows ink to go through that 5 cm^2 (green area on Figure2.24)). Below the screen is a vacuum table which holds the membrane in place while printing. The setup can be either manually or pneumatically operated.

Figure 2.24 is a representation of a typical screen used in screen printing, the area in the middle is the only area on the screen where the ink can pass through the screen. The outer dark area is the aluminium frame over which the screen is stretched.

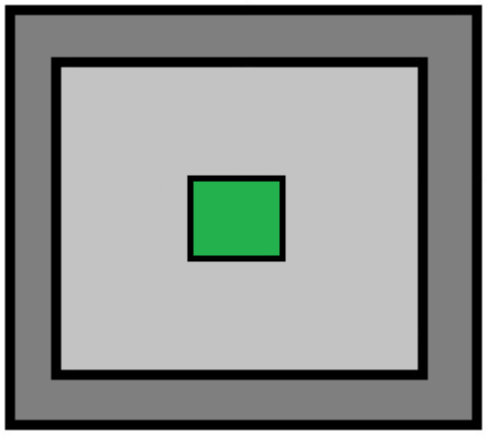

Figure 2.24: Typical screen used for screen printing.

2.5 Conclusion

The world energy consumption is constantly increasing, resulting in an increased demand on the finite resources available. Furthermore, current energy sources are predominantly based on fossil fuels, which are all carbon emitting energy sources. With global warming becoming an international focus point, alternative energy sources (green energy) are receiving significant attention. Most of these alternative energy sources are attractive because they produce little or no carbon emissions, resulting in low or no impact on the environment. The thermochemical and electrochemical cycles discussed in this chapter are some of the alternative sources potentially contributing to the demand of global green energy. The technology is, however, not yet on par with the hydrogen production capabilities of the fossil fuel production processes because of the new and unique challenges it faces.

Over the last few decades, advances in the electrolyser industry have brought about a viable and sustainable technology for the alternative production of hydrogen. The various electrolyser components are discussed in this chapter together with the problems they face. All the discussed components are vital to the working of the electrolyser, each one contributing to its efficiency.

MEA manufacturing techniques are constantly developing and changing with better and newer techniques being published regularly. The MEA development techniques discussed in this chapter are a few of the most popular techniques currently available. They each offer their own advantages and disadvantages. Usually the manufacturing technique is chosen based on its required application, for example for mass scale production, the doctor blade technique will probably be a suitable candidate. If small scale laboratory production is the aim, techniques like spraying or screen printing are two very suitable techniques due to the attained accuracies.

Chapter 3: Experimental

3.1 Introduction

This chapter describes the experimental procedures that were followed to meet the objectives of this study, i.e. the founding of MEA and GDE manufacturing capabilities at the NWU to form part of the PEM characterization techniques to be used in SO_2 depolarised electrolysis. Figure 3.1 shows the outlay of the experimental protocol followed. The catalyst ink preparation is discussed in Section 3.2, the GDE manufacturing in Section 3.3, MEA manufacturing in Section 3.4 and the characterization of the manufactured GDEs and MEAs in Section 3.5.

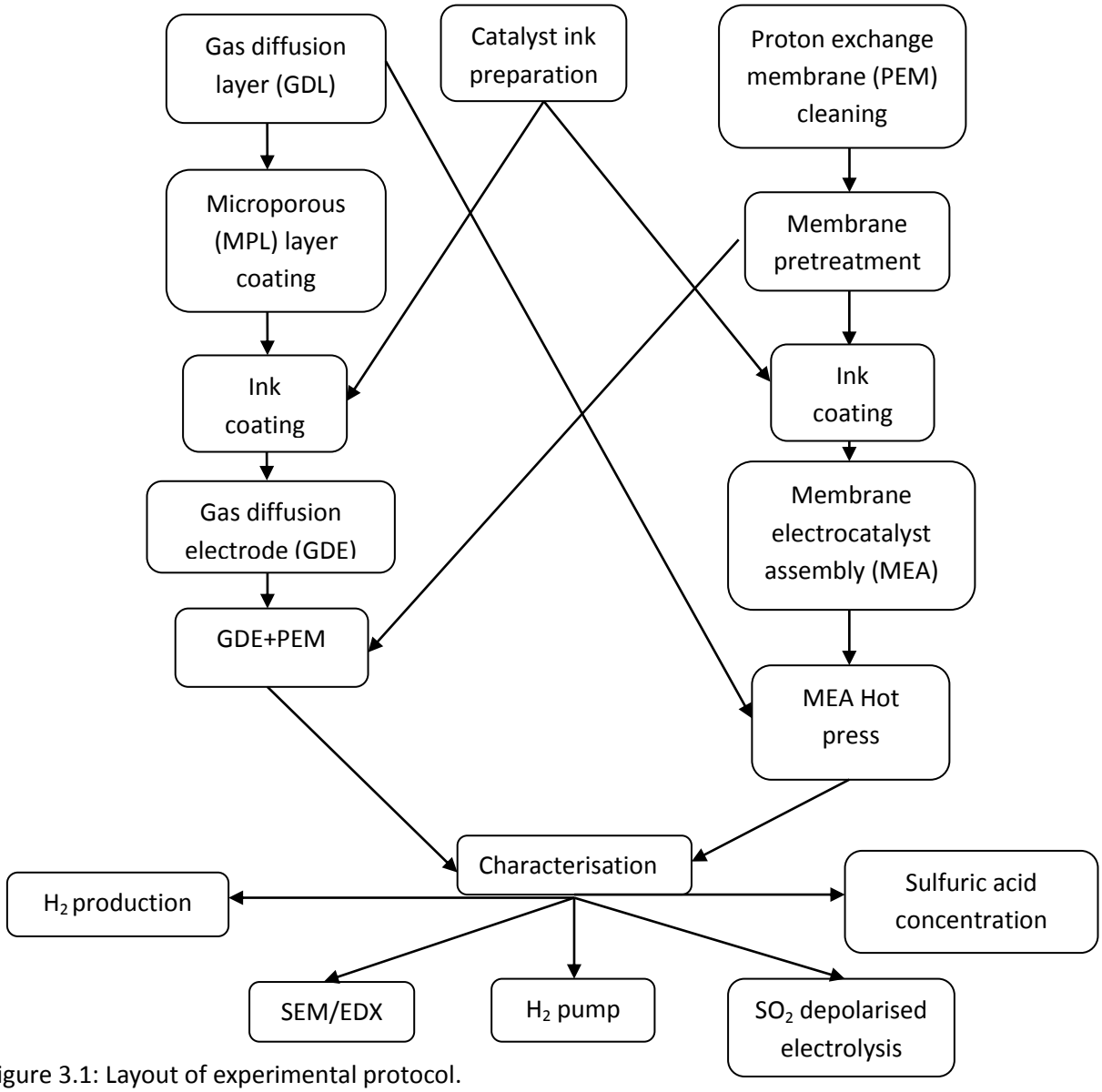

Figure 3.1: Layout of experimental protocol.

Both GDEs and MEAs were made in-house and compared to commercial GDEs and MEAs, respectively. Most of the study was done on Nafion® 117 for benchmarking purposes. The membrane results were subsequently compared to sPSU-PBIOO and sFS-PBIOO membranes. Table 1 outlines the GDEs and MEAs evaluated. Experimental runs 1-4 evaluated the in-house-built GDEs. Runs 1-3 tested the GDEs with a GDL thickness of 0.1mm and run 4 tested the in-house-built GDE with a GDL thickness of 0.19 mm. Runs 1-4 all had 6 MPLs and runs 1-3 had 0.3, 0.6 and 0.9 mg Pt/cm^2 CL loadings, respectively. Run 4's CL loading was determined from the performance of runs 1-3's H_2 pump testing results (Section 2.5.2.3) and was compared to runs 5 & 6, which were the commercial GDEs with a GDL thickness of 0.19 mm. The GDE in run 4 also had a GDL thickness of 0.19mm. Nafion was used as a PEM for all GDE testing and none of the GDEs were hot pressed. Runs 7-9 tested the in-house-built Nafion®-based MEAs with catalyst loadings of 0.3, 0.6 and 0.9 mg Pt/cm^2, respectively and were compared to run 10, which evaluated the commercial MEA with a catalyst loading of 0.3 mg Pt/cm^2. Runs 11 -13 tested the in-house-built sPSU-PBIOO-based MEAs with catalyst loadings of 0.3, 0.6 and 0.9 mg Pt/cm^2, respectively and were compared to run 14, which tested the MEA obtained from ZSW. Run 15 evaluated the in-house-built sFS-PBIOO MEA and was compared to the sPSU-PBIOO MEAs. All MEAs used GDLs with a thickness of 0.1 mm and were hot pressed, except for the MEA obtained from ZSW, which was not hot pressed.

Table 3.1: GDE's and MEA's evaluated using H_2 pump and SO_2 depolarized electrolysis

Experimental run	GDL (Toray™ carbon paper)	MPL (layers)	GDE Loading (mg Pt/cm^2)	PEM	MEA Loading (mg Pt/cm^2)	MEA (hot press)
1	EC-TP1-030	6	0.3	Nafion® 117	-	no
2	EC-TP1-030	6	0.6	Nafion® 117	-	no
3	EC-TP1-030	6	0.9	Nafion® 117	-	no
4	EC-TP1-**060**	6	To be determined(a)	Nafion® 117	-	no
5	EC-TP1-**060**	Not known	0.3(b)	Nafion® 117	-	no
6	EC-TP1-**060**	Not known	0.6(b)	Nafion® 117	-	no
7	EC-TP1-030	-	-	Nafion® 117	0.3	yes
8	EC-TP1-030	-	-	Nafion® 117	0.6	yes
9	EC-TP1-030	-	-	Nafion® 117	0.9	yes
10	EC-TP1-030	-	-	Nafion® 117	0.3 (c)	yes
11	EC-TP1-030	-	-	sPSU-PBIOO	0.3	yes
12	EC-TP1-030	-	-	sPSU-PBIOO	0.6	yes
13	EC-TP1-030	-	-	sPSU-PBIOO	0.9	yes
14	EC-TP1-030	-	-	sPSU-PBIOO	0.6 (d)	no
15	EC-TP1-030			sFS-PBIOO	(e)	yes

(a) Loading will be chosen according to the results of runs 1-3.
(b) GDEs obtained from *Giner*, Inc. and *Giner* Electrochemical Systems, LLC (GES).
(c) MEA obtained from Ion Power, Inc.
(d) sPSU-PBIOO MEA obtained from ZSW.
(e) Loading will be chosen according to the results of runs 11-13.

3.2 Catalyst ink preparation

The ink, which was prepared according to the protocol presented in Figure 3.2, was used both for MEA and GDE manufacturing (this protocol was adapted by Prof V. K. Ramani from Illinois Institute of Technology, USA - personal communication). Catalyst (500mg) (platinum, nominally 20% on carbon black, Alfa Aesar, A Johnson Matthey Company) was mixed with deionized (DI) water (2g) and 20 wt% Nafion® solution (2ml) (D2021 alcohol-based, Ion Power Inc). This mixture (1) was stirred for 10 min using a magnetic stirrer (BOECO) and then sonicated for 2 hours in an ultrasonic bath (Eumax, UD200SH-6L).

To mixture 1, 4g of ethylene glycol (Merck (PTY) LTD) and 12g isopropanol (Merck (PTY) LTD) were added. This mixture (2) was again stirred for 1 hour using a magnetic stirrer and subsequently sonicated for 2 hours. This second step was repeated up to three times if homogeneity had not been reached after the first cycle. Homogeneity was achieved when the ink was entirely liquid and no dry or un-dissolved particles remained. Ink was stored on a magnetic stirrer to ensure that homogeneity was maintained. Ink was used within three days after manufacturing.

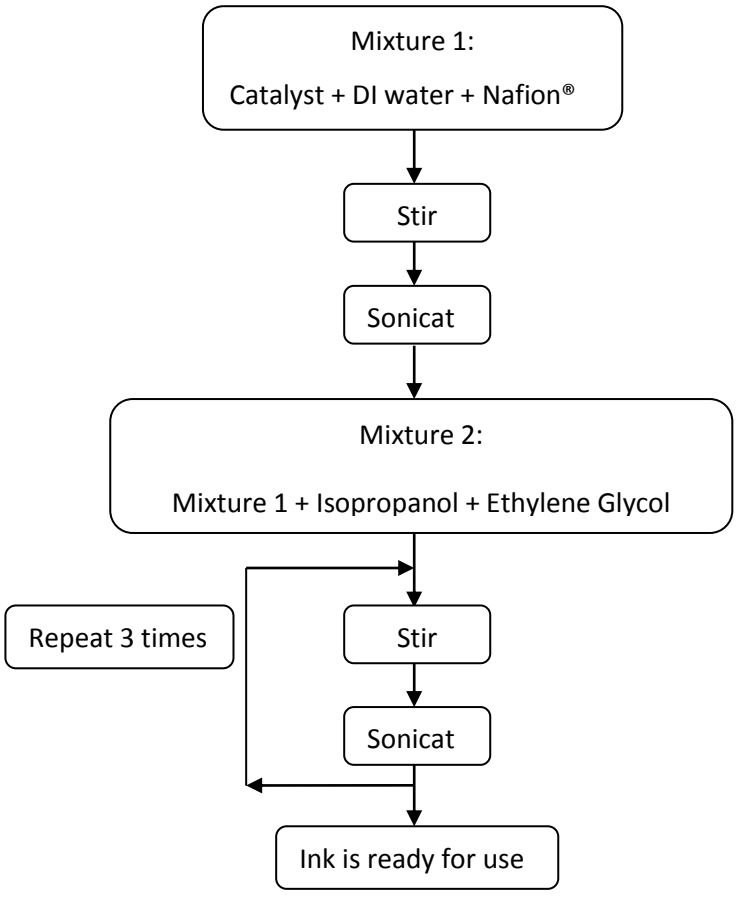

Figure 3.2: Flow diagram illustrating the method used for the preparation of the catalyst ink.

3.3 GDE manufacturing

Before coating the GDLs with the catalyst ink prepared in Section 3.2, an initial microporous layer was applied to them, both the anodic and cathodic GDL, to reduce their porosity and surface roughness.

3.3.1 Microporous layer (MPL) coating of GDLs

500mg Carbon powder (Vulcan XC-72R, Carbot Co.) was mixed with 12g isopropanol, 4g ethylene glycol and 4g DI water. Using a magnetic stirrer, the mixture was stirred for 10 minutes, sonicated for 2 hours and then stirred again for 1 hour with a magnetic stirrer. This ink was then applied to the anode GDL (25 cm^2 EC-TP1-030 Toray™ carbon paper (untreated) supplied by Electrochem, Inc) using a screen printer (Model F1-20, Systematic Automation INC). The GDL (25cm^2) was placed under a screen (KEIP BROS. TRADING CO. PTY LTD) with a 25 cm^2 open printing area. The air pressure was set at 8bar on the vacuum table (Model 80-VCTB-000C, Systematic Automation INC). The GDL was placed in the centre of the screen printing area to ensure that the loading was deposited in the centre of the GDL. The GDL was then coated with the ink by applying 2ml of ink onto the screen just above the open printing area before initiating the screen printing cycle. One screen printing cycle was started by pressing the footswitch of the screen printer. Air pressure forced the lift cylinder to lower the carriage assembly. Once the carriage assembly was at its lowest point, the print flood switch was released manually. The print stroke occurred and the squeegee travelled across the screen forcing the ink through the screen. After the squeegee head had reached its pre-adjusted stroke limit, a solenoid was automatically activated and the printer carriage automatically lifted to its original position, which completed one printing cycle. This cycle was repeated 6 times to ensure the formation of a defect free microporous layer. The coated GDL was then air dried at 120˚C for 1 hour in an evaporation oven (Binder, FP series) to remove all remaining solvent. The same process was used for the microporous layer coating of the cathodic GDL (25 cm^2 EC-TP1-030 Toray™ carbon paper (Teflon™ treated), Electrochem). Six MPL coatings were also applied to the anodic and cathodic EC-TP1-060 Toray™ carbon paper GDLs used in runs 4-6 shown in Table 1.

3.3.2 Catalyst layer (CL) coating of microporous-layered GDLs

For this study, GDEs of 25 cm^2 and loadings of 0.3, 0.6, and 0.9 mg Pt/cm^2 were manufactured from the microporous-layered GDLs (using a spraying technique (Spray gun: Iwata revolution, compressor: Puma and in-house-built spraying table)). None of the manufactured GDEs were hot pressed. The manufactured GDEs were then compared to commercially available GDEs (*Giner*, Inc. and *Giner* Electrochemical Systems, LLC (GES)) with a platinum loading of 0.3 mg Pt/cm^2 and 0.5 mg Pt/cm^2 by means of a H_2 pump and SO_2-depolarized electrolysis (Section 3.5). The GDEs were not hot pressed to the PEM ($64cm^2$) (Nafion® 117 supplied by Ion Power Inc) because of the fragility of the carbon paper used to manufacture them.

The same catalyst coating technique was used to coat the microporous-layered GDLs made from EC-TP1-060 Toray™ carbon paper (0.19 mm thick). The amount of Pt loaded was based on the best results obtained from the EC-TP1-030 Toray™ carbon paper (0.11mm thick) GDE results. The influence of the thickness of the GDE was determined by comparing the H_2 pump and SO_2-depolarized electrolysis results obtained with the EC-TP1-030 to the EC-TP1-060-based GDEs

3.4 MEA manufacturing

3.4.1 Cleaning of proton exchange membranes (PEMs)

Before MEA manufacturing, the Nafion® 117 PEMs (supplied by Ion Power Inc) ($64cm^2$), the sPSU-PBIOO blend PEMs ($64cm^2$), as well as the sFS PBI-OO PEMs ($64cm^2$) (sPSU-PBIOO and sFS-PBIOO PEMs supplied by Dr. Jochen Kerres, University of Stuttgart, Institute of Chemical Process Engineering) were boiled in 3 wt% aqueous H_2O_2 (Merck (PTY) LTD) for 60 minutes to remove all residual organic and inorganic impurities[80]. Subsequently the PEMs were washed 3 times in 500ml boiling DI water to remove any residual H_2O_2. After washing, the PEMs were further handled with gloves (Microflex, nitrile).

3.4.2 Catalyst layer (CL) coating

The MEAs were manufactured using a spraying technique. The Nafion® 117 PEMs were cut into 64 cm^2 squares, before being clamped in an in-house-made frame with eight wing nuts and bolts, which had a 25 cm^2 square hole in the middle (Figure 3.3). Once fixed in the frame, the PEMs were dried in a convection oven at 50°C (Labotec, Eco Therm) overnight. The dry PEMs and frame were weighed to get a base weight. A catalyst coating was obtained by spraying a homogeneous layer of catalyst ink onto the PEM. The PEM and frame combination was weighed after each spray coating in order to determine the correct catalyst loading. Before weighing, the coating was dried using a hair drier.

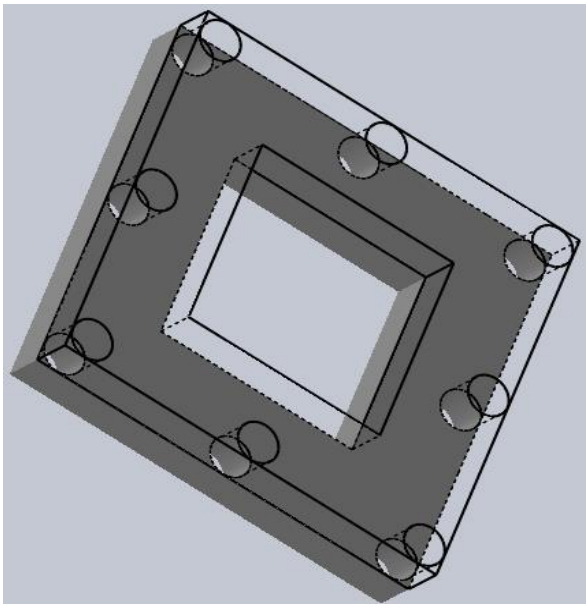

Figure 3.3: PEM drying and spraying frame.

MEAs were manufactured with a loading of 0.3, 0.6, 0.9 mg Pt/cm^2, which was subsequently compared to commercially available Nafion® 117 MEAs (supplied by Ion Power Inc) with a platinum loading of 0.3 mg Pt/cm^2 using an H_2 pump and SO_2-depolarized electrolysis (see Section 3.5).

sPSU-PBIOO blend MEAs with loadings of 0.3, 0.6, 0.9 mg Pt/cm^2 were manufactured in the same way as the Nafion® 117 MEAs and were subsequently compared to a spray coated sPSU-PBIOO MEA with a loading of 0.6 mg/cm^2 Pt/C (obtained from the Zentrum für Sonnenenergie- und Wasserstoff-Forschung (ZSW)) using H_2 pump and SO_2 depolarized electrolysis (see Section 3.5). Using the loading of the best performing sPSU PBI-OO blend MEA, a MEA was manufactured using a sulfonated fluorophenyl sulfone polybenzimidazole (sFS PBI-OO) blend PEM and comparing it to the sPSU PBI-OO blend MEA using an H_2 pump and SO_2-depolarized electrolysis. For the H_2 pump and SO_2-depolarized electrolysis, EC-TP1-030 Toray™ carbon paper (supplied by Electrochem, Inc) was used as GDL, irrespective of the MEA tested.

The amount of platinum catalyst per cm^2 on the PEM was calculated using the following equation:

$$L = A_{Ga} * \left(\frac{100}{P}\right) * L_d * (\frac{100}{N}) /1000 \qquad (1)$$

Where: L= loading (mg Pt/cm^2)

A_{Ga}= Geometric active catalyst area (cm^2).

P= % Pt/C.

L_d= Desired loading (mg Pt/cm^2).

N= wt% Nafion® in Nafion® solution.

3.4.3 MEA hot press

Only the Nafion® 117 (supplied by Ion Power Inc) MEAs were hot pressed. The Pt coated MEAs were placed on a hot press (CARVER, **12-12H)** between the platens (containing two Teflon blocks with a thickness of 8 millimetres used for the pressing of MEAs) and pressed for 5 minutes at 120˚C at a pressure of $20kg/cm^2$ on the active area. The hot pressing was done to strengthen the catalyst layer and PEM bond in order to prevent the catalyst layer from peeling off the PEM when it is rehydrated before use in an electrolyser.

The actual temperature between the platens and Teflon blocks was measured at 120°C, 130°C, 140°C and 160°C to ensure that hot pressing took place close to the glass transition temperature of Nafion® 117 i.e. ±120°C[81]. This was achieved by wedging a thermocouple electrode (FLUKE) between the two Teflon blocks as close to the middle as possible and taking temperature measurements every 5 minutes for 45 minutes, because the platens heat evenly, it was assumed that the Teflon blocks would heat evenly as well. A temperature profile over time curve was then obtained showing the true temperature between the two Teflon blocks.

3.5 MEA and GDE characterisation

In this Section the characterisation of the manufactured MEAs and GDEs is discussed. In Section 3.5.1, SEM characterisation of the manufactured MPL-coated GDLs, GDEs and MEAs is described. In Section 3.5.2 the experimental setup, operation and characterisation of GDEs and MEAs (Table 1) by electrolysis is presented.

3.5.1 SEM

A FEI Quanta 200 ESEM system was used to investigate the visual surface of the MEAs and the GDEs as well as the dispersion of elements in the catalyst layer. SEM micrographs were taken of GDLs with 3, 6 and 9 microporous layers using carbon black ink to determine how many layers were required to provide a thin and effective surface for the catalyst coating. SEM micrographs of uncoated GDLs were used for comparative purposes. SEM micrographs were also taken of a GDL with the optimised microporous layer and a catalyst layer of 0.3 mg Pt/cm^2 before and after hot pressing for comparative purposes. Finally, SEM micrographs were taken of a Nafion® 117 MEA with a loading of 0.3 mg Pt/cm^2 before and after SO_2-depolarized electrolysis.

3.5.2 H_2 pump and SO_2 -depolarised electrolysis

Both H_2 pump and SO_2-depolarized electrolysis were used as characterisation techniques. The H_2 pump was used to ensure correct assembly of the electrolyser cell by determining the proton conductivity across the PEM and the travel of electrons via an external circuit. SO_2-depolarized electrolysis was used to obtain polarization curves, efficiency in terms of hydrogen produced and sulfuric acid concentration in order to determine the efficiency of the manufactured GDEs and MEAs. A single setup was used both for the H_2 pump and the SO_2-depolarised electrolysis.

3.5.2.1 Electrolyser setup

Figure 3.4 shows the experimental setup that was used to characterise the manufactured MEAs and GDEs. N_2, H_2, or SO_2 was supplied via R1, R2 and R3. R2 and R3 were used for flushing, testing as well as SO_2 operation. Water was fed from GV3 using a peristaltic pump (Watson-Marlow 323, PP2), which is the catholyte vessel to the cathode side of the electrolyser (E1) (*in-house-built*). After the water left the electrolyser, it was sent to a separator (GV2) to separate the gases from the liquids. The gases were then passed through to a scrubber (GV4) which absorbed the sulphur containing species. Hydrogen was sent to a flash back arrestor (V15) before leaving the system. The separated water was returned to GV3 using a peristaltic pump (Watson-Marlow 323, PP1) from where it was reintroduced to the cathode via V5. The unreacted SO_2 and produced H_2SO_4 were sent to a second separator (GV1) from where the SO_2 was re-circulated.

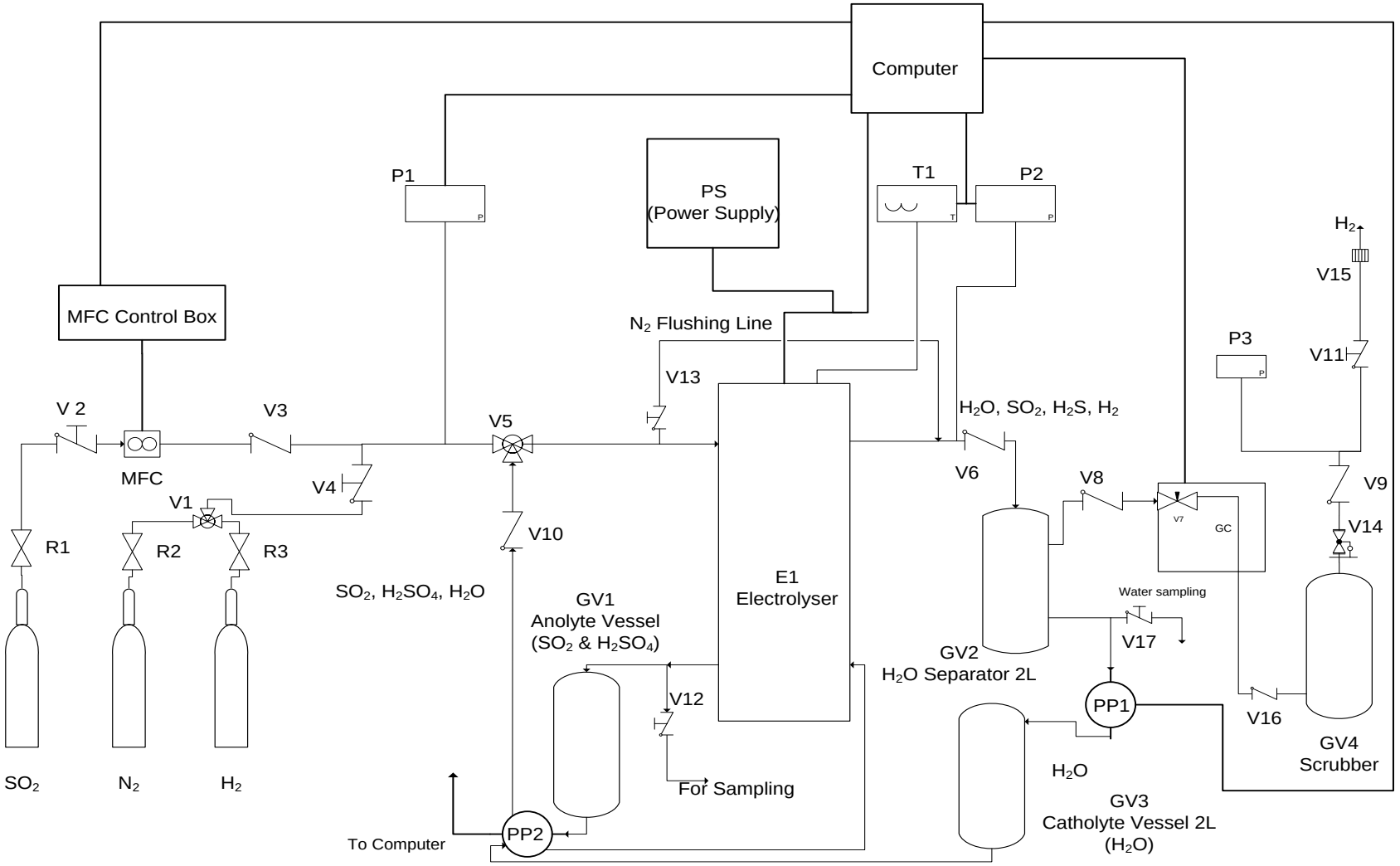

Figure 3.4: Schematic representation of the SO_2-depolarized electrolyser setup[82].

3.5.2.2 Flushing

Prior to a H_2 pump test and SO_2-depolarized electrolysis, the entire system had to be pressure tested to ensure that no leaks existed. N_2 was used to pressurise the system to 150KPa. The system was tested for one hour for any possible leaks which would be detected via a pressure drop on the pressure meters (Instrumentation specialties INC). When no leaks were detected, N_2 was again flushed through the entire system at 1 bar for 15 minutes to ensure that no oxygen remained in the system.

3.5.2.3 H_2 pump

The effectiveness of the MEAs or GDEs was subsequently tested using the H_2 pump test. For this, H_2 was used to first flush the anode. After the flushing and saturation of the anode with H_2, the MEAs or GDEs were tested by supplying a current to the cell. For an effective MEA or GDE, a 1A/cm^2 should be achieved for H_2 oxidation at the anode and the cathode consuming not more than 0.2V for the H^+ reduction. A positive test confirms that the protons successfully migrated through the PEM while the electrons travelled via an external circuit from the anode to the cathode without major resistance.

3.5.2.4 SO_2-depolarized electrolysis

After completing the N_2 flushing and H_2 testing was completed, SO_2 was introduced into the system by connecting SO_2 (via V2) to the system. Pre-heated DI water, heated to 88°C using a water bath (Julabo FP 50) (not shown in Figure 3.3) was subsequently supplied to the electrolyser cell at 100 mL/min while heating the endplates of the electrolyser to 80°C using heating pads.

Before initiating operation, contact between the SO_2 gas and the electrode had to be ensured while the scrubber solution (GV4) was circulated to ensure total sulphur chemisorption. Saturation and flushing of the anode compartment was achieved by flushing SO_2 at 20cm^3/minute to the anode for 1 minute, ensuring that all H_2 had been removed. After flushing was completed, a current density of 200mA/cm^2 (5A) was applied over the electrolyser cell. When a stable voltage had been attained for at least 2-3 minutes, the current density was increased by 20mA/cm^2 increments to 1000mA/cm^2 or the maximum limit of the PEM. At each current, the cell potential was noted and from this polarization curves were obtained. To prevent irreversible corrosion of the carbon of the bipolar plates as well as the carbon contained in the GDEs and MEAs, the applied voltage was kept below 1.2V.

3.5.2.5.1 H_2 production

During SO_2-depolarized electrolysis operation, a bubble flow meter (in-house-made) was used to note the amount of hydrogen produced, which was used to calculate the efficiency by comparing the experimental amount of hydrogen produced to the theoretical amount of hydrogen producible in terms of the SO_2 delivered.

3.5.2.5.2 Sulfuric acid concentration

During SO_2-depolarized electrolysis operation, the sulfuric acid concentration was determined at every current density ramp and titrated against sodium hydroxide (1M, supplied by Merck (PTY) LTD) using a phenolphthalein indicator to determine the sulfuric acid concentration. For the titration the acid was diluted 100 times.

3.5.2.5.3 Hydrogen production efficiency

During SO_2-depolarized electrolysis operation the amount of H_2 produced was measured, this was then compared to the theoretical hydrogen produced and from this the efficiency was calculated.

Chapter 4: Results and discussion

4.1 Introduction

This chapter describes and discusses the results obtained using the experimental procedures described in Chapter 3. Since the purpose of this study was to manufacture and characterize GDEs and MEAs for SO_2-depolarized electrolysis, Sections 4.2 and 4.3 deal with the manufacturing of the GDEs and MEAs, respectively. Subsequently, the results of GDE manufacturing are presented and discussed in Section 4.4. Most of the results in Section 4.2 (MPL coating, CL coating) and Section 4.3 (CL coating and CL hot pressing) were obtained using SEM analysis. Subsequently, the characterisation results pertaining to H_2 pump, SO_2-depolarized electrolysis, hydrogen production and hydrogen production efficiency from the MEAs presented in Table 1, Chapter 3 are discussed in Section 4.4.

4.2 GDE manufacture

To obtain a defect free and thin CL, the GDL was first coated with a MPL. In this section, both the MPL coating (Section 4.3.1) and the subsequent CL coating (Section 4.3.2) results are presented. A comprehensive range of SEM micrographs was taken, showing every step of the manufacturing step from the uncoated gas diffusion layer (GDL), for both Teflon treated and untreated GDLs to, the catalyst layer coating, including hot pressing of the GDEs.

4.2.1 MPL coating

To determine the optimum MPLs, both the Teflon-treated GDL (thickness 0.11 mm) to be used on the anode side of the electrolyser, and the untreated GDL (thickness 0.11 mm) to be used on the cathode side of the electrolyser, were coated with 3, 6 and 9 consecutive MPL coatings and subsequently visually analysed using SEM. As mentioned previously, the MPL is important for the manufacture of a defect free GDE, providing a smooth enough surface for the sufficient deposition of the catalyst layer to the GDL[83]. Furthermore, without such an MPL, the catalyst ink would seep into the carbon fibres, blocking the pores and thereby lowering the effectiveness of the GDL, while simultaneously reducing the amount of catalyst that is available on the membrane surface for the catalytic electrolysis[84].

In Figures 4.1 and 4.2, the top and side view of both the Teflon-treated and untreated GDLs prior to MPL deposition are shown respectively. In Figure 4.1, the Teflon polymer can clearly be seen in between the carbon fibres when compared to Figure 4.2 indicated by the arrow in Figure 4.1, resulting in its hydrophobic properties. The hydrophobicity is necessary on the anode side of the reaction cell to limit the loss of water that would otherwise permeate through the cathode and the PEM, which would result in lower cell performance[84]. When comparing Figure 4.2 with Figure 4.1, it is clear that the covering between the carbon fibres is as expected much less for the untreated GDL as indicated by the green arrow. The observed material in between the fibres visible in Figure 4.2 probably consists of residual compounds (ex. binding agent) from the GDL manufacturing process.

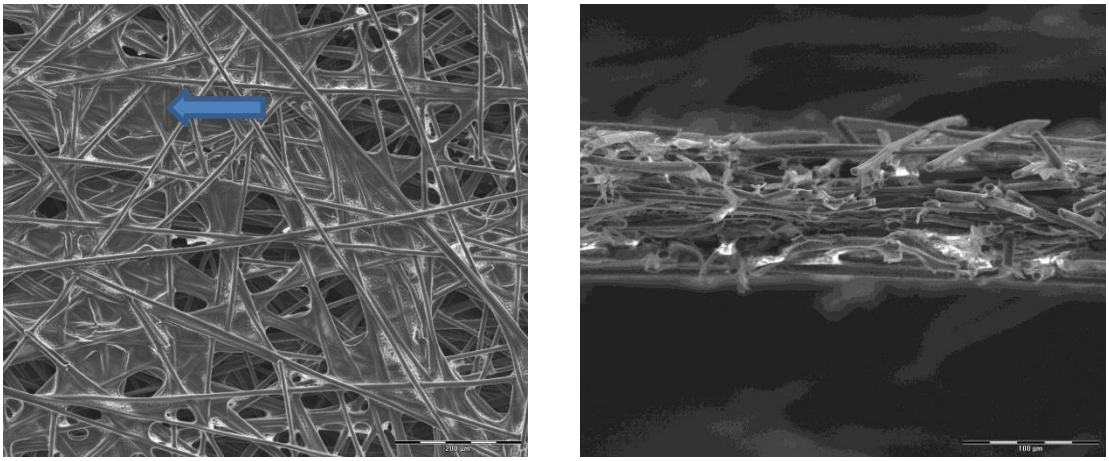

Figure 4.1: Top and cross sectional view of Teflon treated GDL prior to MPL coating.

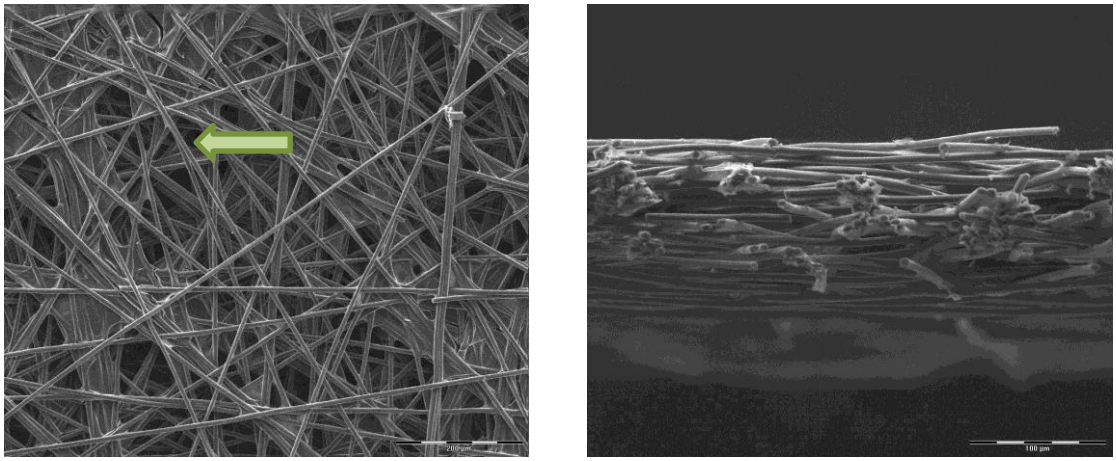

Figure 4.2: Top and cross sectional view of untreated GDL prior to MPL coating.

When comparing the 3 times MPL-coated GDL shown in Figures 4.3 and 4.4 for the Teflon treated and untreated GDL, respectively, the visual surface porosity has decreased slightly due to the MPL coatings for both GDLs as expected. While this decrease does show the successful deposition of the MPL coating technique, the amount deposited was not yet enough to significantly reduce the surface roughness or catalyst seepage into the GDL during CL deposition.

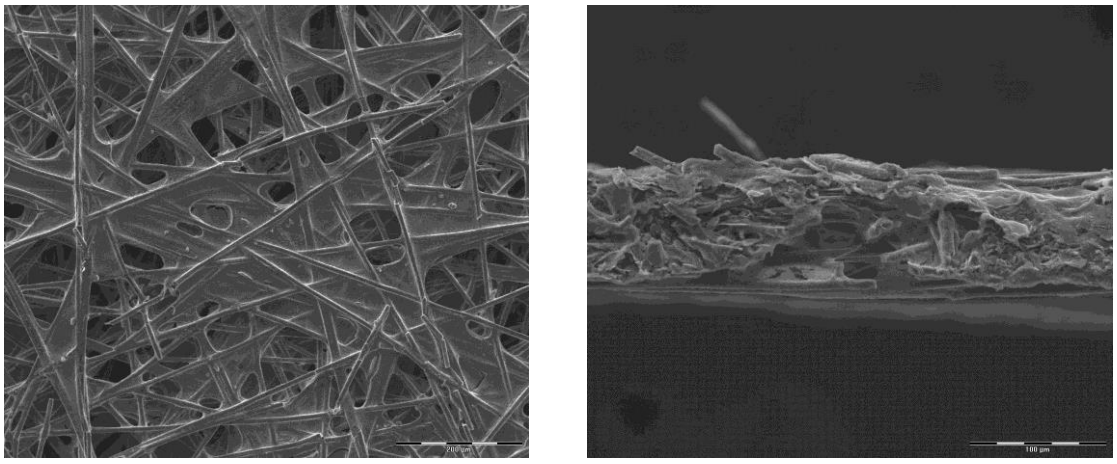

Figure 4.3: Top and cross sectional view of Teflon treated GDL with three MPL coatings applied.

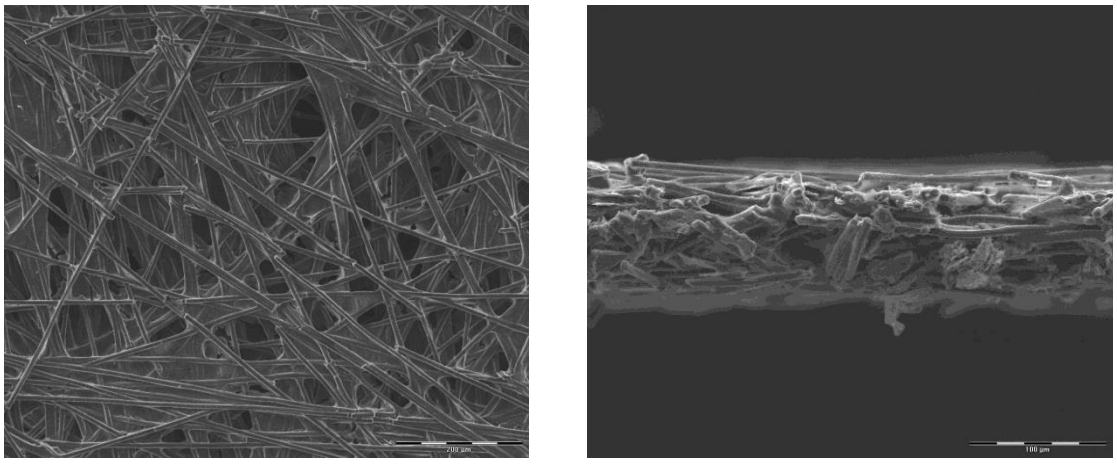

Figure 4.4: Top and cross sectional view of untreated GDL with three MPL coatings applied.

In Figures 4.5 and 4.6, the GDLs that had been coated with 6 MPLs are presented. A further reduction in terms of surface roughness compared to the 3-layered MPL-coated GDL is clearly visible both for the Teflon treated and untreated GDLs. However, as will be shown in Section 4.4, this 6 layered GDL still had adequate porosity to ensure gas and water permeability properties while simultaneously providing a smooth surface for a defect free catalyst deposition.

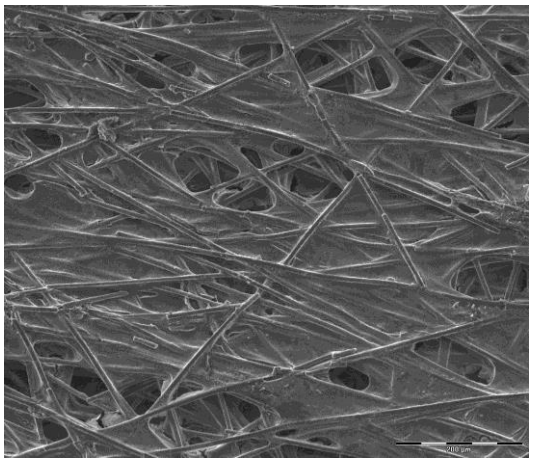

Figure 4.5: Top view of Teflon treated GDL with six MPL coatings applied.

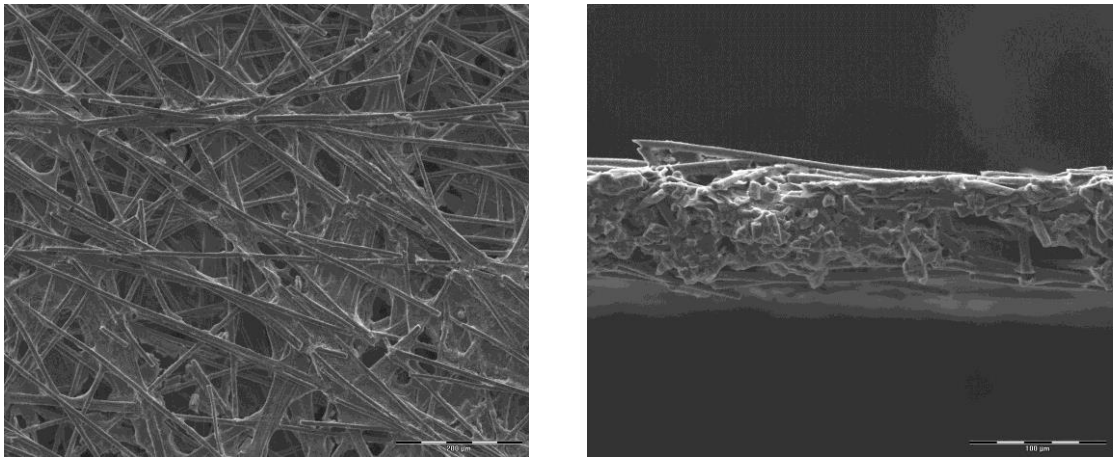

Figure 4.6: Top and cross sectional view of untreated GDL with six MPL coatings applied.

Finally, a nine-layered MPL was prepared and evaluated. Figures 4.7 and 4.8 show the top and cross sectional views of these GDLs containing nine-layered MPL coatings. From Figure 4.7, it can be seen that the carbon fibres have almost been completely sealed by the MPL coating, which would significantly reduce the flow of gases and liquids through the GDL, thereby increasing the mass transport limitation which is known to be a vital contributor to current density[85]. While the MPL-coated, untreated GDL (Figure 4.8) still shows some openings between the carbon fibres, which can be attributed to the initial untreated GDL having a more open structure due to the absence of the Teflon to begin with, it is also clear from Figure 4.8 that in some areas the MPL was so thick that cracks occurred during drying. The different drying rates experienced by the multiple coatings probably have contributed to the formation of stress cracks. According to these results, the 6-layered GDL was clearly the best candidate for CL coating and was therefore used for the CL coatings of the rest of the in-house-coated GDEs.

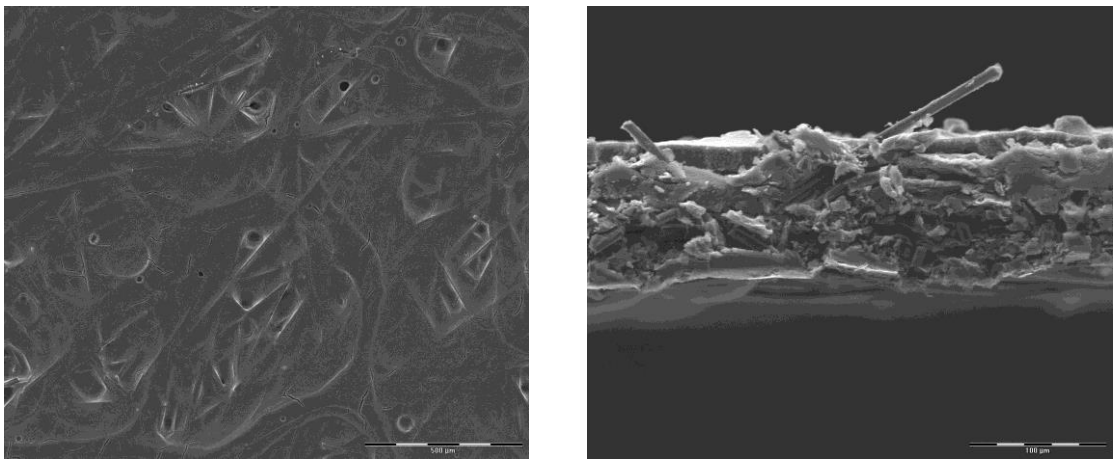

Figure 4.7: Top and cross sectional view of Teflon treated GDL with nine MPL coatings applied.

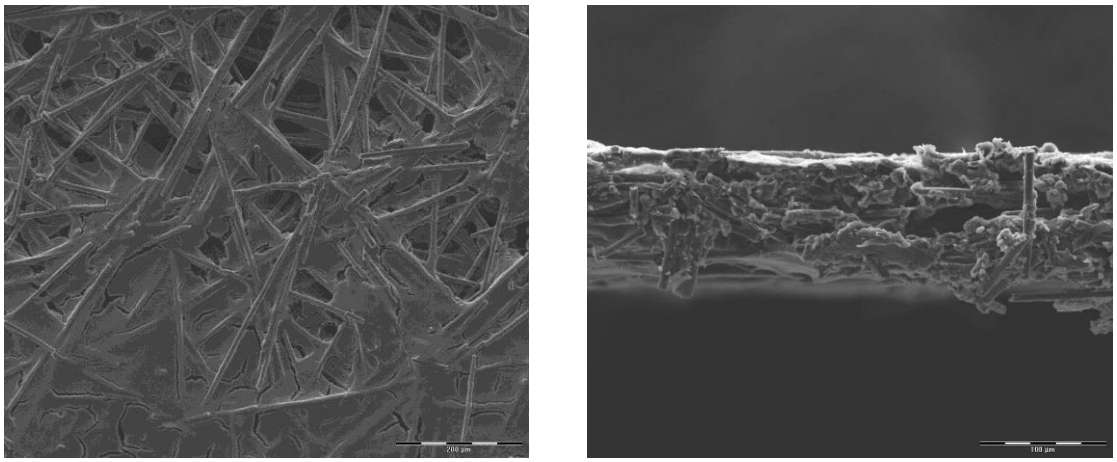

Figure 4.8: Top and cross sectional view of untreated GDL with nine microporous layer coatings applied.

4.2.2 CL coating

After optimising the MPL coatings, the next step entailed the CL deposition on the MPL coated GDL. To illustrate the suitability of the CL deposition technique, a 0.3 mg Pt/cm^2 GDE was prepared using the 6-layered MPL-coated GDLs, the SEM micrographs of which are shown in Figures 4.9 and 4.10 for the Teflon-treated and untreated MPL-coated GDLs, respectively.

To illustrate the various coatings, a higher magnification of the cross section of the Teflon-treated GDE was used for the cross sectional view presented in Figure 4.9. From the SEM micrographs, the CL (A) , MPL (B) and GDL (C) that forms the three layered sandwich called a GDE is visible (Figure 4.9). The regularity in thickness seen for both the MPLs and CLs was confirmed from other sections of the cross sectional view of the GDE. From the top view, the homogeneous coating of the CL can be seen. The cracks observed are normal and resulted from the drying process as has been observed by Pfrang et al[86]. These optimised GDEs were subsequently used in H_2 pump testing as well as SO_2-depolarized electrolysis (performance will be discussed in Section 4.4).

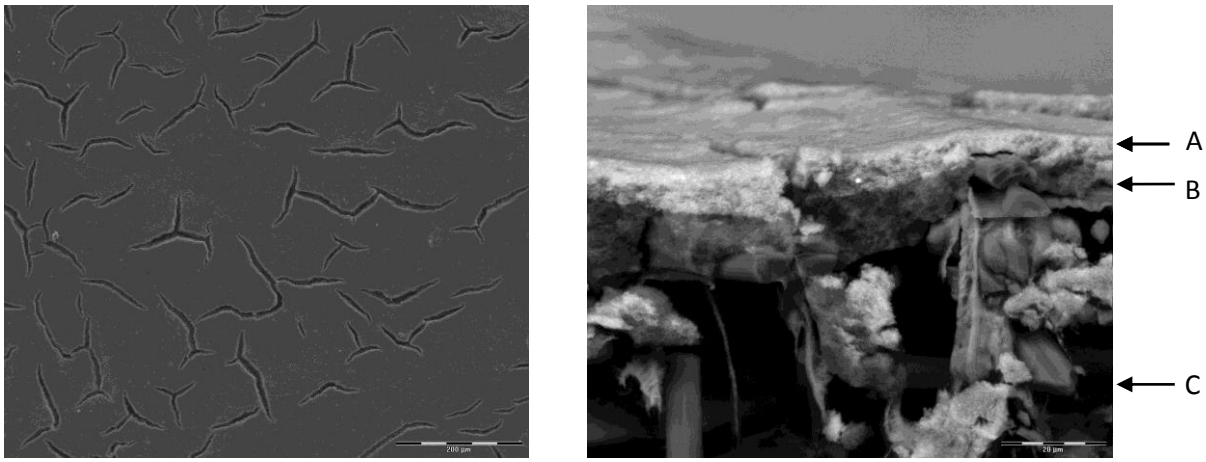

Figure 4.9: Top and cross sectional view of optimised Teflon-treated GDE with a 0.3 mg Pt/cm^2 catalyst coating where A is the CL, B is the MPL and C the GDL.

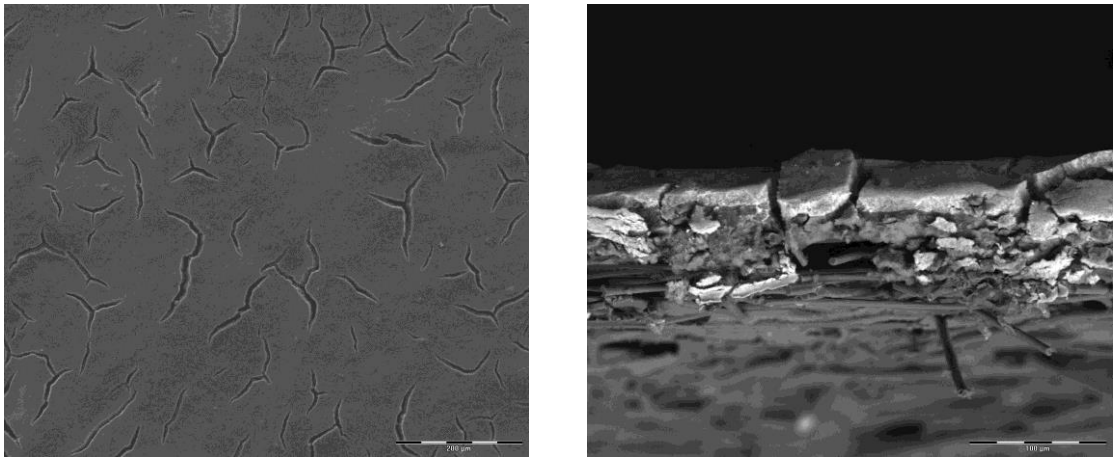

Figure 4.10: Top and cross sectional view of optimised untreated GDE with a 0.3 mg Pt/cm^2 catalyst coating.

4.2.3 Hot press

To determine the effect of hot pressing of the GDE, a 0.3 mg Pt/cm^2 coated GDE was hot pressed at 120°C for 5 minutes. No significant change in the appearance of the surface was visible when comparing the hot pressed (Figure 4.11) to the non-pressed surface (Figure 4.10). Although not visible in this image, it has been shown that hot pressing can often cause large cracks over the surface of the GDE, which compromise the ability of the GDE to regulate gas diffusion, resulting in current density losses and thus lower performance[87]. Furthermore, according to literature, hot pressing can often result in the crushing of the GDE, which has the same effect as over-clamping within an electrolysis cell, causing increased mass transport resistance[87]. In view of the disadvantages mentioned and the fact that no difference was observable between the pressed and the hot pressed examples, it was decided that all GDEs used for the electrolysis study (Experiments 1-6; Table 1, Chapter 3) would not be hot pressed. The optimum GDE therefore consisted of a composite containing an untreated + Teflon treated GDL, a six-layered MPL and a CL containing at least 0.3 mg Pt/cm^2 which was not hot pressed.

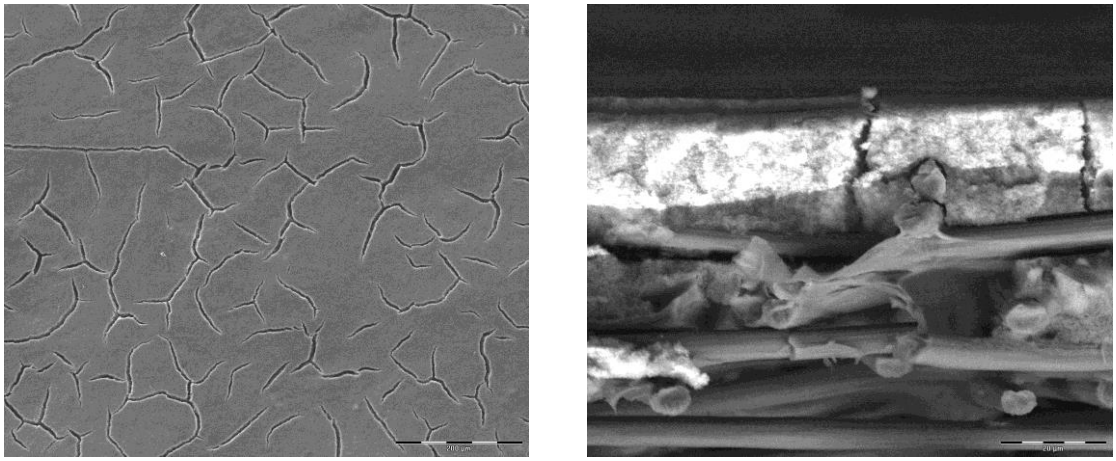

Figure 4.11: Top and cross sectional view of optimised untreated GDE with a 0.3 mg Pt/cm^2 catalyst coating after hot pressing.

4.3 MEA manufacture

Having manufactured and optimized the GDEs, the next step prior to electrolysis was to manufacture an MEA from a PEM by addition of a CL and to determine the suitability and necessity of hot pressing for this combination. Both for the Nafion® and PBI based MEAs, 0.3, 0.6 and 0.9 mg Pt/cm^2 CL loadings were prepared for SO_2-depolarized electrolysis. For the purpose of optimizing the MEA manufacturing, only the results for Nafion® are shown. The optimised procedures according to the results obtained for Nafion® were then used as is for the PBI MEA manufacture.

4.3.1 Catalyst coating

Figure 4.12 shows the surface structure of a 0.3 mg Pt/cm^2 CL-coated Nafion-based PEM before hot pressing. It is clear from the images that the CL was rough and not distributed well across the PEM. This translated into a weaker bond between the CL and PEM which would thus result in lower performance. It is clear from this that hot pressing would most probably be required for the MEAs.

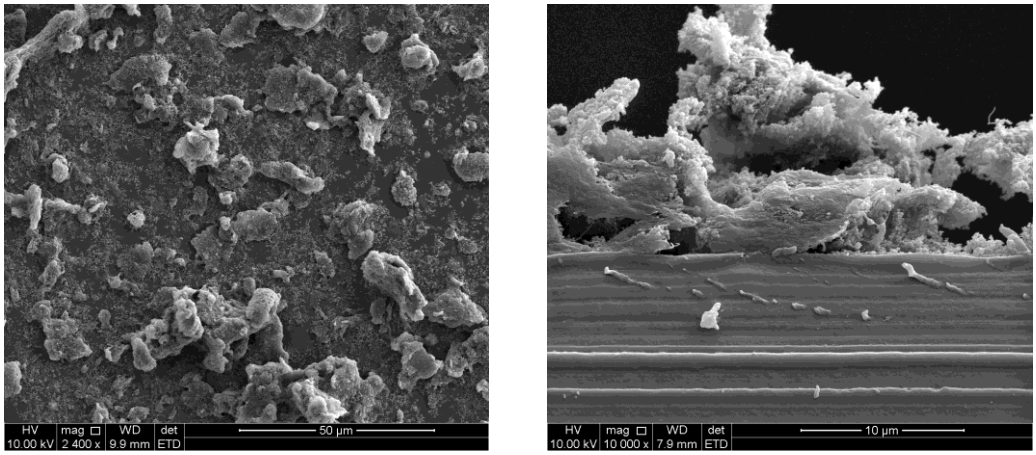

Figure 4.12: Top and cross section view of a 0.3 mg Pt/cm^2 CL-coated Nafion® PEM after spray coating and before hot pressing.

4.3.2 Hot press optimisation

In this section the hot press optimization results are shown and discussed. Because of the importance of the temperature at which hot pressing is done[83], it was necessary to first determine the actual temperature between the MEA and the Teflon block's interface prior to actual hot pressing to determine whether this temperature would correspond to the displayed temperatures. In Figure 4.13, the temperature profile at the interface is shown for those temperatures that fall into the range suggested for Nafion® MEA hot pressing. According to Figure 4.13, it is clear that the temperature became consistent after approximately 30 minutes, irrespective of the set temperature. Furthermore, it is apparent that, for all temperatures, the actual measured temperature at equilibrium was significantly lower (between 21-25%) than the temperature indicated by the equipment. Therefore, to attain the desired hot pressing temperature of 120°C, all MEAs were manufactured using a hot pressing temperature set at 160°C. This temperature was maintained for 45 minutes to ensure adequate time for reaching the temperature equilibrium, including the time required for hot pressing. Since the same binder was used for the preparation of the CL ink for the Nafion® as well as the PBI MEAs, 160°C was also used for PBI MEA hot pressing.

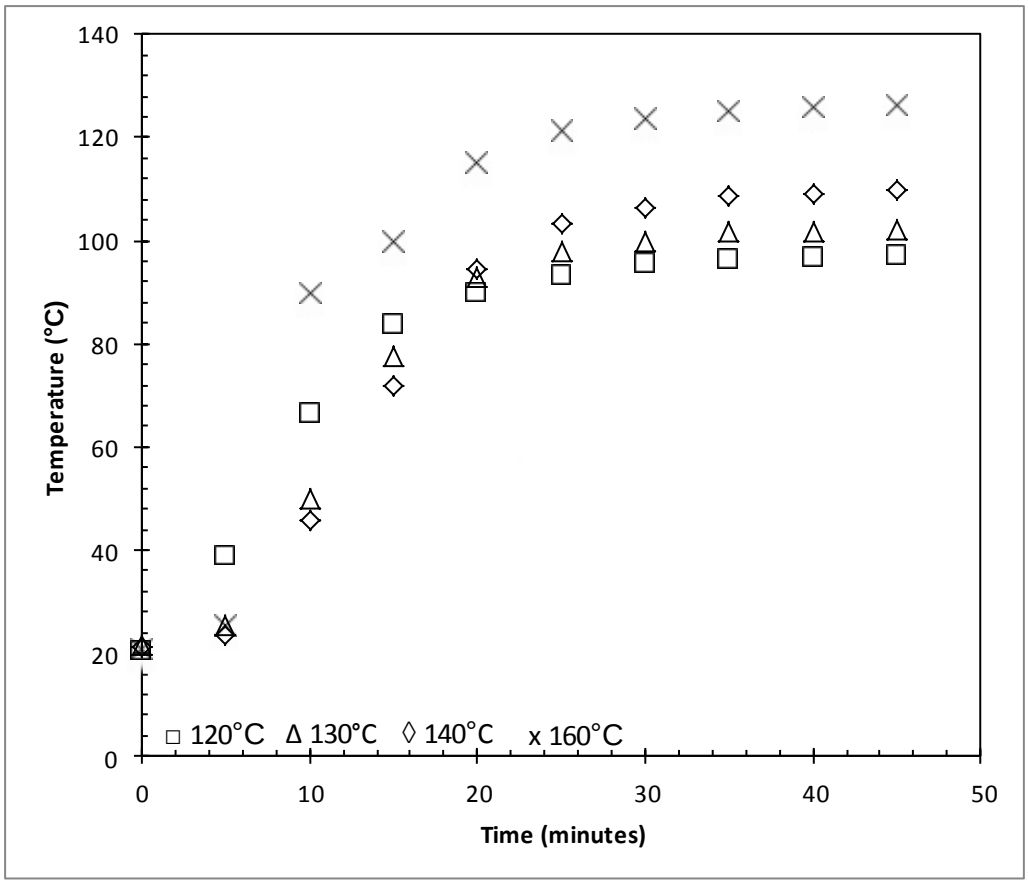

Figure 4.13: Temperature against time trends for hot pressing of in-house-coated MEA's.

Figure 4.14 shows two SEM micrographs (top and cross sectional) of the 0.3 mg Pt/cm^2 MEA Nafion® after hot pressing. When comparing Figure 4.14 to Figure 4.12, it is clear, as has been confirmed by literature[88], that hot pressing had a significant effect on the surface of the CL by smoothing the CL and securing an even distribution of the CL on a micro level, thereby ensuring better contact adhesion between the PEM and CL and a larger surface area of catalyst available. This change is caused by the hot pressing temperature being close to the glass transition temperature (120˚C) of the Nafion® PEM and the Nafion® binder, causing the two layers to form a strong bond in the presence of the pressure (20kg/cm^2) applied.

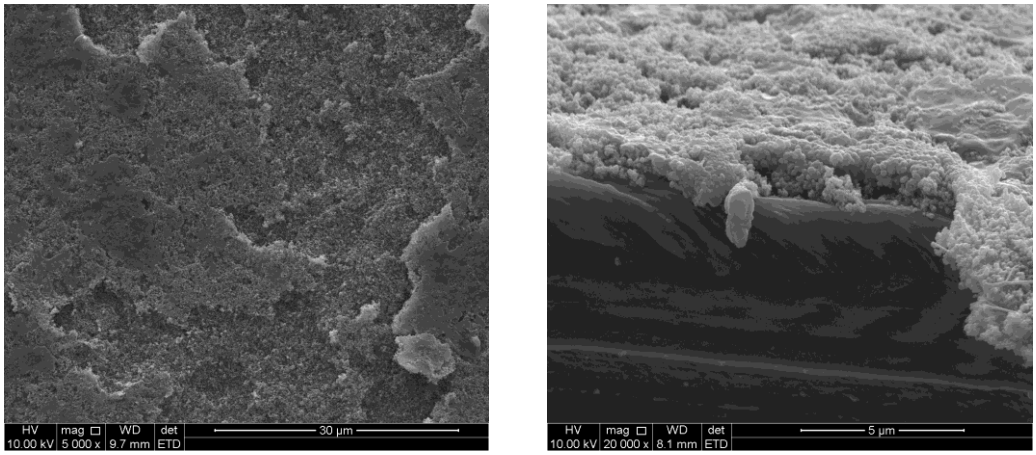

Figure 4.14: Top and cross sectional view of a 0.3 mg Pt/cm^2 CL-coated Nafion® PEM after hot pressing for 45 minutes at approximately 120°C.

4.4 GDE and MEA characterisation

After synthesis and characterization, the performance of both GDEs and MEAs was evaluated in terms of SO_2-depolarized electrolysis. For comparative purposes, the in-house-manufactured GDEs and MEAs were also compared to commercial GDEs and MEAs. To facilitate the discussion in view of the many different GDEs and MEAs evaluated, a list of all the GDEs and MEAs tested as well as their respective symbols and abbreviations used in further discussions is presented in Table 4.1.

Prior to SO_2-depolarized electrolysis (Section 4.4.2), the GDEs and MEAs performance in terms of the H_2 pump test (Section 4.4.1) was determined by means of polarization curves. As part of the SO_2 electrolysis, the H_2 (Section 4.4.3), as well as H_2SO_4 (Section 4.4.4) production of the GDEs and MEAs was determined and discussed. Finally, the MEAs and GDEs were evaluated in terms of their efficiency as described in Section 4.4.5.

Table 4.1: Abbreviations and symbols used for GDEs and MEAs evaluated.

GDE and MEA	Manufacturer	Thickness (mm)	Pt loading (mg Pt/cm^2)	Abbreviation	Symbol
GDE (for all GDE studies Nafion® 117 was used as PEM)					
EC-TP01-030	In-house	0.11	0.3	GDE-1	◆
EC-TP01-030	In-house	0.11	0.6	GDE-2	■
EC-TP01-030	In-house	0.11	0.9	GDE-3	▲
EC-TP01-060	In-house	0.19	0.3	GDE-01	◊
EC-TP01-060	Giner	0.19	0.3	GDE-02	□
EC-TP01-060	*Giner*	0.19	0.6	GDE-03	Δ
MEA (for all MEA studies a EC-TP01-030 GDL was used)					
Nafion® 117	In-house	0.171	0.3	NAF-1	x
Nafion® 117	In-house	0.171	0.6	NAF-2	ж
Nafion® 117	In-house	0.171	0.9	NAF-3	-
Nafion® 117	Ion-Power	0.171	0.3	NAF-4	–
Nafion® 117	(1)	0.171	0.5	NAF-5	o
sPSU-PBIOO	In-house	0.0306	0.3	PBI-1	●
sPSU-PBIOO	In-house	0.0306	0.6	PBI-2	+
sPSU-PBIOO	In-house	0.0306	0.9	PBI-3	▶
sPSU-PBIOO	ZSW	0.0306	0.6	PBI-Z	⊕
sFS-PBIOO	In-house	0.046	0.3	PBI-S	■

(1) The commercial MEAs characterised in the study of Krüger M-dissertation[89] had been obtained from Ion power.

4.4.1 H_2 pump

H_2 pump testing is an essential tool to determine whether the MEA and GDE fabrication had been done properly, as it can be used to determine whether suitable contact exists between the PEM, CL and GDL by determining the overall cell resistance. According to literature, the initiation voltage of the reaction should be below ≈ 0.3V[89]. It was shown that, for all the GDEs and MEAs evaluated (Figure 4.15-4.17), the initiation voltage was above zero throughout, due to the internal resistance of the electrolyser cell, which varied between 18 and 32 mΩ, but below the required 0.3V. All H_2 pump tests were done at 70°C and none of the MEAs and GDEs were run above 13A to ensure their integrity was maintained for SO_2-depolarized electrolysis.

4.4.1.1 GDE H_2 pump test

Generally it can be seen from all the polarization curve data (Figure 4.15) that there were negligible differences between the different catalyst loadings on the GDEs, confirming previous results presented by Lee et al[90] and Staser et al[91]. From the results, it is also clear that the H_2 pump testing for the in-house-coated GDEs were comparable to that of the commercial GDEs, which is interesting also in view of the difference in thickness of the commercial and in-house GDEs (in-house coated GDL was 0.11mm while the commercial GDL was 0.19 mm thick). For all GDEs a H_2 pump testing result of 0.08-0.12 V @ 400mA/cm^2 was obtained, showing a near linear increase in voltage with increasing current density.

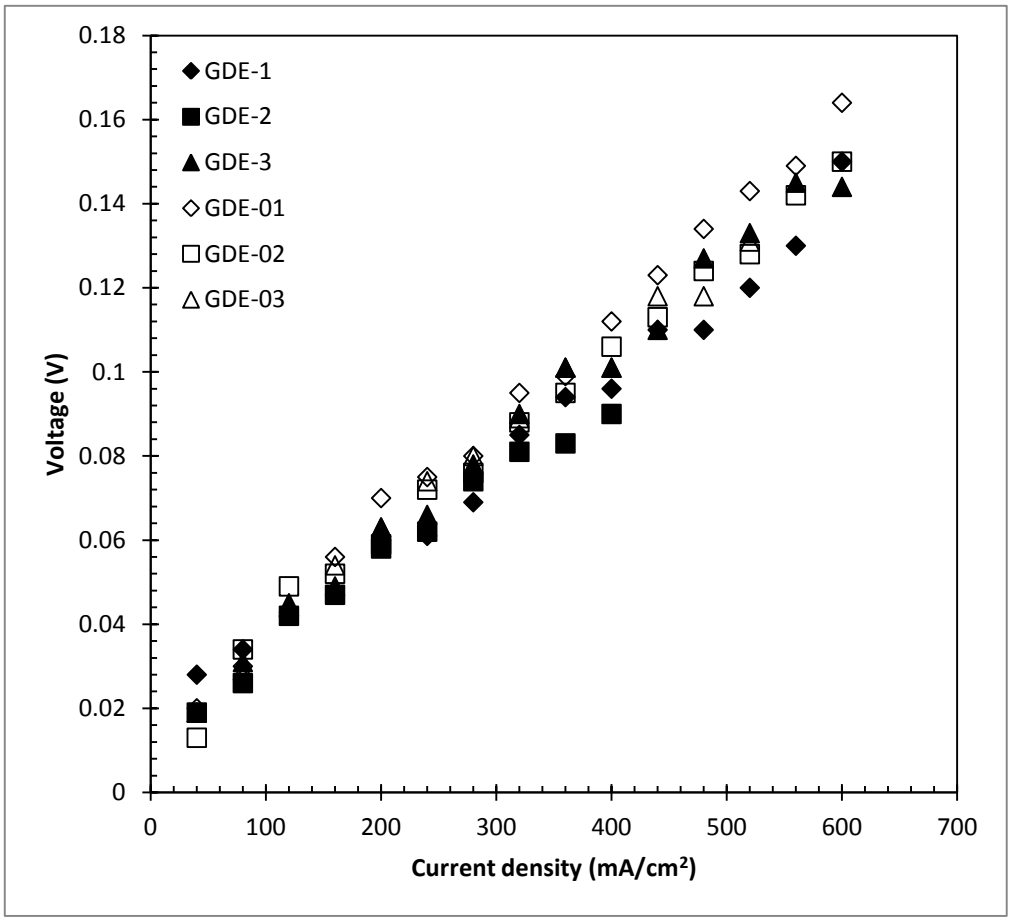

Figure 4.15: Polarization curves of Nafion®-based, in-house-coated, and commercial GDEs.

4.4.1.2 MEA H_2 Pump test

Due to the large amount of different MEAs tested, the H_2 pump test results of the Nafion®-based MEAs and the PBI-based MEAs were presented separately in Figures 4.16 and 4.17, respectively. When considering Figure 4.16, showing the polarization curves for the Nafion®-based in-house-coated and commercial MEAs, it is clear that approximately 0.1V @ 400 mA was obtained for most MEAs (excluding NAF-1), confirming that sufficient contact between the PEM, CL and GDL had been obtained. Although the H_2 data for the 0.3 mg Pt/cm^2-loaded in-house-manufactured MEA (NAF-1) deviated significantly during the H_2 pump section test, no deviation was observed for the 0.3 mg Pt/cm^2 (NAF 1) coated MEA using electrolysis conditions (see Section 4.4.2), Subsequently, the H_2 pump test variation can probably be ascribed to a higher contact resistance or GDL shifting during electrolyser cell assembly. As results show, the manufacturing of the in-house-coated MEAs was comparable to the -obtained Nafion®-based MEAs. It also seems that similar performances were obtained when comparing the MEAs' results to the H_2 pump results obtained using GDEs (Figure

4.15). NAF-5 was not included in this section because it is reference data obtained from Krüger et al[82].

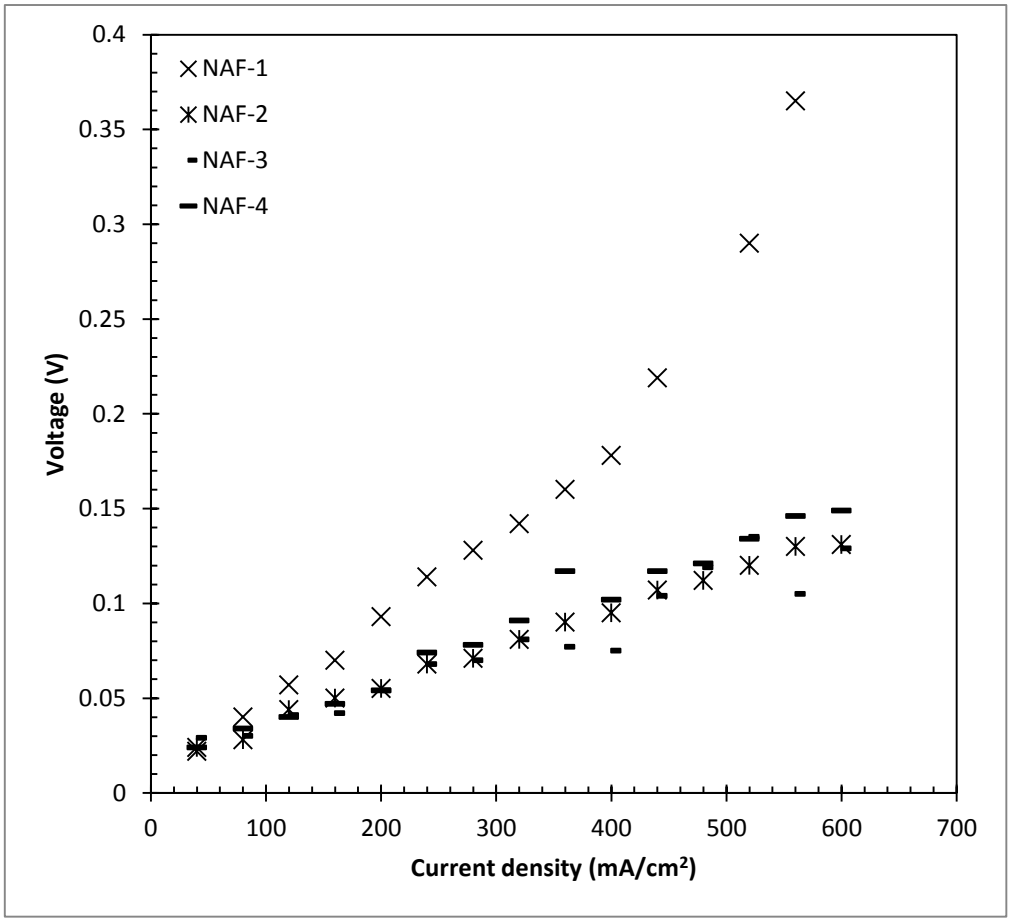

Figure 4.16: Polarization curves of Nafion® based MEA's.

While the optimization of the GDE and MEA manufacture techniques was done using Nafion PEMs, a further aim of the study was to use the optimized conditions to manufacture specific PBI-based MEAs i.e. a sPSU – PBIOO and sFS – PBIOO blend PEM obtained from the group of Kerres (Stuttgart, Germany). The sFS-PBIOO MEA (sFS-S) was manufactured with a 0.3 mg Pt/cm^2 CL before being hot-pressed at 120°C for 45 minutes, while the sPSU-PBIOO MEAs (PBI-1, PBI-2, PBI-3) were coated with 0.3, 0.6 and 0.9 mg Pt/cm^2 CL, respectively.

In Figure 4.17, the polarization curves of sPSU-PBIOO MEAs with different catalyst loadings (0.3, 0.6 and 0.9mg Pt/cm^2) and sFS-PBIOO (0.3 mg Pt/cm^2) are presented. H_2 pump testing was not done on the sPSU-PBIOO MEA made by ZSW (Germany) (PBI-Z) (0.3 mg Pt/cm^2), as the MEA had already been used for SO_2-depolarized electrolysis, which compromised the MEA in terms of H_2 pump testing. According to Figure 4.17, the sFS-PBIOO in-house-coated MEA (PBI-S) significantly out-performed the sPSU-PBIOO MEAs. Since sPSU-PBIOO and sFS-PBIOO both use the same transport mechanism[92],

the improved performance can probably be ascribed to the partially fluorinated sFS-PBIOO backbone and its subsequent higher acidity. This higher acidity of the partially fluorinated sFS backbone leads to a higher dissociation degree of the -SO_3H groups resulting in higher proton conductivity[93].

When comparing all the evaluated GDEs and Nafion®-based MEAs in terms of the H_2 pump test, it is clear that all GDEs and MEAs performed in the same range (0.08-0.1 V @ 400 m A/cm^2), except for the 0.3 mg Pt/cm^2 Nafion MEA which performed slightly worse. These results of the successfully completed H_2 pump test confirm that the manufactured GDEs and MEAs were of a comparable quality and integrity with commercial GDEs and MEAs and hence would probably be suitable for SO_2-depolarized electrolysis.

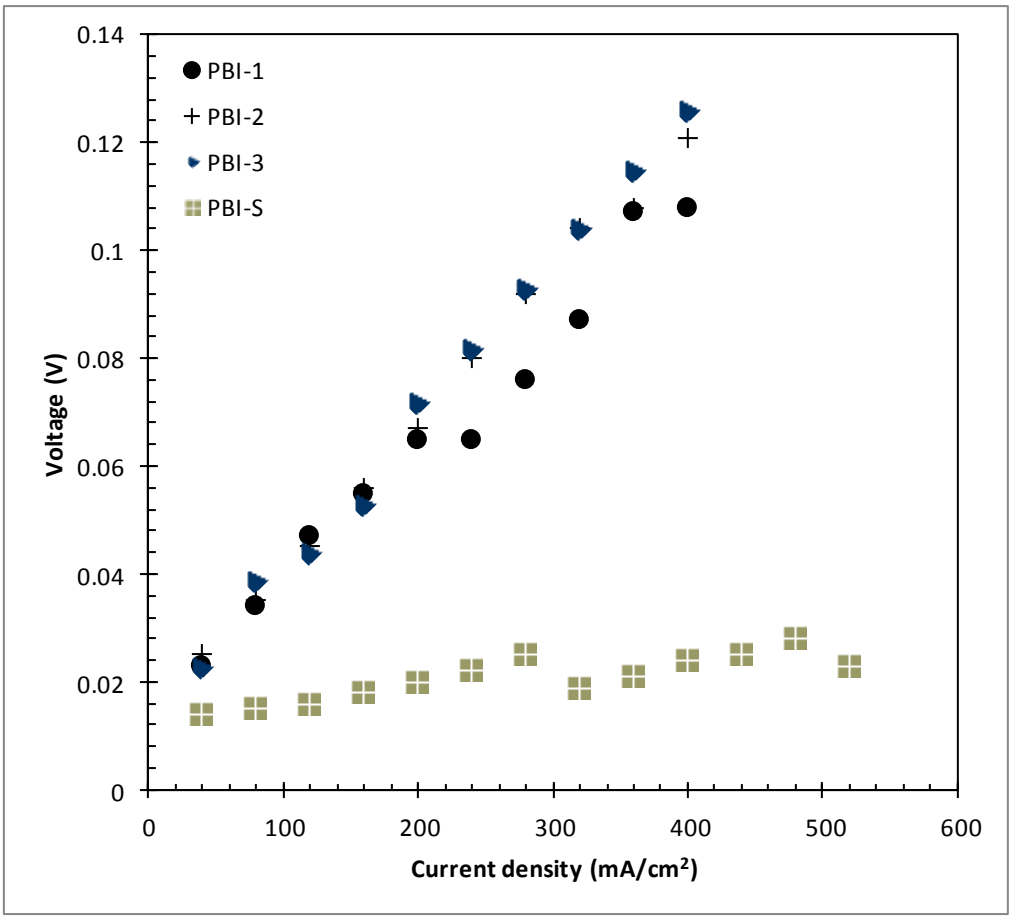

Figure 4.17: Polarization curves of sPSU-PBIOO and sFS-PBIOO-based, in-house-coated MEAs.

4.4.2 SO_2-depolarized electrolysis

In this section, different facets pertaining to SO_2-depolarized electrolysis are discussed. Initially, SO_2-depolarized electrolysis was used to determine how the in-house-coated MEAs and GDEs compared to commercial MEAs and GDEs in terms of the obtained polarization curves. Simultaneously, the data was used for the Nafion®-based MEAs to compare how the commercial MEAs compared to the in-house-coated PBI-based MEAs. Polarization curves were generated for all the in-house-coated MEAs and GDEs, commercial MEAs and GDEs, as well as for the sPSU-PBIOO MEA obtained from ZSW (Section 4.4.2).

During operation of the SO_2-depolarized electrolysis, both the hydrogen production as well as the concentration of sulfuric acid produced was measured, which is discussed in Section 4.4.3 and Section 4.4.4, respectively. To confirm the repeatability of the results, the published results obtained by Krüger et al[89] were used to correlate the data obtained from this SO_2-depolarized electrolysis study using the exact same setup (Figure 4.19).

4.4.2.1 GDE polarization curves

In addition to the determination of the effect of the catalyst loading, the scope of this part of the study was extended to also evaluate the effect of GDE thickness on the performance. For this purpose, GDEs with three different catalyst loadings (0.3, 0.6, 0.9 mg Pt/cm^2) made from a 0.11 mm GDL, as well as a 0.3 mg Pt/cm^2 coated GDE made from 0.19 mm GDL were prepared. Using a 0.19mm GDL had the added advantage that it facilitated the comparison with the 2 commercial GDEs (0.3 and 0.6 mg Pt/cm^2) which had also been prepared on a 0.19 mm thick GDL . In this way the in-house-coated GDEs could be compared to the commercial GDEs where catalyst loading as well as GDL thickness was taken into account.

In Figure 4.18, the polarization curves of the in-house-coated and commercial GDEs are presented. It is clear that the performance of the three in-house-coated MEAs (GDE-1, GDE-2 and GDE-3) varied, where the 0.3 mg Pt/cm^2 (GDE-01) loading performed the worst and the 0.9 mg Pt/cm^2 (GDE-3) loading performed the best. This is interesting because at these catalyst loading levels, according to literature, the loading should not have any significant effect on the performance (See Section 4.4.1)[90,91,94]. This variation could possibly be accredited to the assembly of the electrolyser cell being slightly different for each of the GDEs, for example due to GDEs shifting during assembly or due to the pressure on the GDEs in the cell from assembly being slightly different each time. On the other hand, it could mean that, for this specific setup, 0.3 mg catalyst was not yet enough to reach the plateau where a further increase in catalyst would not result in a further improvement in efficiency,

which seems likely considering the step-wise increase in performance with increased catalyst content.

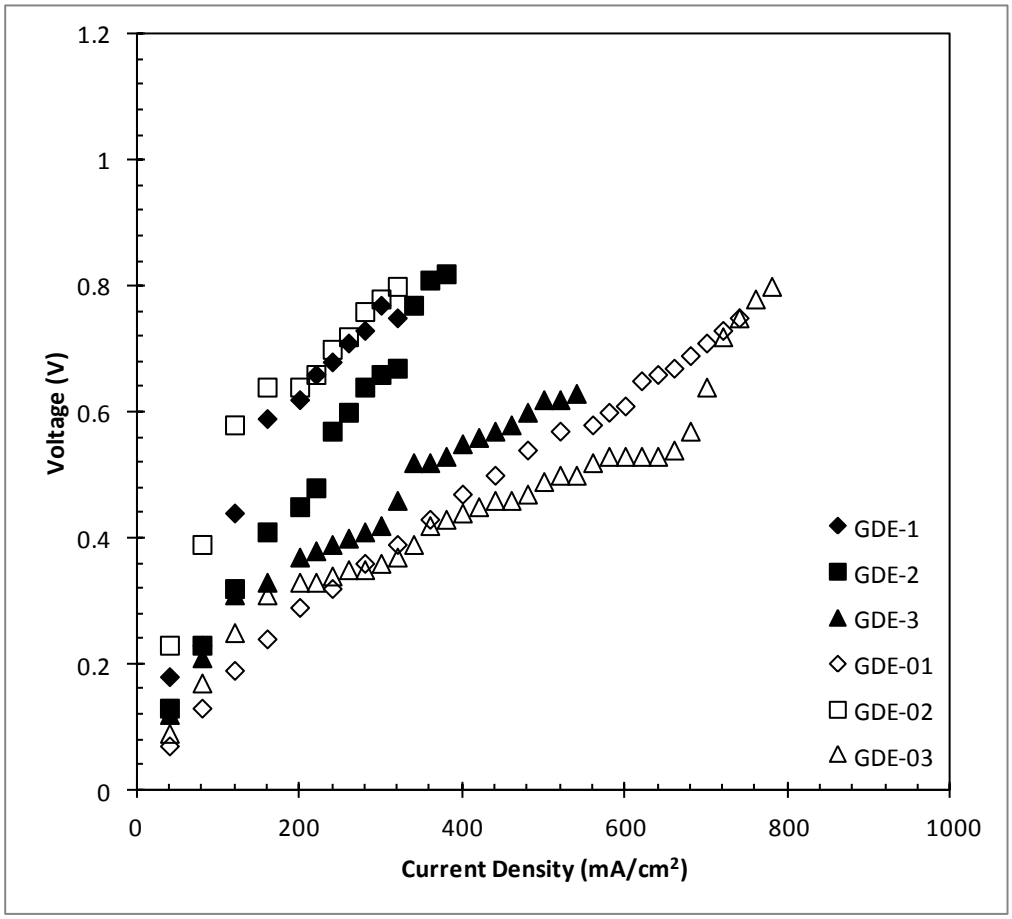

Figure 4.18: SO_2-depolarized electrolysis polarization curves for in-house-coated and commercially-obtained GDEs.

It is also clear from this Figure that the commercial 0.6 mg Pt/cm^2 (GDE-03) GDE performed the best, while the 0.3 mg Pt/cm^2 commercial GDE (GDE-02) performed the worst, which could again point to the observation of increasing performance with increasing load made with the in-house-made GDEs, However, after opening the cell containing GDE-02, it became apparent that the GDE had been crushed during operation, which could possibly have been caused by the large difference in gasket thickness to GDE ratio (0.1mm thick Teflon gaskets vs. the 0.19 mm thick). It is well known that the compression should ideally be around 60%-65% compression[95] where larger compression rations would lead to GDE crushing and flooding, resulting in increased resistance and lower performance[96].

When only comparing GDE-01 and GDE-03, it seems as if the commercial GDE with the higher catalyst loading GDE-03 (0.6 mg Pt/cm^2) performed similar to or marginally better than the in-house-built GDE with the lower loading (GDE-01; 0.3 mg Pt/cm^2). It is, however, difficult to establish

whether this difference in voltage was significant and if so, whether this was due to manufacturing of the in-house GDE or due to the fact that the loading was lower. It can therefore be stated that the in-house-manufactured GDE yielded a similar performance than the commercial GDE, confirming the suitability of the in-house manufacturing technique.

When considering the possible influence of the thickness of the GDE, is clear from Figure 4.18 that the thicker GDEs (0.19 mm) generally performed better than the thinner GDEs (0.11 mm). Since their bulk density, porosity and surface roughness are almost identical, the two GDLs mainly differ in their gas permeability (2500 ml/mm (0.11 mm GDL) and 1900 ml/mm (0.19 mm GDL)[97]). While the higher gas permeability seems to suggest a possible higher performance, the higher gas permeability of the 0.11 mm GDL makes it more susceptible to flooding than the 0.19 mm GDEs, possibly resulting in the lower SO_2-depolarised electrolysis performance.

4.4.2.2 MEA polarization curves

In Figure 4.19, the polarization curves of the in-house-coated Nafion-based MEAs are presented and compared to the commercial Nafion-based MEAs' data, obtained from Krüger et al[7]. It is clear that all the MEAs performed within a comparable range of the reference MEA (NAF-5), confirming what has been observed in Section 4.4.1[90,91,94]. Of the in-house-coated MEAs, the 0.3 mg Pt/cm^2 MEA (NAF-1) produced the best results, though it did not produce any hydrogen, which will be discussed in Section 4.4.3. The in-house-coated 0.6 (NAF-2) and 0.9 (NAF-3) mg Pt/cm^2 MEAs performed similar in the mid current density range, comparable with both NAF-1 and NAF-4. Similarly to what had been observed for the GDEs, the commercial 0.3 mg Pt/cm^2 (NAF-4) produced better results than the in-house-manufactured NAF-2 and NAF-3 below 200mA/cm^2,while also performing better than NAF-1 above 200mA/cm^2 .

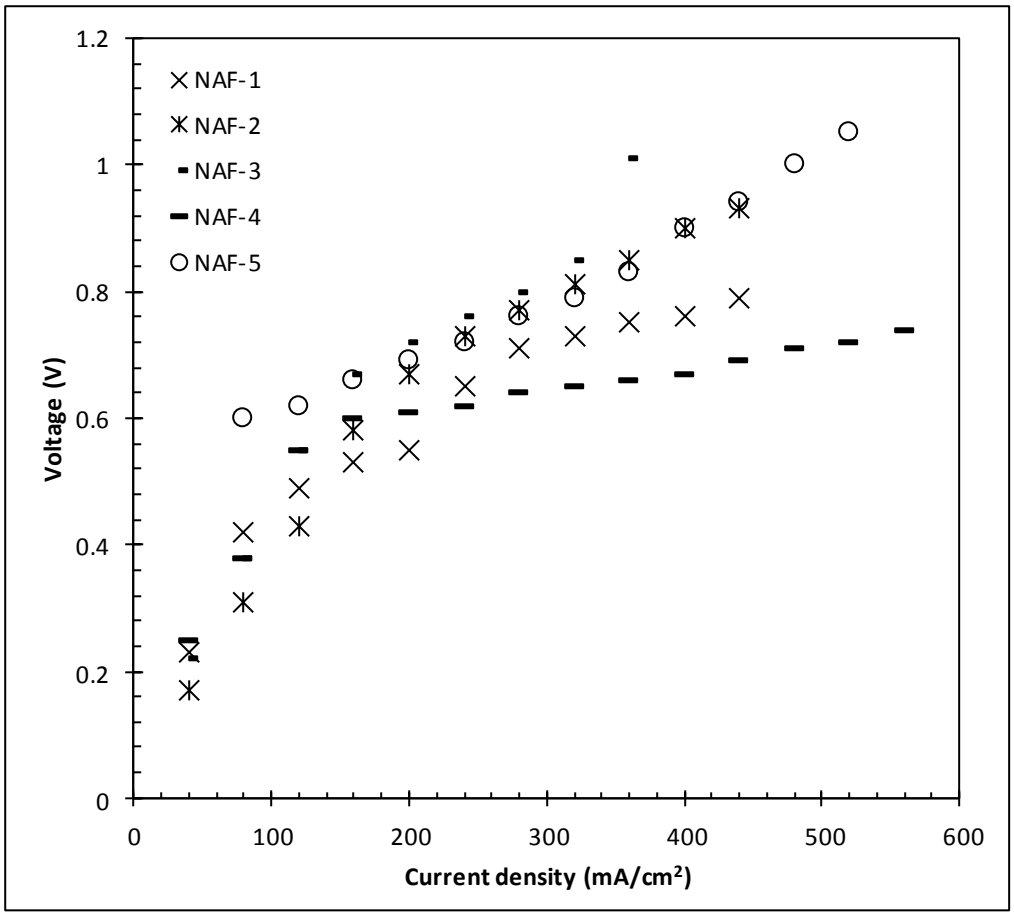

Figure 4.19: SO_2-depolarised electrolysis polarization curves for in-house-coated and commercial Nafion®-based MEAs.

In Figure 4.20, the polarization curves of the three in-house-manufactured sPSU-PBIOO with catalyst loadings of 0.3 (PBI-1), 0.6 (PBI-2) and 0.9 (PBI-3) Pt/cm^2 are presented and compared both to the sPSU-PBIOO MEA manufactured by ZSW (PBI-Z), as well as to the in-house-manufactured sFS-PBIOO (PBI-S). PBI-1 clearly yielded the best performance but, as had been observed with the 0.3 mg Pt/cm^2 Nafion® MEA (NAF-1), did not generate any hydrogen, which will be discussed in Section 4.4.3. When comparing the in-house-coated sPSU-PBIOO curves with the curves of the sPSU-PBIOO MEA obtained from ZSW (PBI-Z), it is clear that the 0.6 mg Pt/cm^2 MEA (PBI-2) performed slightly better (approximately 0.82 V @ 300mA) than the 0.6 mg Pt/cm^2 MEA obtained from ZSW (PBI-Z) (0.84 V @ 300mA), whereas the 0.9 mg Pt/cm^2 (PBI-3) performed worse (1 V @ 300mA) than both the in-house-coated 0.6 mg Pt/cm^2 MEA (PBI-2) and the ZSW MEA (PBI-Z). Taking the hydrogen pump test results from Section 4.4.1.2 into account, where the PBI-3 compared favourably with the other PBI-based MEAs, the worse performance of the PBI-3 during SO_2 electrolysis could only be ascribed to an over-potential caused by the assembly process. It is clear that the sFS-PBIOO (PBI-S) performed well, i.e. better than all the sPSU-PBIOO MEAs, except for PBI-1. The reason for this is, as

has been previously stated in Section 4.4.1.2, the higher acidity of the partially fluorinated sFS backbone leading to a higher dissociation degree of the -SO_3H groups and a subsequent higher proton conductivity. In addition, the sFS-PBIOO has more active -SO_3H groups available for proton conductivity as has been described by Katzfuß et al[93].

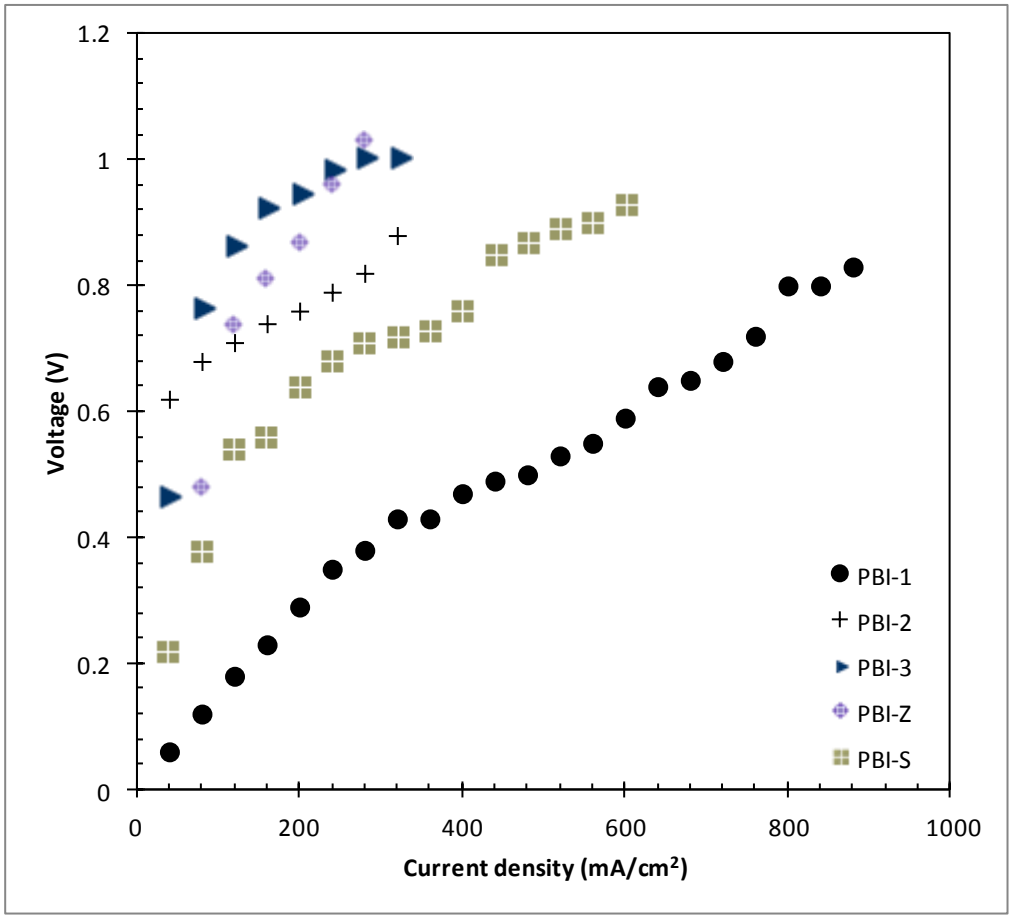

Figure 4.20: SO_2-depolarised electrolysis polarization curves in sPSU-PBIOO and sFS-PBIOO MEAs.

When comparing the GDEs and MEAs at 200 and 320 A/cm^2 (Table 4.2), it becomes apparent that for the GDEs, the best performance was attained with the higher catalyst loadings (GDE-3 and GDE-03), with the exception of GDE-01, which performed exceptionally well in spite of its 0.3 mg Pt/cm^2 loading. When considering the results obtained with the MEAs, the Nafion-based MEAs performed slightly better than the PBI-based MEAs, with the exception of PBI-1, which yielded exceptionally good VI curves. In general, the GDEs yielded lower voltages (0.45±0.14V) than the Nafion-based (0.64±0.07V) or PBI-based (0.70±0.26V) MEAs at 200mA/cm^2, suggesting their suitability for this application. It is interesting to note that the Nafion® MEAs VI curves were slightly more linear and consistent in their voltage increase with less variance between the different MEAs, which could have

resulted from the difference in thickness of the Nafion® (0.156 mm) vs. the sPSU-PBIOO (0.0306 mm)[98].

Table 4.2 Voltages of GDEs and MEAs tested at 200 mA/cm^2 and 320 mA/cm^2, respectively.

GDE and MEA	Symbol	Abbreviation	V (at 200 mA/cm^2)	V (at 320 mA/cm^2)
GDE				
EC-TP01-030	◆	GDE-1	0.62	0.75
EC-TP01-030	■	GDE-2	0.45	0.67
EC-TP01-030	▲	GDE-3	0.37	0.46
EC-TP01-060	◊	GDE-01	0.29	0.39
EC-TP01-060	□	GDE-02	0.64	0.8
EC-TP01-060	Δ	GDE-03	0.33	0.37
MEA				
Nafion® 117	x	NAF-1	0.55	0.73
Nafion® 117	ж	NAF-2	0.67	0.81
Nafion® 117	-	NAF-3	0.72	0.85
Nafion® 117	—	NAF-4	0.61	0.69
Nafion® 117	o	NAF-5	-	-
sPSU-PBIOO	●	PBI-1	0.29	0.43
sPSU-PBIOO	+	PBI-2	0.76	0.88
sPSU-PBIOO	▶	PBI-3	0.95	1.01
sPSU-PBIOO	⊕	PBI-Z	0.87	-
sFS-PBIOO	■	PBI-S	0.64	0.72

4.4.3 Hydrogen production

In this section the hydrogen production obtained during the SO_2-depolarised electrolysis is presented and discussed.

4.4.3.1 GDE hydrogen production

In Figure 4.21, the hydrogen production results for all the in-house-made and commercial GDEs are presented. Since none of the GDEs were hot pressed onto the PEMs, it can be assumed that sulfur deposition on the cathode influenced the GDEs performance in that increased sulfur deposition would shorten the lifetime of the GDLs and GDEs by blocking their pores. In terms of H_2 produced by the 0.11 mm thick in-house-coated GDE (GDE -1, -2 and -3), the 0.6 mg Pt/cm^2 (GDE-2) GDE performed the best, followed by the 0.3 mg Pt/cm^2 (GDE-1) GDE and then the 0.9 mg Pt/cm^2 (GDE-3) GDE, which corroborates well with the SO_2-depolarised electrolysis results from Figure 4.18. It was

also found that the 0.19 mm GDEs produced more hydrogen than the 0.11 mm GDEs, which again is in line with the polarization curves (See Section 4.4.2.1). Similarly, the low H_2 production of the 0.6 mg Pt/cm^2 (GDE-03) when compared to the 0.19 mm thick GDEs correlates with the polarization curves presented in Section 4.4.2.1.

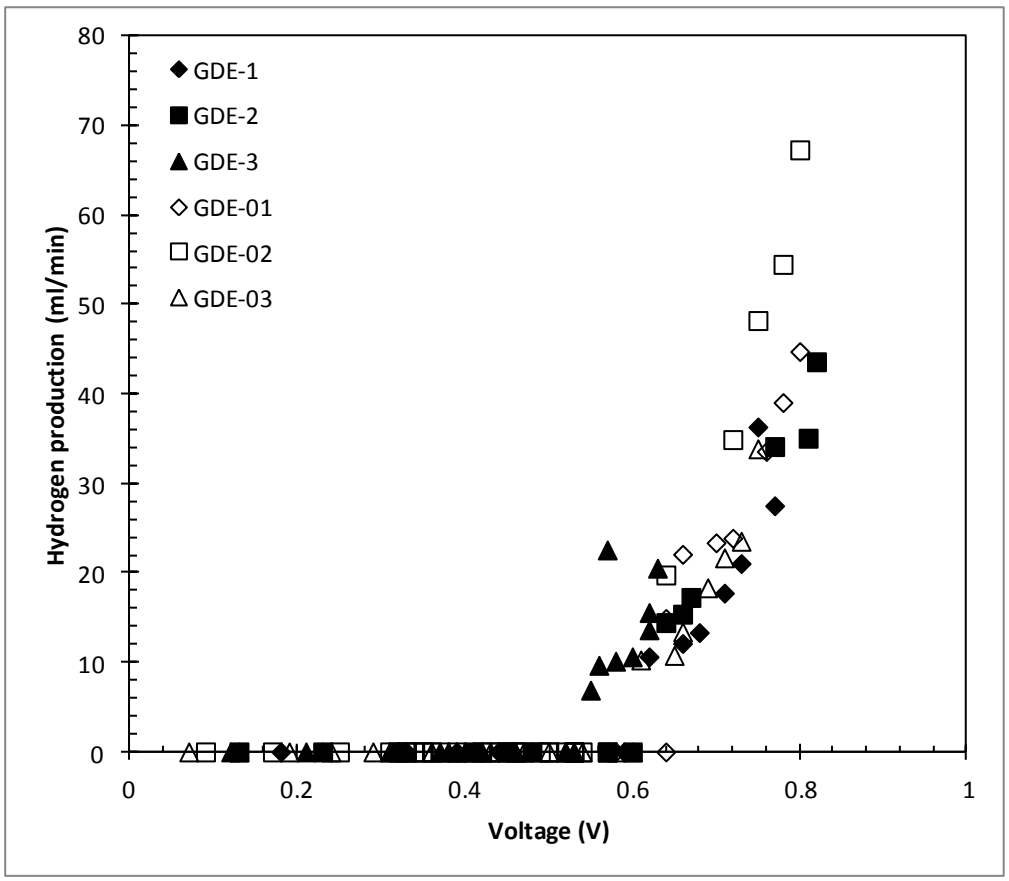

Figure 4.21: Hydrogen production of the in-house-coated and commercially-obtained GDE's.

4.4.3.2 MEA hydrogen production

Some correlation was obtained from the NAF MEAs between the polarization curves shown in Figure 4.19 and the hydrogen production shown in Figure 4.22. For example NAF-4, which had the best polarization curve, also had the highest hydrogen production. However, while according to Figure 4.19 NAF-1 performed second best in terms of SO_2-depolarised electrolysis, followed by NAF-2 and then NAF-3, respectively; in terms of hydrogen production (Figure 4.22) NAF-2 performed second best, followed by NAF-3 and only then NAF-1. Although, apart from NAF-1, a clear pattern emerges in terms of NAF-4, which performed the best, followed by NAF-2 and then NAF-3 according to Figure

4.19 and Figure 4.22. As mentioned previously, the 0.3 mg Pt/cm^2 (NAF-1) MEA did not produce any hydrogen. It is possible that side chain reactions occurred which resulted in the formation of H_2S.

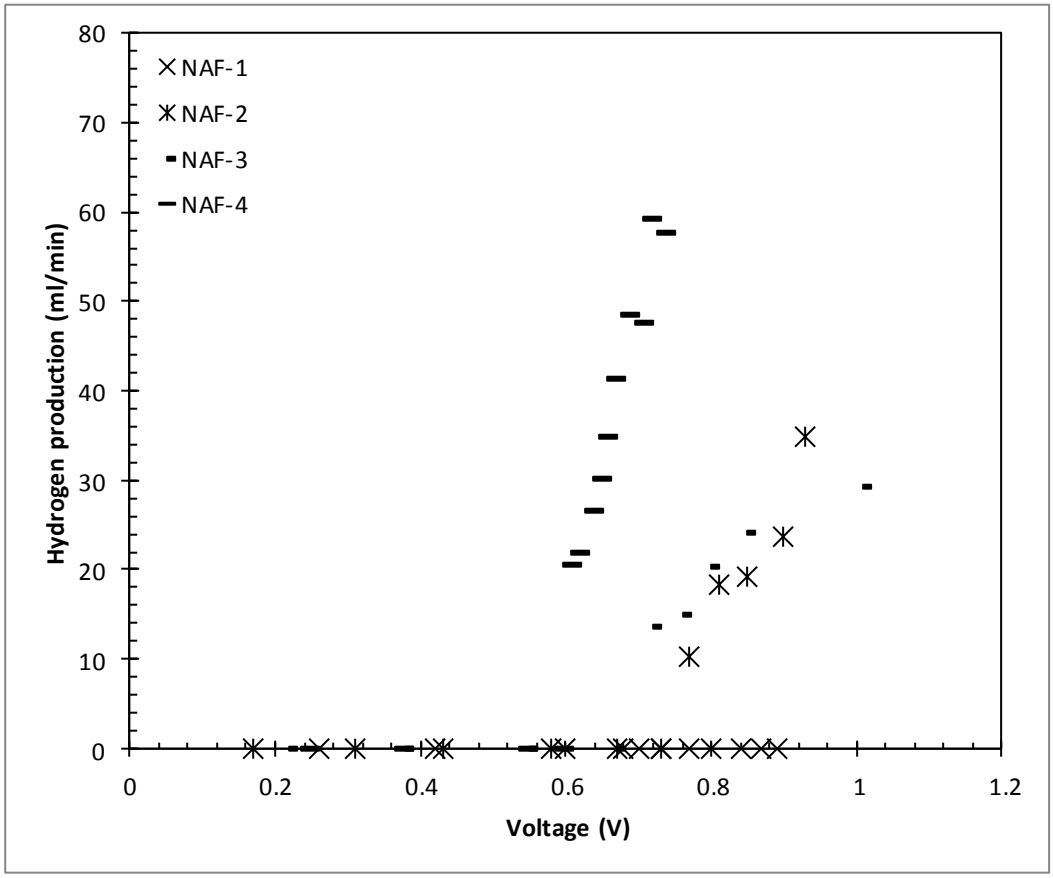

Figure 4.22: Hydrogen production of the in-house-coated and commercially-obtained MEAs

In Figure 4.23, a photo is shown of the permeated water from the cathode side of the electrolyser. The observed milky colour is typical of H_2S in the water[89]. Although the hydrogen production of the in-house-coated MEAs was in a reasonable range compared to the commercial MEAs, a temperature increase would undoubtedly increase the hydrogen production as has been shown by Krüger et al[89]. It is interesting to note that the VI curves of the in-house-manufactured MEAs were in closer proximity to the commercial MEAs (NAF-4) performance when compared to the hydrogen production, whereas the commercial MEAs performed significantly better than the in-house-manufactured MEAs.

Figure 4.23: Permeated SO_2 in feed water vessel resulting in H_2S formation.

In Figure 4.24, the H_2 production of the PBI-based membranes is presented. It is interesting to note that the in-house-coated 0.3 mg Pt/cm^2 sPSU-PBIOO MEA, as previously the NAF-1, also containing only 0.3 mg Pt/cm^2, did not generate any hydrogen. In accordance to the previously discussed Nafion-based MEAs, hydrogen production only occurred above 0.6V, where the hydrogen production decreased in the order of PBI-2>PBI-3>PBI-S>PBI-1. When comparing these results to the VI curves obtained during SO_2-depolarised electrolysis (Figure 4.20), i.e. PBI-1>PBI-S>PBI-2>PBI-Z>PBI-3, it becomes apparent that for the PBI-based MEAs no clear correlation between hydrogen production and actual VI curves could be observed. It is assumed that, due to the thinness of the PBI based membranes, the SO_2 crossover was higher than for the Nafion-based MEAs, which would result in better VI curves but lower hydrogen production.

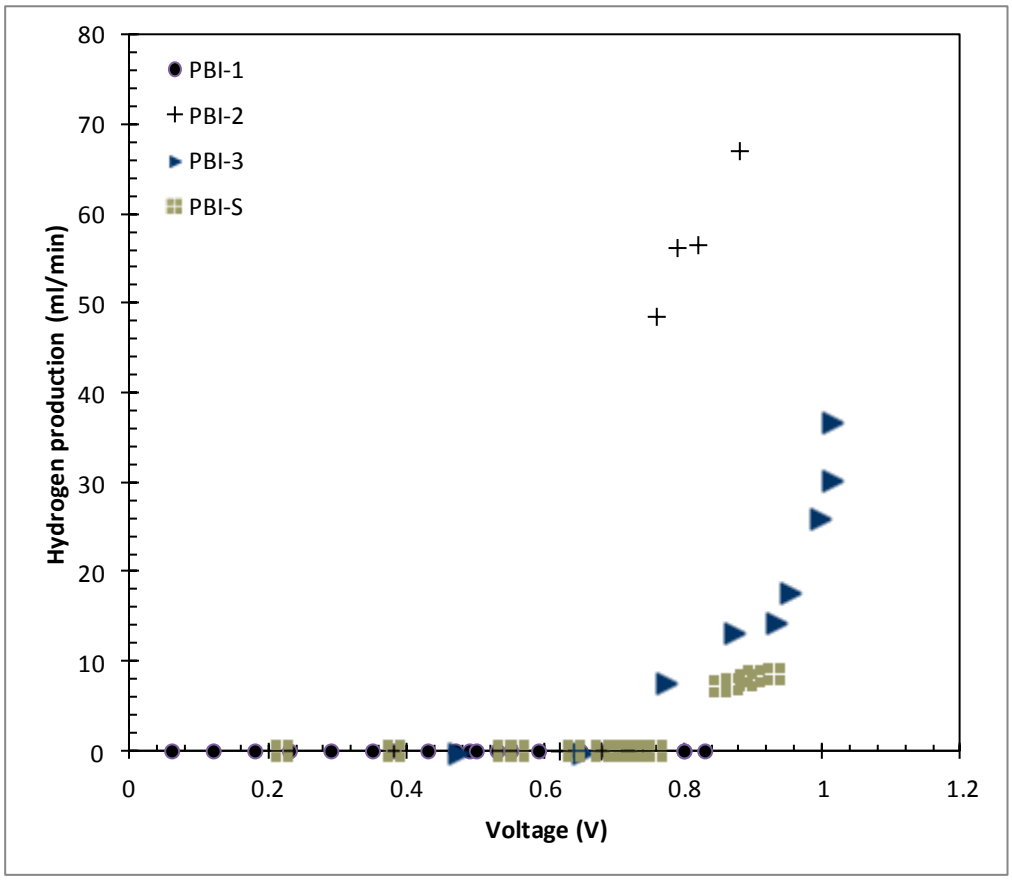

Figure 4.24: Hydrogen production of the in-house-coated PBI-based MEAs.

4.4.4 H_2SO_4 concentration

According to the theoretical reactions, one mole of sulfuric acid is produced for every one mole of hydrogen produced (see Section 2.2.4). The sulfuric acid concentration is therefore another variable that can yield further information on the process itself and its efficiency. Apart from the direct correlation between hydrogen production and acid concentration, the acid concentration also influences the durability and the lifetime of the GDEs and MEAs used in SO_2-depolarised electrolysis as has been shown in the work done by Schoeman et al[99]. In addition, the acid concentration also influences the water flux and electro-osmotic drag inside the membrane, thereby directly influencing the operation voltage and thus the efficiency of the overall process within the electrolyser cell[94].

4.4.4.1 GDE H_2SO_4 concentration

In Figure 4.25, the acid concentration as a result for all of the GDEs tested is presented. It is clear that the same trend is observed in Figure 4.25 that was observed during hydrogen production (Figure 4.21). Similarly, when comparing the in-house-coated 0.3 mg Pt/cm^2 (0.19 mm) and 0.6 mg Pt/cm^2 commercial GDE, a comparable trend was observed, showing consistent correlation between the hydrogen production and the acid concentration. The only deviation is the commercial 0.3 mg Pt/cm^2,which produced higher acid concentrations than the in-house-coated 0.3 and 0.6 mg Pt/cm^2 GDEs. The 0.9 mg Pt/cm^2 GDE's acid production also correlated with its polarization and hydrogen production curves.

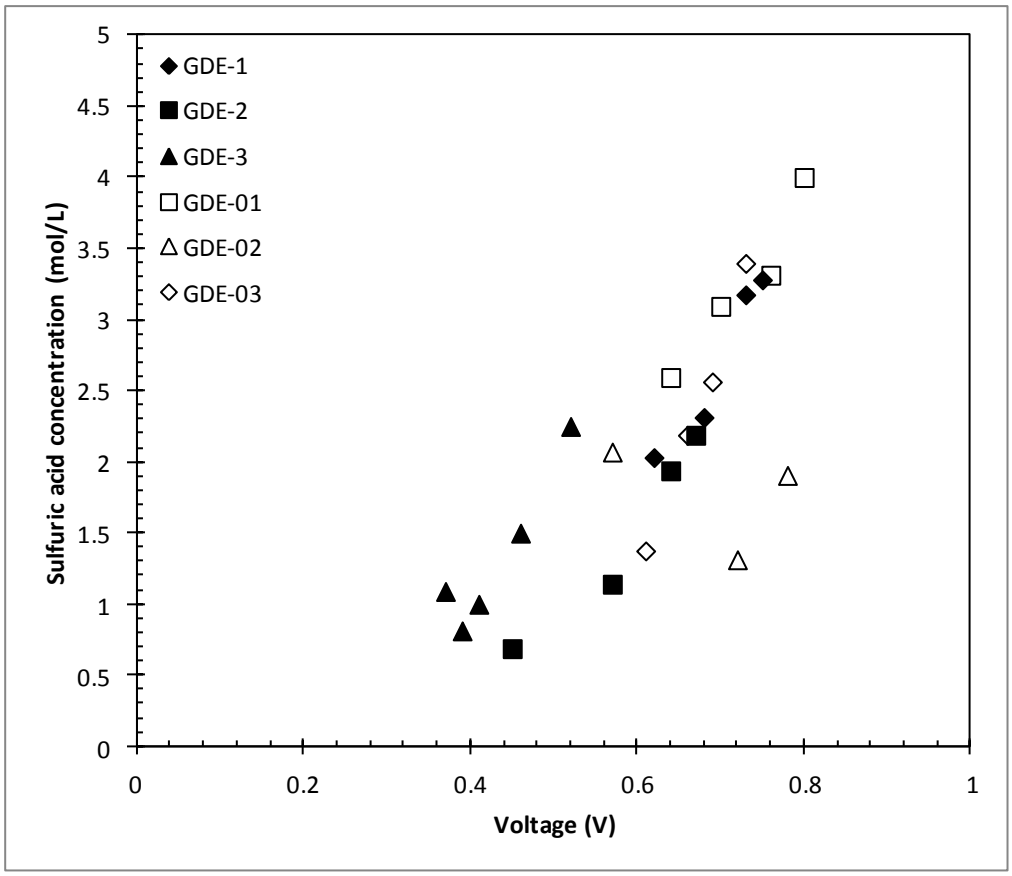

Figure 4.25: GDE H_2SO_4 concentration.

4.4.4.2 MEA H_2SO_4 concentration

In Figure 4.26, the acid concentrations produced by the tested Nafion® MEAs are presented. As stated in Section 4.4.2.2, the in-house-coated 0.3 mg Pt/cm^2 MEA (NAF-1) did not produce any hydrogen and similarly no acid was produced. For the other Nafion-based MEAs, the acid concentrations produced were in the same range as the hydrogen production. The 0.6 and 0.9 mg Pt/cm^2 MEAs produced almost exactly the same acid concentrations, although at different current densities, which correlates with their hydrogen production curves in Figure 4.22. The 0.3 mg Pt/cm^2 commercial MEA (NAF-4) showed slightly higher acid concentration results which were to be expected considering its superior polarization curve in Figure 4.19 and hydrogen production curve in Figure 4.22.

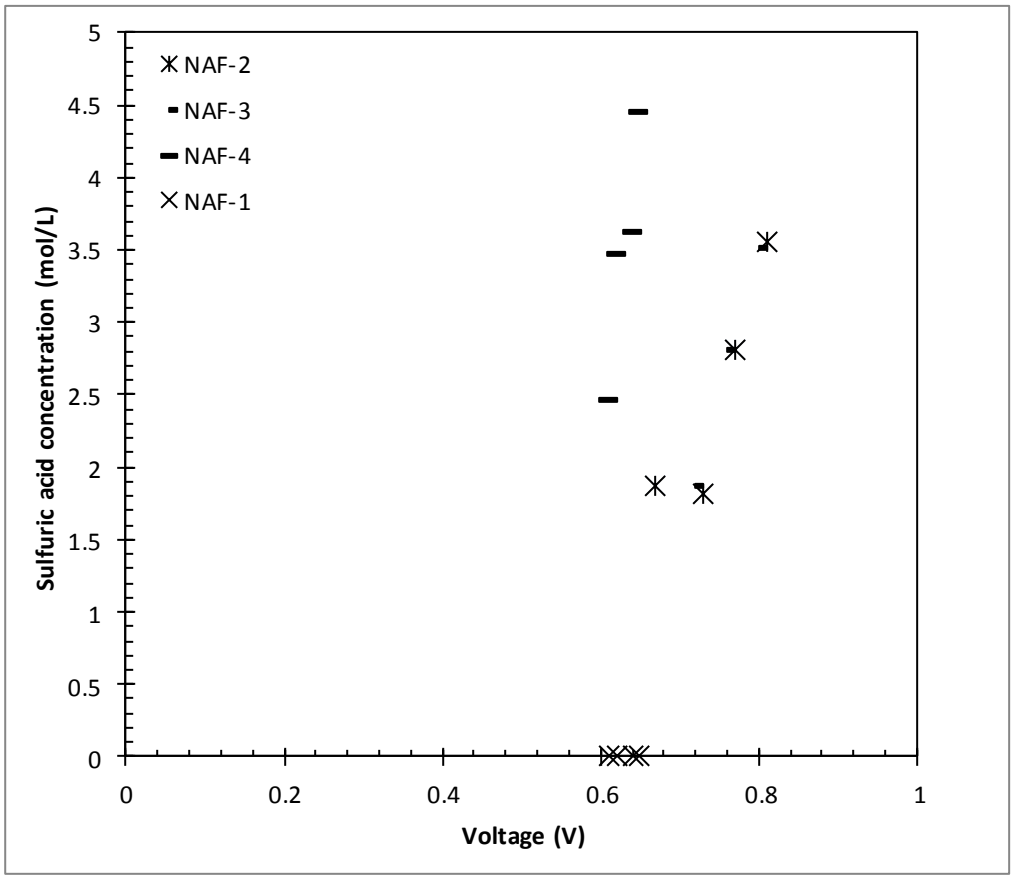

Figure 4.26: Nafion®-based MEA H_2SO_4 concentration.

In Figure 4.27, the acid concentration results of only those PBIOO MEAs that generated hydrogen are presented. According to the hydrogen production of the sPSU-PBIOO MEAs (Figure 4.24), the 0.6 mg Pt/cm^2 sPSU-PBIOO MEA (PBI-2) produced more hydrogen at similar current densities than the 0.9 mg Pt/cm^2 sPSU-PBIOO MEA (PBI-3), which had been related to its better polarization curve performance. In Figure 4.27, the same correlation can be seen for the acid production, i.e. the 0.6 mg Pt/cm^2 sPSU-PBIOO MEA produced higher acid concentrations in line with its better polarization curve performance and thus overall better efficiency, although sulfuric acid was produced at current densities approximately 100 mA higher than the 0.9 mg Pt/cm^2 sPSU-PBIOO MEA. Similarly, the sFS-PBIOO MEA showed low hydrogen production results (Figure 4.24), which was confirmed in terms of the acid concentrations generated by the sFS-PBIOO MEA shown in Figure 4.27.

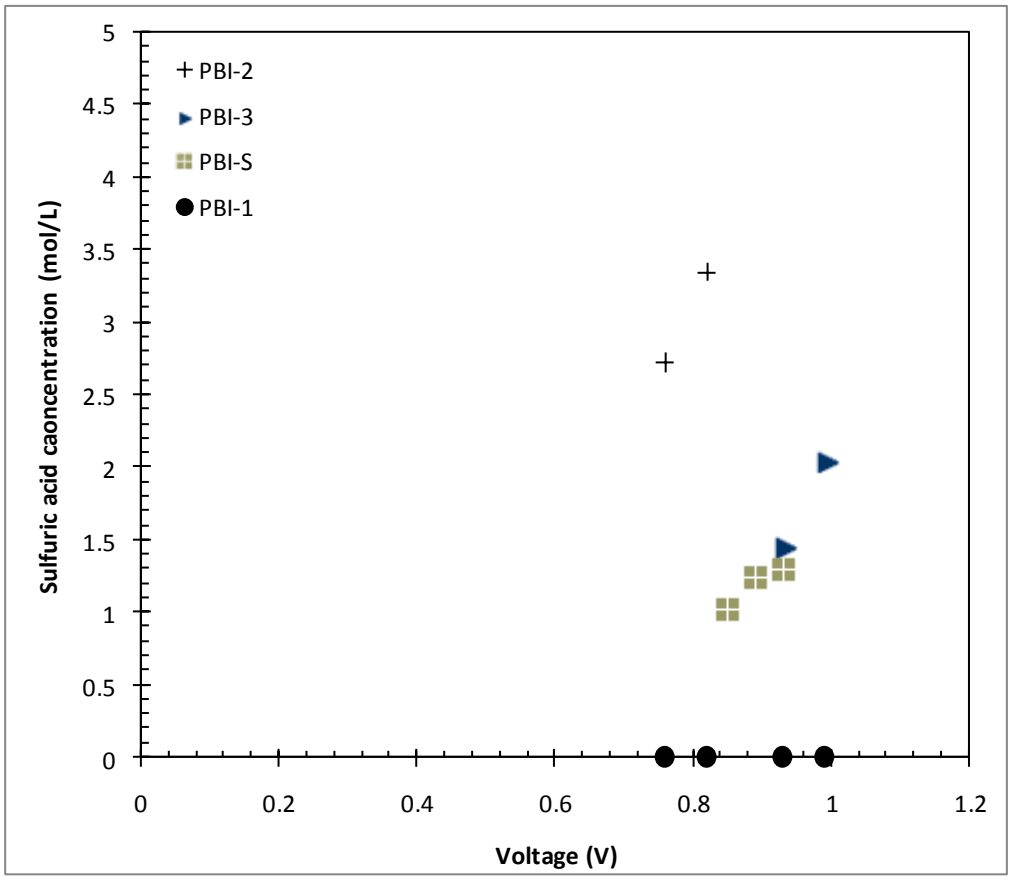

Figure 4.27: PBI-based MEA H_2SO_4 concentration.

4.4.4.3 Mole/s H_2 vs. Mol/L/s H_2SO_4

In Figure 4.28, an example using NAF-4 of the ratio between hydrogen production and acid production is shown. As stated in Section 4.4.4, it is theoretically true that one mole of acid should be produced for every mole of hydrogen produced. When considering Figure 4.28, it is clear that significantly more H_2SO_4 was produced than hydrogen, while the positive slope confirms that hydrogen production did increase with an increase in the acid production. There are two possible factors that might explain this deviation of the slope from unity. In the first place, it is possible that some of the protons produced did not migrate through the membrane, but were washed away with the formed H_2SO_4, which would result in a decrease of the pH. Since the H_2SO_4 concentration was determined by acid-base titration, these added protons would therefore skew the amount of H_2SO_4 measured. On the other hand, it was shown in Figure 4.23 that a significant amount of SO_2 crossover occurred, resulting in a decrease in the hydrogen produced, while not affecting the H_2SO_4 produced.

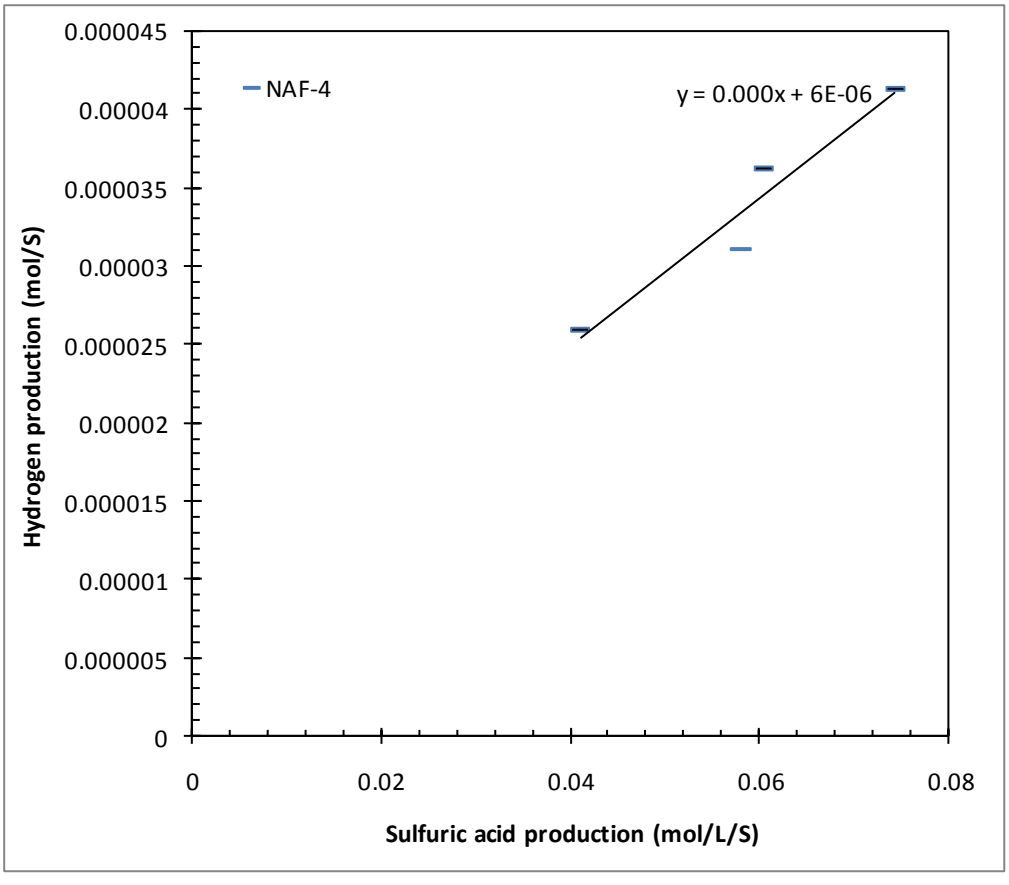

4.28: Nafion®-based MEA H_2/H_2SO_4 mole ratio

4.4.5 Hydrogen production efficiency

In this section the hydrogen production efficiencies of the tested GDEs and MEAs are presented and discussed. Hydrogen efficiency was calculated by calculating the difference between the theoretical and actual amount of hydrogen produced by firstly calculating the charge used during the process:

$$Q = I \times t \quad (1)$$

Where Q is the charge (Coulomb), I is the current (Amperes) and t is time (seconds). The charge can be calculated by equation 2:

$$n_e = \frac{Q}{F} \quad (2)$$

Where n_e is the mole of electrons produced and F is the faradic constant of 94685 C (A.s). Using reaction scheme (3) and (4), the actual moles amount of hydrogen produced can be calculated from the measured hydrogen produced:

$$2e^- + 2H^+ \rightarrow H_2 \quad (3)$$

$$n_{H_2} = 1/2 n_e \quad (4)$$

From the actual and theoretical moles of hydrogen, the efficiency was calculated in terms of percentage.

4.4.5.1 GDE efficiency

It is clear from Figure 4.29, that although most GDEs had similar hydrogen production efficiencies, GDE-02 (65%@ 0.79 V) had the highest efficiency, while GDE-01 had the worst efficiency (15%@ 0.76V). This confirms previous results where GDE-02 produced both the most hydrogen and the most sulfuric acid. In addition, GDE-02 delivered the best polarization curves (Figure 4.18), whereas GDE-01 delivered the worst at lower voltages but improved slightly as the voltage increased. On average, GDE-1 performed 16% lower, GDE-2 performed 12% lower and GDE-3 performed 36% lower than GDE-02.

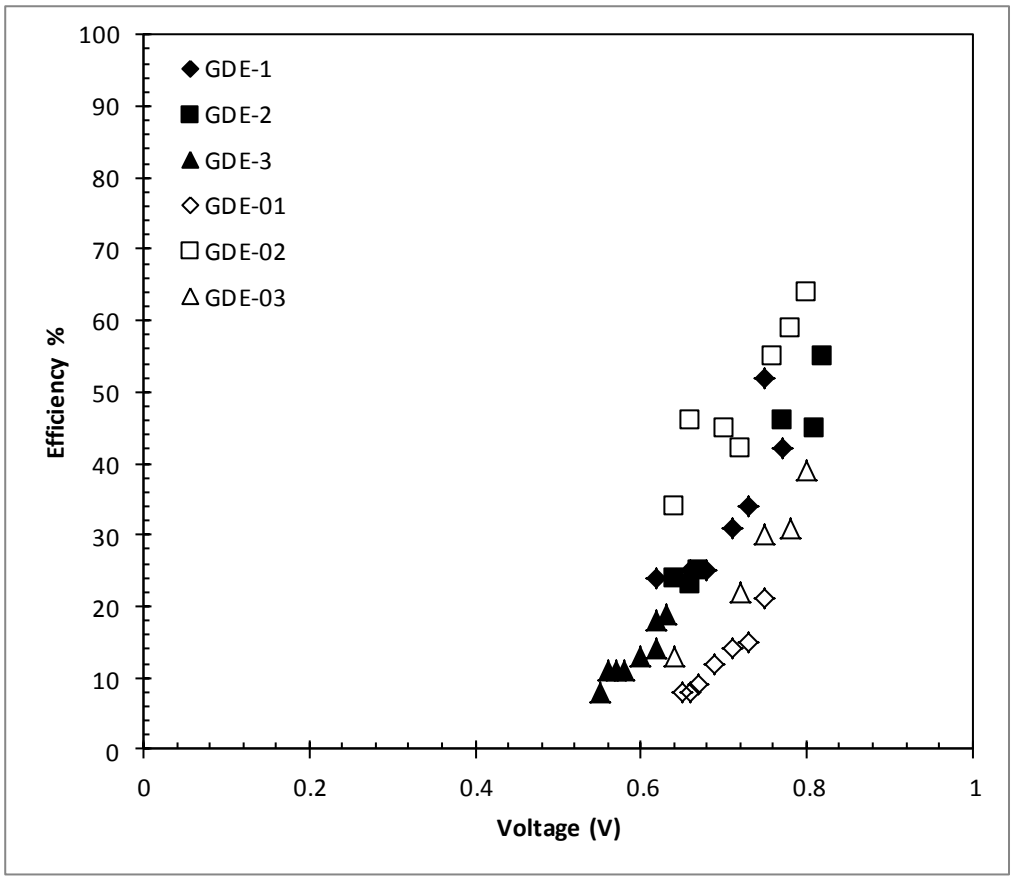

Figure 4.29: Hydrogen production efficiencies of GDEs.

4.4.5.2 MEA efficiency

It is clear from the hydrogen production (Figure 4.22) that the same trend was obtained as can be observed in Figure 4.30. In Figure 4.22, the best performing MEA in terms of hydrogen generation was NAF-4 and in Figure 4.26 the same tendency was observed for H_2SO_4 production. In Figure 4.22, NAF-2 is the second best performing MEA in terms of hydrogen production, which correlated with the H_2SO_4 production in Figure 4.26. The weakest performing MEA, NAF-3, was the weakest performing MEA in both Figures 4.22 and 4.30. In terms of polarization curves (Figure 4.19), NAF-4 was again the best performing MEA and NAF-3 the weakest performing MEA. Because of the higher efficiencies obtained from the MEAs tested, the difference in manufacturing between the in-house and commercial MEAs is clearer than for the comparison between the in-house-made and commercially-obtained GDEs.

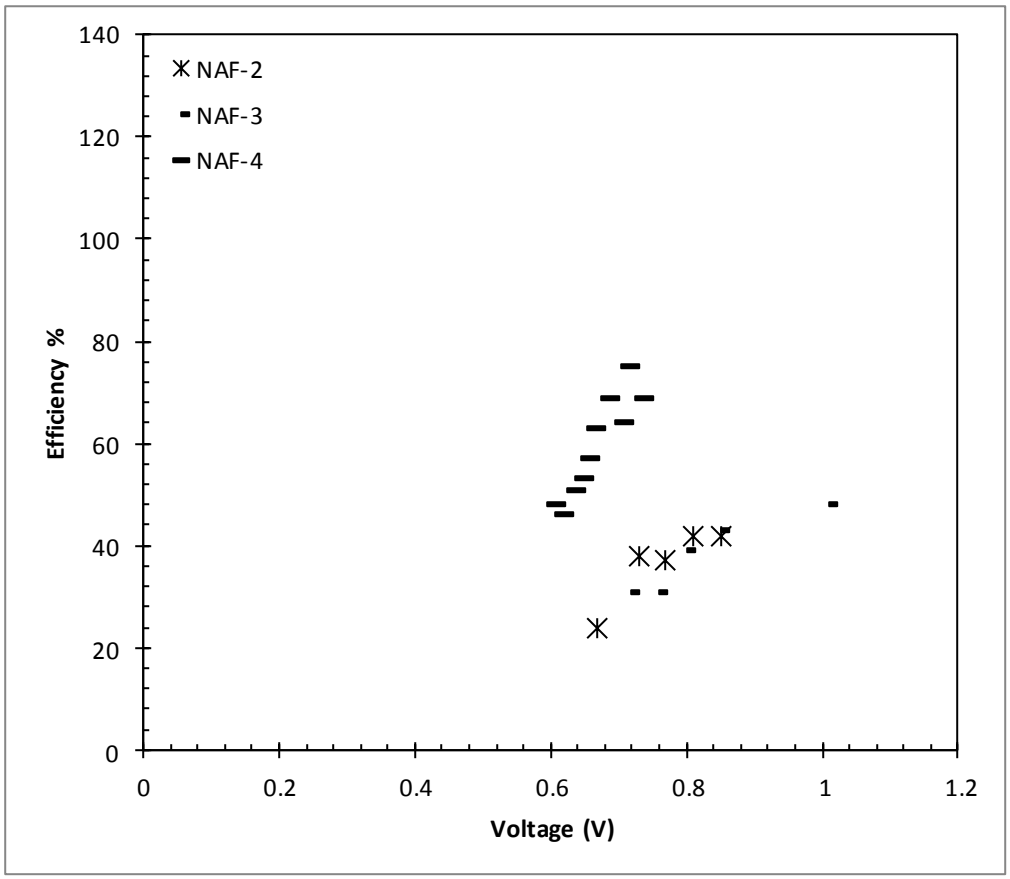

Figure 4.30: Hydrogen production efficiencies of Nafion®-based MEAs.

In Figure 4.31, the efficiencies of the PBI-MEAs are presented. In Figure 4.31, only the 0.6, 0.9 mg Pt/cm^2 sPSU-based MEAs (PBI 2, 3) and the 0.3 mg Pt/cm^2 (sFS-S) sFS-based MEA was presented (reasons discussed in previous sections). Apart from the MEAs where no hyrogen was produced, the sFS-based MEA (sFS-S) performed the weakest both in terms of hydrogen production (Figure 4.24) and efficiency (Figure 4.31). Similarly to the correlation between Figure 4.31 and Figure 4.24, the 0.6 mg Pt/cm^2 sPSU-based MEA (PBI 2) generated the best hydrogen production efficiencies. It is interesting to note that the efficiency for both PBI-2 and PBI-3 decreased as the current density increased, showing that the PBI-based MEAs had a higher hydrogen production efficiency at lower current densities.

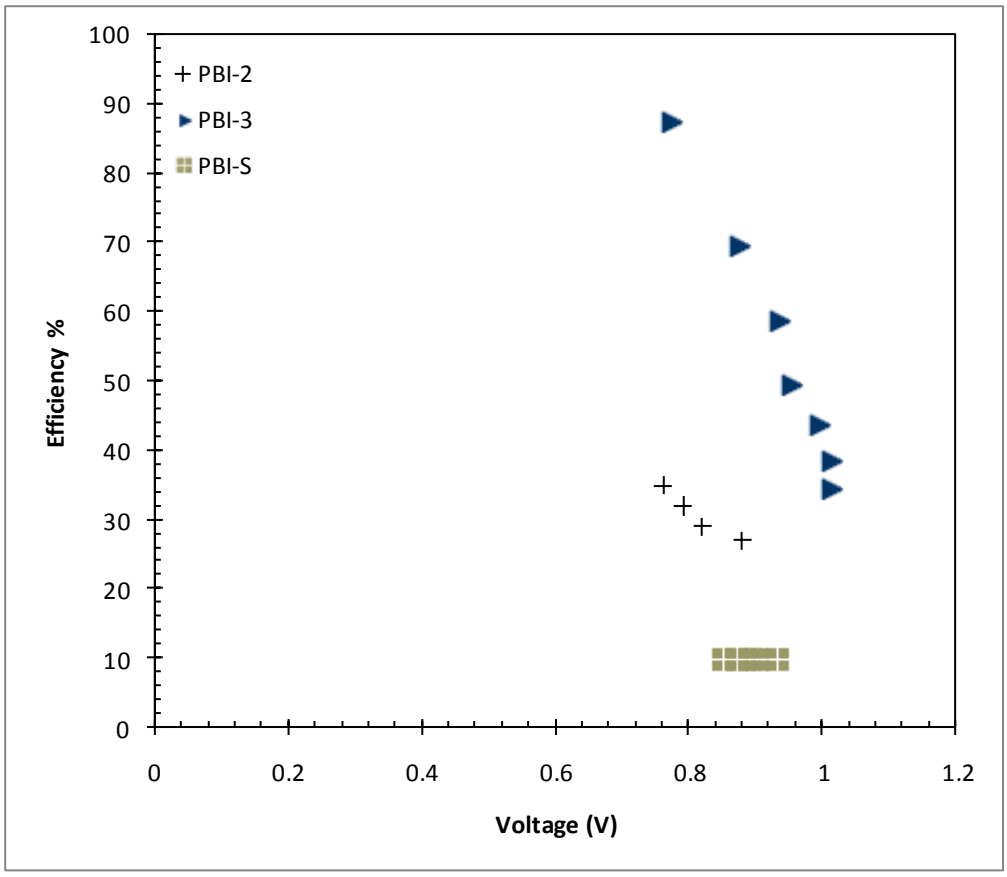

Figure 4.31: Hydrogen production efficiencies of PBI-based MEAs.

4.5 Conclusion

From the experimental data shown it can be concluded that both MEA and GDE manufacturing was successfully accomplished. It is clear from this study that the Nafion®-based MEAs performed the most consistently, which is currently regarded as the benchmark PEM, while the GDEs gave a generally lower voltage at 200 and 320 mA/cm^2. The in-house-manufactured Nafion® MEAs showed the best performance in terms of comparable results to the commercial Nafion® MEAs. They were also more handling friendly, showing less expansion and crimping during wetting and drying than the PBIOO MEAs. They were also less prone to tearing during hot pressing because of their increased thickness compared to that of the PBIOO MEAs. The GDEs performed more inconsistently compared to the Nafion® MEAs, possibly because of the absence of hot pressing, which made these GDEs more prone to elemental sulfur build-up on the cathode. In addition, the GDEs were more prone to crushing.

The PBIOO MEAs performed relatively well in terms of consistency, but because of their low thickness they were prone to SO_2 crossover, which impaired performance. The sFS-PBIOO gave better polarization curves but lower hydrogen production and lower acid production. It was also interesting to note that their hydrogen production efficiency decreased as the current density was increased.

Chapter 5: Evaluation and recommendations

5.1 Introduction

The purpose of this study was to establish MEA and GDE manufacturing capacities at the North-West University, Potchefstroom, South Africa for the characterisation of proton exchange membranes to be used in SO_2-depolarised electrolysis (HyS process). In order to establish the manufacturing techniques, a number of different MEAs and GDEs were manufactured. Firstly, different catalyst loadings were applied onto different PEMs in order to manufacture the MEAs. Subsequently, both microporous layers and different catalyst loadings were applied to GDLs to form GDEs. All of the manufactured (in-house-built) MEAs and GDEs were subsequently compared to various commercial MEAs and GDEs in order to measure the level of established manufacturing. Both MEAs and GDEs were evaluated using SEM before being characterised by hydrogen pump testing and SO_2-depolarised electrolysis, during which VI curves were obtained, while both the hydrogen and H_2SO_4 produced were measured.

5.2 Manufacturing techniques

5.2.1 Ink preparation

The recipe used for the ink preparation was suitable and did not give any problems during the catalyst ink preparation and subsequent use.

5.2.2 Screen printing

Although the screen printing was initially thought to be an effective and easy technique to develop for MEA and GDE manufacturing, it proved significantly more challenging. The main problem with the technique was related to the screens used on the printer as the commercially available screens were too dense for this application, thereby limiting the amount of ink able to pass through it. As a result numerous coatings were needed in order to achieve the required catalyst loading, making this technique laborious and time-consuming. In addition, the physical printing process onto the PEM, as well as the amount of coatings required, caused the already applied catalyst coatings to detach from the PEM surface. A second problem arose from the drying of the PEM during coating, which caused the PEM to shrivel. Although the screen printer could not be used meaningfully for the catalyst coating, the technique was, however, suitable for the microporous layer coatings applied prior to GDE manufacturing. Where fewer layers were required, as for example in the case of the microporous layer, the screen printer produced even and consistent layers of ink on the GDL.

5.2.3 Catalyst ink spraying

Because of the limitations posed by the screen printing technique, a spray painting setup was designed and manufactured. For this setup, specific frames were built which fit onto the spray table, in which the PEM could be clamped, leaving only the area exposed onto which the catalyst layer was sprayed. With the optimised ink composition and the simplicity of the technique, the spraying was easy and repeatable catalyst loadings were obtained. Care had to be taken not to spray too much ink onto the PEM, as this would cause blotching, resulting in an uneven CLs. One of the common drawbacks of this technique was the small amount of ink loss which occurs when the ink is in the aerosol state between the spraying and the contact with the PEM. Apart thereof however, the spraying technique proved to be successful both for MEA and GDE manufacture.

5.2.4 Hot pressing

As previously shown in literature[100], hot pressing was shown to be vital in producing effective and reliable MEAs. This can be ascribed to, as previously discussed in Chapters 3 and 4, the more intimate CL/PEM bond resulting from the hot pressing. Problems experienced during hot pressing included the tearing of thinner PEMs upon removal of the Teflon blocks, especially the PBI-based PEMs, which had a thickness of only 0.0306 mm. GDL hot pressing was problematic as the applied pressures combined with the elevated temperatures tended to lead to GDL cracking, which obviously led to adverse results during electrolyser operation. For this reason the in-house-manufactured GDEs were not hot pressed.

5.3 Characterisation

5.3.1 SEM Micrographs

SEM micrographs were taken for each step of the GDE manufacturing process, thereby giving a visual documentation of the various steps. The results showed that the most suitable MPL thickness was chosen and that the CL was applied effectively onto the MPL, as was confirmed by the H_2 pump and SO_2-depolarised electrolysis results. The SEM micrographs also corroborated the problems discussed above with the hot pressing of the GDLs, GDEs and thin PEMs.

5.3.2 H_2 pump testing

H_2 pump testing was done to ensure both proper cell assembly and that proper proton exchange occurred, thereby confirming whether the MEA and GDE manufacturing had been carried out correctly. While the general setup used had been built during a previous study[101], a new electrolysis cell had to be built for this study as the new bipolar plates did not fit into the old electrolysis cell. In addition, the old electrolysis cell had become compromised by the continuous SO_2 interaction which led to the corrosion of the flow fields inside the bipolar plates. The scrubber had also been replaced due to leakage resulting from NaOH corrosion.

5.3.3 SO_2-depolarised electrolysis

SO_2-depolarised electrolysis presented many challenges, mainly because an effective protocol of operation had to be developed for this study. Initially, SO_2 crossover presented major problems. At low current densities (below 200 m A/cm^2), SO_2 crossover was prevalent, which led to elemental sulfur deposition on the cathode, water lines and cathodic flow field, thereby poisoning the catalyst and destroying the catalyst membrane interface. In addition, the sulphur build up on the cathode caused higher over-potentials and thus lower efficiencies, while the sulfur build-up in the flow field caused blockages, which meant that the entire electrolyser cell had to be taken apart and cleaned regularly. Similarly, sulfur build-up in the water lines resulted in poisoned feed water and the occurrence of side chain reactions, including H_2S formation. In collaboration with Dr S Stone (Giner Electrochemical Systems, LLC (GES)), a suitable protocol was developed. The use of the optimised protocol led not only to the attainment of higher current densities, but also improved the reproducibility of the results, while contributing to a reduction in the SO_2 crossover. As stated in Chapter 4, in some cases GDE crushing was observed, which was ascribed to the differences between the gasket and GDE thicknesses, obviously resulting in lower performances.

In order to compare the VI curves of the GDEs and MEAs evaluated, it is possible to compare the voltages at a specific current. In Figure 5.1, the voltages for the best performing GDEs and MEAs are shown at 320 and 380 mA/cm^2. From this depiction it is clear that the best performance was obtained by the PBIOO-based in-house-manufactured PBI MEA (PBI-1), followed by the commercially-obtained GDEs, and thirdly by the commercially obtained Nafion-based MEAs. When only taking the in-house-manufactured GDEs and MEAs into account, GDE-3, NAF-1 and PBI-1 performed best overall while the worst overall performing GDEs and MEAs were GDE-02, NAF-3 and PBI-3.

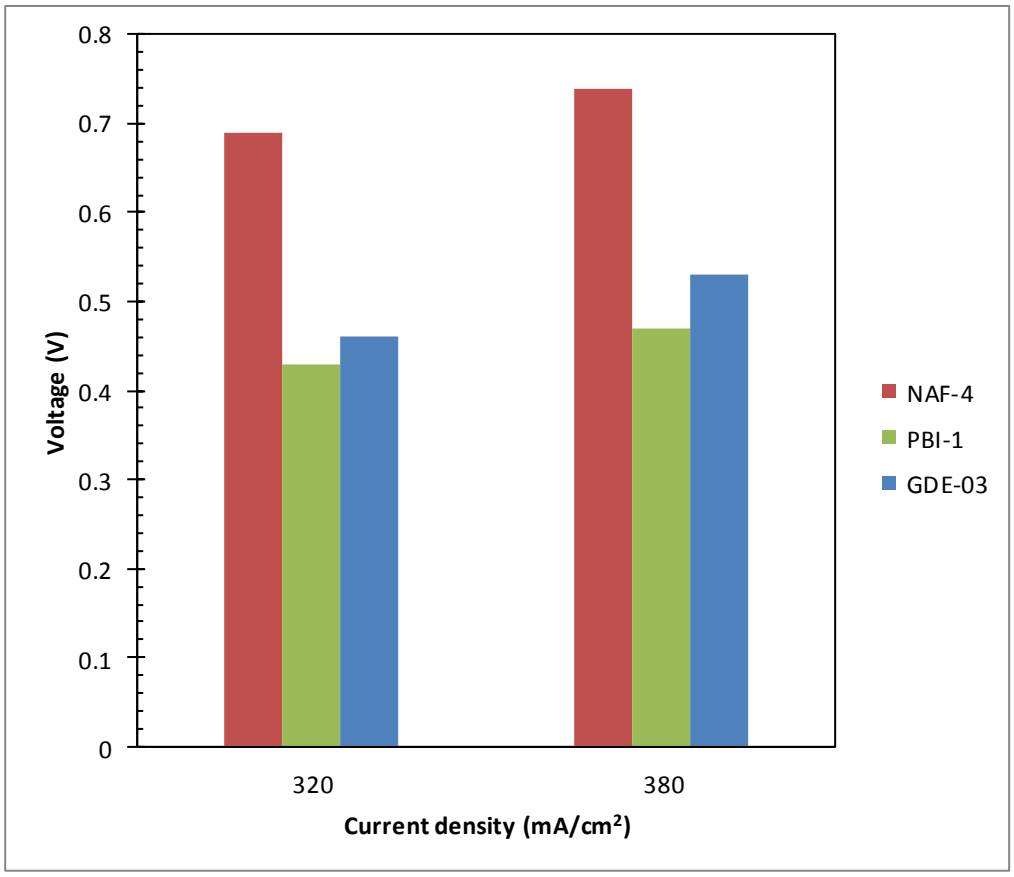

Figure 5.1 Best performing GDE and MEAs during SO_2-depolarised electrolysis.

5.3.4 Hydrogen production

Hydrogen production measurements yielded some further challenges. To remove the crossed-over SO_2, the produced gas was passed through two scrubbers containing NaOH. The bubbling through the scrubbers required a slight pressure build-up on the cathode before the gas would start bubbling through the solutions. As a result, hydrogen measurements at low current densities were often not measurable due to the pressure build-up and release. At higher current densities, with subsequent higher hydrogen amounts produced, the measurement of hydrogen became more consistent and repeatable.

5.3.5 H_2SO_4 concentrations

The amount of sulfuric acid needed to ensure accurate titrations took a relatively long time (approximately 5-7 min. per Ampere) on average to produce, this part of the characterisation had significant error margins (10-20%) as the SO_2 crossover and feed solution poisoning restricted the operational time limit of the electrolyser.

5.3.6 Hydrogen production efficiency

Hydrogen production efficiencies were calculated using a series of equations that were based on theoretical hydrogen production vs. experimental hydrogen production. In view of the variations experienced during hydrogen production described in Section 5.3.4, the results from the calculated hydrogen production efficiency obviously displayed the same variations. However, since the errors arising from the hydrogen production were consistent, the data was comparable in terms of the different MEAs and GDEs tested.

5.4 Recommendations

For the GDE and MEA manufacturing process the following recommendations could be made:

- More suitable screens in terms of pore size could be manufactured which would make screen printing more suitable for CL coating by reducing the amount of coatings required.
- Specialized pressing blocks could be manufactured to more effectively fix the MEA in its position inside the spraying frame, thereby reducing the handling required while eliminating potential shrivelling of the PEM during hot pressing.
- The thin PEMs should be prepared with slightly higher thicknesses, which would eliminate the tearing observed during MEA manufacturing, PEM drying and wetting.

For the characterisation process the following recommendations could be made:

- Gaskets with varying thicknesses should be obtained to eliminate GDE or MEA crushing.
- A setup could be devised facilitating the measurement of both the hydrogen and H_2SO_4, while hopefully simultaneously increasing the accuracy of the determinations.
- A wider variety of PBIOO and Nafion®-based MEAs could be tested in future to obtain a more extensive overview on their performance according to their proton conductivity, thickness and SO_2 crossover.
- A high pressure setup could be built to lessen SO_2 crossover.

5 References

[1] http://www.ren21.net/REN21Activities/Publications/GlobalStatusReport/GSR2010/tabid/5824/Default.aspx. Date of access: 17 August. 2011.

[2] D. W. Connell. 2005. Basic concepts of environmental chemistry. New York: Taylor & Francis group 261p.

[3] http://www.esrl.noaa.gov/gmd/webdata/ccgg/trends/co2_data_mlo.png. Date of access: 17 August. 2011.

[4] http://www.alternative-energy-news.info/technology/hydro/. Date of access: 17 August. 2011.

[5] B. Parida, S. Iniyan, R. Goic. Review of solar photovoltaic techniques. Renewable and sustainable energy reviews 2011; 15: 1625 – 1636.

[6] K. Benlarbi, L. Mokrani, M. S. Nait-Said. A fuzzy global efficiency optimization of a photovoltaic water pumping system. Solar energy 2004; 77: 203 – 216.

[7] M. Kolhe, K. Agbossou, J. Hamelin, T.K. Bose. Analytical model for predicting the performance of photovoltaic array coupled with a wind turbine in a stand –alone renewable energy system based on hydrogen. Renewable energy 2003; 28: 727 – 742.

[8] http://www.eco-h2o.co.za/2010/03/11/cape-could-get-500-wind-turbines/

[9] G. Wei, Y. Wang, S. Huang, Q. Gao, Z. Wang, L. Xu. The stability of MEA in SPE water electrolysis for hydrogen production. Int j hydrogen energy 2010; 35: 3951 – 3957.

[10] M. Ni, M. K. H. Leung, D. Y. C. Leung. Energy and exergy analysis of hydrogen production by a proton exchange membrane (PEM) electrolyzer plant. Energy conversion and management 2008; 49: 2748 – 2756.

[11] K. Hou, R. Hughes. The kinetics of methane steam reforming over Ni/α-Al_2O catalyst. Chemical engineering journal 2001; 82: 311 – 328.

[12] S. C. Dantas, J. C. Escritori, R. R. Soares, C. E. Hori. Effect of different promoters on Ni/$CeZrO_2$ catalyst for autothermal reforming and partial oxidation of methane. Chemical engineering journal 2010; 156: 380 – 387.

[13] G. F. Naterer, V. N. Daggupati, G. Martin, K.S. Gabriel, Z. L. Wang. Thermochemical hydrogen production with a copper-chlorine cycle, II: Flashing and drying of aqueous cupric chloride. Int j hydrogen energy 2008; 33: 5451 – 5459.

[14] X. Vitart, P. Charles, P. Anzieu. A general survey of the potential and the main issues associated with the sulfur-iodine thermochemical cucle for hydrogen production using nuclear heat. Progress in nuclear energy 2008; 50: 402 – 410.

[15] H. Zhang, G. Lin, J. Chen. Evaluation and calculation on the efficiency of a water electrolysis system for hydrogen production. Int j hydrogen energy 2010; 35: 10851 – 10858.

[16] S. K. Lee, C. H. Kim, W. C. Cho, K. S. Kang, C. S. Park, K. K. Bae. The effect of Pt loading amount on SO_2 oxidation reaction in an SO_2-depolarized electrolyzer used in the hybrid sulfur (HyS) process. Int j hydrogen energy 2009; 34: 4701 – 4707.

[17] H. Zhang, G. Lin, J. Chen. Evaluation and calculation of the efficiency of a water electrolysis system for hydrogen production. Int j hydrogen energy 2010; 35: 10851 – 10858.

[18] R. P. Viswanath. A patent for generation of electrolytic hydrogen by a cost effective and cheaper route. Int J hydrogen energy 2004; 29: 1191 – 1194.

[19] M. B. Gorensek. Hybrid sulfur cycle flowsheets for hydrogen production using high-temperature gas-cooled reactors. Int j hydrogen energy 2011; 36: 12725 – 12741.

[20] S. Ranganathan, E. B. Easton. Ceramic carbon electrode-based anodes for the use in the Cu-Cl thermochemical cycle. Int J hydrogen energy 2010; 35: 4871 – 4876.

[21] A. Konieczny, K. Mondal, T. Wiltowski, P. Dydo. Catalyst development for thermocatalytic decomposition of methane to hydrogen. Int J hydrogen energy 2008; 33(1):264-272.

[22] G. F. Naterer, K. Gabriel, Z. Wang. 2008. Recent advances in nuclear-based hydrogen production with the thermochemical copper-chlorine cycle. 16th International Conference on Nuclear Engineering. Orlando, Florida May 11 – 15.

[23] J. A. Basco, M. A. Lewis, M. Serban. 2004. Kinetic study of the hydrogen and oxygen production reactions in the copper-chloride thermochemical cycle, in AIChE; Spring national meeting.

[24] M. A. Lewis, M. S. Ferrandon, D. F. Tatterson, P. Mathias. Evaluation of alternative Thermochemical cycles – Part III: Further development of the Cu-Cl cycle. Int J hydrogen energy 2009; 34: 4136-4145.

[25] M. A. Lewis, J. G. Masin, P. A. O'Hare. Evaluation of alternative thermochemical cycles, Part I: The methodology. Int J hydrogen energy 2009; 34: 4115 – 4124.

[26] X. Vitart, P. Charles, P. Anzieu. A general survey of the potential and the main issues associated with the sulfur-iodine thermochemical cycle for hydrogen production using nuclear heat. Progress in Nuclear Energy 2008; 50: 402 – 410.

[27] J. H. Norman, G. E. Besenbruch, L. C. Brown, D. R. O'Keefe, C. L. Allen. Thermochemical water splitting cycle, Bench scale investigations and process engineering. DOE/ET/26225, 1981.

[28] M. K. Hadji-Kali, V. Gerbaud, P. Lovera, O. Baudouin, P. Florquet, X. Joulia, J. M. Borgard, P. Carles. Bunsen section thermodynamic model for hydrogen production by the sulfur-iodine cycle. Int J hydrogen energy 2009; 34: 6625 – 6635.

[29] B. J. Lee, H. C. NO, H. J. Yoon, H. G. Jin, Y. S. Kim, J. I. Lee. Development of a flow sheet for iodine-sulfur thermo-chemical cycle based on optimized Bunsen reaction. Int J hydrogen energy 2009; 34: 2133-2143.

[30] L. C. Brown, G. E. Besenbruch, R. D. Lentsch, K. R. Schultz, J. F. Funk, P. S. Pickard, et al. High efficiency generation of hydrogen fuels using nuclear power – final technical report of the period August 1, 1999 through September 30, 2002. General Atomics report GA-A24285, Rev. 01; December 2003.

[31] H. Zhang, G. Lin, J. Chen. Evaluation and calculation on the efficiency of water electrolysis system for hydrogen production. Int J Hydrogen energy 2010; 35: 10851 – 10858.

[32] G. Wei, L. Xu, C. Huang, Y. Wang. SPE water electrolysis with SPEEK/PES blend membranes. Int J Hydrogen energy 2010; 35:7778-7783

[33] M. Ni, M. K. H. Leung, D. Y. C. Leung. Energy and exergy analysis of hydrogen production by proton exchange membrane (PEM) electrolyzer plant. Energy conservation and management 2008; 49: 2748 – 2756.

[34] G. Wei, Y. Wang, C. Huang, Q. Gao, Z. Wang, L. Xu. The stability of MEA in SPE water electrolysis for hydrogen production. Int J hydrogen energy 2010; 35: 3951 – 3957.

[35] M. S. Wilson, S. Gottesfeld. Thin film catalyst layers for polymer electrolyte fuel cell electrodes. Journal of applied electrochemistry 1992; 22: 1-7.

[36] P. Millet, N. Mbemba, S. A. Grigoriev, V. N. Fateev, A. Aukauloo, C. Etie'vant. Electrochemical performances of PEM water electrolysis cells and perspectives. Int J hydrogen energy 2010; xxx: 1-9.

[37] Y. Gong, E. Chalkova, N. Aknifiev, V. Balashov, M. Fedkin, S. N. Lvov. Development of CuCl-HCl electrolysis for hydrogen production via Cu-Cl thermochemical cycle. Nuclear production of hydrogen. Fourth information exchange meeting, Oakbrook, Illinois, USA, 14-16 April 2009. DOI: 10.1787/9789264087156 – en.

[38] F. Jomard, J. P. Feraud, J. P. Caire. Numerical modeling for preliminary design of the hydrogen production electrolyzer in the Westinghouse hybrid cycle. Int J hydrogen energy 2008; 33: 1142–1152.

[39] L. E. Brecher, S. Spewock, C. J. Warde. The Westinghouse sulfur cycle for the thermochemical decomposition of water. Int J Hydrogen energy 1977; 2: 7-15.

[40] R. H. Colón-Mercando, D. T. Hobbs. Catalyst evaluation for a sulfur dioxide-depolarized electrolyzer. Electrochemistry communications 2007; 9: 2649 –2653.

[41] P. Sivasubramanian, R. P. Ramasamy, F. J. Freire, C. E. Holland, J. W. Weidner. Electrochemical hydrogen production from thermochemical cycles using a proton exchange membrane electrolyzer. Int J hydrogen energy 2007; 32: 463 – 468.

[42] E. Middleman, W. Kout, B. Vogelaar, J. Lenssen, E. de Waal. Bipolar plates for PEM fuel cells. Journal of power sources 2003; 118: 44 – 46.

[43] D. H. Jeon, S. Greenway, S. Shimpalee, J. W. Van Zee. The effect of serpentine flow-field design on PEM fuel cells. Int J hydrogen energy 2008; 33: 1052 – 1066.

[44] K. Tüber, A. Oedegaard, M. Hermann, C. Hebling. Investigation of fractal flow-fields in portable proton exchange membrane and direct methanol fuel cells. Journal of power sources 2004; 131: 175 – 181.

[45] C. Hartnig, T. J. Schmidt. On a new degradation mode for high-temperature polymer electrolyte fuel cells: How bipolar plate degradation affects cell performance. Electrochimica acta 2011; xxx: xxx – xxx.

[46] J. H. Chun, K. T. Park, D. H. Jo, S. G. Kim, S. H. Kim. Numerical modeling and experimental study of the influence of GDL properties on performance in a PEMFC. Int j hydrogen energy 2011; 36: 1837 – 1845.

[47] V. Gurrau, M. J. Bluemle, E. S. De Castro, Y. Tsou, J. A. Mann Jr, T. A. Zawodzinski Jr. Characterization of transport properties in gas diffusion layers for proton exchange membrane fuel cells 1. Wettability (internal contact angle to water and surface energy of GDL fibers). Journal of power sources 2006; 160: 1156 – 1162.

[48] K. S. S. Naing, Y. Tabe, T. Chikahisa. Performance and liquid water distribution in PEFCs with different Anisotropic fiber directions of the GDL. Journal of power sources 2011; 196: 2584 – 2594.

[49] J. Ge, A. Higier, H. Liu. Effect of gas diffusion layer compression on PEM fuel cell performance. Journal of Power sources 2006; 159: 922 – 927.

[50] Y. Gao, G. Q. Sun, S. L. Wang, S. Zhu. Carbon nanotubes based gas diffusion layers in direct methanol fuel cells. Energy 2010; 35: 1455 – 1459.

[51] C. Pan, Q. Li, J. O. Jenses, R. He, L. N. Cleemann, M. S. Nilson, N. J. Bjerrum, Q. Zeng. Preparation of gas diffusion electrodes for high-temperature proton exchange membrane fuel cells. Journal of power sources 2007; 172: 278 – 286.

[52] U. Pasaogullari, C. Y. Wang. Liquid water transport in gas diffusion layer of polymer electrolyte fuel cells. Journal of the electrochemical society 2004; 151 (3): 399 – 406.

[53] G. Sasikumar, J. W. Ihm, H. Ryu. Dependence of optimum Nafion content in catalyst layer on platinum loading. Journal of power sources 2004; 132: 11 - 17.

[54] J. Zhang. PEM fuel cell electro catalysts and catalyst layers: fundamentals and applications 2008. 889 - 916.

[55] D. Lee, S. Hwang. Effect of loading and distributions of Nafion ionomer in the catalyst layer for PEMFCs. Int J hydrogen energy 2008; 33: 2790 – 2794.

[56] V. Mehta, J. S. Cooper. Review and analysis of PEM fuel cell design and manufacturing. Journal of power Sources 2003; 114: 32 – 53.

[57] S. K. Lee, C. Kim, W. C Cho, K. S. Kang, C. S. Park, K. K. Bae, The effect of Pt loading amount on SO_2 oxidation reaction in an SO_2- depolarized electrolyzer used in the hybrid sulfur (HyS) process. Int J hydrogen energy 2009; 34: 4701 – 4707.

[58] J. A. Staser, M. B. Gorensek, J. W. Weidner. Quantifying individual potential contributions of the Hybrid Sulfur Electrolyzer. Journal of the electrochemical society 2010; 157: (6) B952 – B958.

[59] P. Costamagna, S. Srinivasan. Quantum jumps in the PEMFC science and technology from the 1960s to the year 2000. Journal of power sources 2011; 102: 242 – 252, 253 – 269.

[60] K. A. Mauritz, R. B. Moore. State of understanding of Nafion. American chemical society 2004; 104: 4535 – 4585.

[61] G. B. Jung, F. B. Weng, A. Su, J. S. Wang, T. L. Yu, H. L. Lin, T. F. Yang, S. H. Chan. Nafion/PTFE/silicate membranes for high temperature proton exchange membrane fuel cells. Int J hydrogen energy 2008; 33: 2413 – 2417.

[62] F. N. Büchi, G. G. Scherer. In-Situ resistance measurements of Nafion® 117 membranes in polymer electrolyte fuel cells. Journal of electroanalytical chemistry 1996; 404: 37 – 43.

[63] A. Mahreni, A. B. Mohamad, A. A. H. Kadhum, W. R. W. Daud, S. E. Lyuke. Nafion/silicon oxide/ phosphotungstic acid nanocomposite membrane with enhanced proton conductivity. Journal of membrane science 2009; 327: 32 – 40.

[64] S. J. Paddison, R. Paul. The nature of proton transport in fully hydrated Nafion. Phys Chem. Chem Phys 2002; 4: 1158 – 1163.

[65] K.D. Kreuer. Proton conductivity: Materials and applications. Chem. Mater 1996; 8: 610-641.

[66] C. A. Edmondson, P. E. Stallworth, M. E. Chapman, J. J. Fontanella, M. C. Wintersgill, S. H. Chung, S. G. Greenbaum. Complex impedance studies of proton-conducting membranes. Solid State Ionics 2000;13: 419-423.

[67] E. P. Jutemar. 2010. Proton-conducting sulfonated aromatic ionomers and membranes by chemical modifications and polycondensations. Sweden Lund University. (Theisis – P.hD.) 64p.

[68] P. Choi, N. H. Jalani, R. Datta. Thermodynamics and proton transport in nafion. Journal of the electrochemical society 2005; 152 (3): E123 – E 130.

[69] Q Li, J O Jensen, R F Savinell, N J Bjerrum. High temperature proton exchange membranes based on polybenzimidazoles for fuel cells. Progress in polymer science 2009; 34: 449 – 477.

[70] Q. F. Li, R H He, J. O. Jensen, N. J. Bjerrum. Approaches and recent development of polymer electrolyte membranes for fuel cells operating above 100˚C. Chem Mater 2003; 15: 4896 – 4915.

[71] E. W. Neuse, Aromatic polybenzimidazoles – syntheses, properties and applications, advanced polymer science 1982; 42: 1 – 42.

[72] E. W. Choe, Catalysts for the preparation of polybenzimidazoles. Journal of applied polymer science 1994; 53: 497 – 506.

[73] L. Paturzo, A. Basile, A. Iulianelli, J. C. Jansen, I. Gatto, E. Passalazqua. High temperature proton exchange membrane fuel cell using a sulfonated membrane obtained via H_2SO_4 treatment of PEEK – WC. Catalysis today 2005; 104: 213 – 218.

[74] E. Drioli, A. Regina, M. Casciola, A. Oliveti, F. Trotta, T. Massari. Sulfonated PEEK –WC membranes for possible fuel cell applications. Journal of membrane sciences 2004; 228: 139 – 148.

[75] NASA. http://www.grc.nasa.gov/WWW/Electrochemistry/doc/fuelcell.html.

[76] L. Sun, R. Ran, G. Wang, Z. Shao. Fabrication and performance test of a catalyst – coated membrane from direct spray deposition. Solid state Ionics 2008; 179: 960 – 965.

[77] I. Park, W. Li, A. Mnathiram. Fabrication of catalyst – coated membrane-electrode assemblies by doctor blade method and their performance in fuel cells. Journal of power sources 2010; 195: 7078 – 7082.

[78] G. Bender, T. A. Zawodzinski, A. P. Saab. Fabrication of high precision PEFC membrane electrode assemblies. Journal of power sources 2003; 124: 114 – 117.

[79] C. S. Kim, Y. G. Chun, D. H. Peck, D. R. Shin. A Novel process to fabricate membrane electrode assemblies for proton exchange membrane fuel cells. Int J hydrogen energy 1998; 23 (11): 1045 – 1048.

[80] L. Sun, R. Ran, G Wang, Z. Shao. Fabrication and performance test of a catalyst-coated membrane from direct spray deposition. Solid state ionics 2008; 179:960 -965.

[81] H. R. Corti, F. Nores-Pondal, M. P. Buera. Low temperature properties of Nafion 117 membranes in water and methanol-water mixtures. Journal of power sources 2006; 161: 799 – 805.

[82] A. J. Krüger. Properties and use of SO_2 for the Hybrid Sulfur Process. Potchefstroom: NWU. (M.Sc Thesis – M.Sc) P86.

[83] J. Zhang. PEM fuel cell electro catalysts and catalyst layers: fundamentals and applications 2008. 889 – 916.

[84] K. D. Baik, S. I. Kim, B. K. Hong, K. Han, M. S. Kim. Effects of gas diffusion layer structure on the open circuit voltage and hydrogen crossover of polymer electrolyte membrane fuel cells. Int J Hydrogen energy 2011; 36: 9916 – 9925.

[85] Y. Hiramitsu, H. Sato, H. Hosomi, Y. Aoki, T. Harada, Y. Sakiyama, Y. Nakagawa, K. Kobayashi, M. Hori. Influence of humidification on deterioration of gas diffusivity in catalyst layer on polymer electrolyte fuel cell. Journal of power sources 2010; 195: 435 – 444.

[86] A. Pfrang, D. Veyret, G. J. M. Jannsen, G. Tsotridis. Imaging of membrane electrode assemblies of proton exchange fuel cells by X-ray computer tomography. Journal of power sources 2011; 196: 5272 – 5276.

[87] V. Radhakrishnan, P. Haridoss. Effect of cyclic compression on structure and properties of gas diffusion layer used in fuel cells. J Int Hydrogen energy 2010; 35: 11107 – 11118.

[88] L. Sun, R. Ran, G. Wang, Z. Shao. Fabrication and performance test of a catalyst-coated membrane from direct spray deposition. Solid State Ionics 2008; 179: 960 – 965.

[89] A. J. Krüger. Properties and use of SO_2 for the Hybrid Sulfur Process. Potchefstroom: NWU. (M.Sc Thesis – M.Sc) P45.

[90] S. K. Lee, C. Kim, W. C Cho, K. S. Kang, C. S. Park, K. K. Bae, The effect of Pt loading amount on SO_2 oxidation reaction in an SO_2- depolarized electrolyzer used in the hybrid sulfur (HyS) process. Int J hydrogen energy 2009; 34: 4701 – 4707.

[91] J. A. Staser, M. B. Gorensek, J. W. Weidner. Quantifying individual potential contributions of the Hybrid Sulfur Electrolyzer. Journal of the electrochemical society 2010; 157: (6) B952 – B958.

[92] Q Li, J O Jensen, R F Savinell, N J Bjerrum. High temperature proton exchange membranes based on polybenzimidazoles for fuel cells. Progress in polymer science 2009; 34: 449 – 477.

[93] A. Katzfuß, K. Krajinovic, A. Chromik, J. Kerres. Partially fluorinated sulfonated poly(arylene sulfone)s blended with polybenzimidazole. Journal of polymer science Part A: Polymer chemistry 2011; 49: 1919 – 1927.

[94] J. A. Staser, J. W. Weidner. Effect of water transport on the production of hydrogen and sulfuric acid in a PEM electrolyzer. Journal of The Electrochemical Society 2009; 156 (1): B16 – B21.

[95] J. Lin, W. Chen, Y. Su, T. Ko. Effect of gas diffusion layer compression on the performance in a proton exchange fuel cell. Fuel 2008; 87: 2420 – 2424.

[96] R. P. Ramasamy, E. C. Kumbur, M. M. Mench, W. Liu, D. Moore, M. Murthy. Investigation of macro- and micro-porous layer interaction in polymer electrolyte fuel cells. Int J hydrogen energy 2008; 33: 3351 – 3367.

[97] Toray carbon fibre paper data sheet. P2.

[98] J. A. Staser, J. W. Weidner. Sulfur dioxide crossover during the production of hydrogen and sulfuric acid in a PEM electrolyzer 2009; 156 (7): B836 – B841.

[99] H. Schoeman, H. M. Krieg, A. J. Kruger, A. Chromik, K. Krajinovic, J. Kerres. H_2SO_4 stability of PBI-blend membranes for SO_2 electrolysis 2012; 37: 603 – 614.

[100] J. Zhang. PEM fuel cell electro catalysts and catalyst layers: fundamentals and applications 2008. 165 - 287.

[101] H. Schoeman, H. M. Krieg, A. J. Kruger, A. Chromik, K. Krajinovic, J. Kerres. H_2SO_4 stability of PBI-blend membranes for SO_2 electrolysis 2012; 37: 603 – 614.